4-1993

Peroxyoxalate chemiluminescence and capillary electrophoresis : new methods for bioanalytical chemistry

Nian Wu
Binghamton University--SUNY

PEROXYOXALATE CHEMILUMINESCENCE AND CAPILLARY ELECTROPHORESIS: NEW METHODS FOR BIOANALYTICAL CHEMISTRY

BY

NIAN WU

B. S., Nanjing Normal University, 1982

M. A., University of Scranton, 1989

DISSERTATION

Submitted in partial fulfillment of the requirements for the degree of
Doctor of Philosophy in Chemistry
in the Graduate School of the State University of New York at Binghamton
1993

Accepted in partial fulfillment of the requirements for the degree of
Doctor of Philosophy in Chemistry
In the Graduate School of the State University of New York at Binghamton

Carmen W. Huie. 4/26/93
Research Advisor

Richard A. Hartwick 4/26/93
Chair, Defense Committee

Udo H. Brinker 4/26/93
Department of Chemistry

David C. Doetschman. 4/26/93
Department of Chemistry

ABSTRACT

The general research objectives lie in the development of new approaches to improve chemical analysis in the area of bioanalytical chemistry. More specifically this thesis is focused on the development and application of new methodologies and instrumentation involving two potentially powerful techniques: 1) Chemiluminescence-a spectroscopic technique in which the generation of fluorescence from the electronically excited state of the molecule is provided by a chemical reaction and 2) Capillary electrophoresis-a separation technique in which small ions as well as large biomolecules can be separated with high efficiency within a narrow capillary under the influence of high voltage.

In chapter 2 a chemiluminescence detection system was descibed for the sensitive and reproducible detection of three dansyl-amino acids separated on thin-layer chromatographic plates involving the peroxyoxalate chemiluminescence (CL) reaction. Synchronization of timing between chemical excitation (spraying of pre-mixed CL reagents onto the plate surface) and subsequent detection of the rapidly changing CL signal was accomplished by coupling a pneumatic nebulizer and an optical fiber to produce a steady stream of reactive aerosol and to transport the CL emission to the detector, respectively. Further study in this area was concentrated on the investigation of those parameters which may affect the analytical application of peroxyoxalate chemiluminescence to thin-layer chromatography using a stopped-scan, kinetic system.

In chapter 3 the observation of light emission from bilirubin in an organic solvent as a result of the peroxyoxalate chemiluminescence reaction is reported for the first time. Analytical utilization of the present observation for the determination of bilirubin in biological materials was evaluated. The visible spectrum of bovine serum in the blue-green region was obtained using the present chemiluminescence method and

was briefly compared with those obtained from absorption and fluorescence methods.

In chapter 4 four major bilirubin species in serum were separated by micellar electrokinetic chromatography (MEKC) with sodium dodecyl sulfate (SDS) in sodium tetraborate-boric acid buffer at pH 8.5. Due to the solubilization of the serum proteins by the SDS micelles, serum samples were injected directly into a fused silica capillary and complete separation of the four bilirubin species was accomplished within *ca.* 10 min. without extensive sample pretreatment. The usefulness of this method was demonstrated for the separation and detection of a number of bilirubin species present in pathological human serum samples. Bovine Serum Albumin (BSA) was used as a run buffer modifier in the MEKC separation of urinary porphyrins and type I and III isomers of coproporphyrin using bile salt micelles. The retention mechanism is described briefly. The results show that using BSA as a run buffer modifier in bile salt and SDS MEKC increases the scope of applications of MEKC to include both hydrophilic and hydrophobic compounds, improves separation efficiency, and increases sample solubilization via pH changes of the run buffer.

In chapter 5 capillary zone electrophoresis was evaluated as a method for the speciation of aluminum in aqueous solution using indirect UV absorption detection. Excellent agreement between experimental and theoretical species concentrations (via the thermodynamic speciation model SOILCHEM) was obtained for solutions with varying ligand/aluminum mole ratios and pH values.

In chapter 6 the feasibility of employing peroxyoxalate chemiluminescence (PO-CL) detection in capillary electrophoresis (CE) was demonstrated using a two-step approach for the CE separation and dynamic elution (elution under pressure) of the analytes. In this approach, potential problems associated with incompatibilities between mixed aqueous-organic solvent and electrically driven separation systems were avoided by switching off the CE power supply at an appropriate time and connecting the CE capillary to a syringe pump to effect dynamic elution. Also, an improved whole

capillary scanning device was constructed which permitted the scanning of capillaries. This device allowed examination of electropherograms during the course of development, and also eliminated the need to handle the capillaries after separation. This design produced noise levels better than the earlier prototype on a separation of test proteins.

ACKNOWLEDGEMENTS

I would like to express my gratitude to professor Huie who supervised my research; professor Hartwick for letting me use his research facilities; professor Brinker, professor Doetschman and professor Cotts for acting as my oral defense committee; Joseph Aiken, William Horvath, Mei Lin, Geoffrey Barker and Peng Sun for their friendship and useful dicussion; Adam Landman and Lisa Sanders for their assistance.

Table of Contents

Abstract ii

Acknowledgement v

Table of Contents vi

List of Tables x

List of Figures xi

CHAPTER 1 INTRODUCTION 1

I. *Objectives* 1

II. *Peroxyoxalate Chemiluminescence* 2

Historical Aspect (2)

The Measurement of Peroxyoxalate Chemiluminescence (5)

Theoretical Aspect (6)

Problemsin the Analytical Application of Peroxyoxalate Chemiluminescence (8)

III. *Capillary Electrophoresis* 10

Historical Aspect (10)

The Principles of Separation and CE instrumentation (12)

Theoretical Aspect (13)

Problems in Capillary Electrophoresis (18)

CHAPTER 2 PEROXYOXALATE CHEMILUMINESCENCE FOR THIN-LAYER CHROMATOGRAPHY 22

I. *The Design of A Chemiluminescence Detection System* 22

Introduction (22)

Experimental (24)

Results and Discussion (28)

Conclusion (31)

II. *Determination of the Parameters Affecting the Application of Peroxyoxalate Chemiluminescence to Thin-Layer Chromatography* 38

Introduction (38)

Experimental (39)

Results and Discussion (42)

Conclusion (46)

CHAPTER 3 LIGHT EMISSION FROM BILIRUBIN FROM THE PEROXYOXALATE CHEMILUMINESCENCE REACTION 58

Introduction (58)

Experimental (60)

Results and Discussion (63)

Conclusion (72)

CHAPTER 4 NEW METHOD FOR THE BIOLOGICAL TETRAPYRROLES ANALYSIS USING MICELLAR ELECTROKINETIC CHROMATOGRPHY . . 78

I. *Separation of Serum Bilirubin Species with Micellar Electrokinetic Chromatography By Direct Sample Injection* 78

Introduction (78)
Experimental (81)
Results and Discussion (83)
Conclusion (91)

II. *Enhanced Separation of Urinary Porphyrins in Micellar Electrokinetic Chromatography with Bovine Serum Albumin as a Buffer Additive* 99

Introduction (99)
Experimental (100)
Results and Discussion (101)
Conclusion (106)

CHAPTER 5 SPECIATION OF ALUMINUM USING CAPILLARY ZONE ELECTROPHORESIS WITH INDIRECT UV DETECTION 116

Introduction (116)
Experimental (118)
Results and Discussion (120)
Conclusion (124)

CHAPTER 6 IMPROVEMENT OF DETECTABILITY IN CAPILLARY ELECTROPHORESIS 130

I. *Peroxyoxalate Chemiluminescence Detection in Capillary Electrophoresis* 130

Introduction (130)

Experimental (132)

Results and Discussion (135)

Conclusion (137)

II. *Improved Detection System for Whole Column Detection in Capillary Electric Focusing* 145

Introduction (145)

Experimental (146)

Results and Discussion (147)

Conclusion (149)

APPENDIX INVESTIGATIONS OF GAS-FLOW PATTERNS WITHIN A CYLINDRICAL GLASS TUBE HAVING IDENTICAL DIMENSIONS AS A GRAPHITE FURNACE ATOMIZER UNDER THE INFLUENCE OF FORCED CONVECTIVE FLOW 153

REFERENCES 166

List of Tables

Table 2-1. Effect of TCPO concentration on background intensity 46

Table 2-2. Effect of H_2O_2 concentration on background intensity 47

Table 2-3. Effect of imidazole concentration on background intensity 48

Table 2-4. Environmental effects on the CL emission. 48

Table 2-5 Maximum CL enhancement 49

Table 2-6 Effects of flow-rate on the CL emission 50

Table 2-7 Comparison of the mass limits of detection between porphyrin free acids and their methyl esters 51

Table2-8 Substrate effect on maximum CL emission and reproducibility. 51

Table 2-9 Linear regression analysis of the CL measurements 52

Table 4-1-1 Detection limits and linearity 92

Table 4-1-2 Reproducibility of migration times and peak areas 92

Table 4-2-1 K' values in different systems. 107

Table 4-2-2 The relative standardard deviation on the reproducibility of migration time and peak areas 108

Table 5-1 Measured (CZE) and predicted (SOILCHEM-SOIL) concentrations of uncomplexed Al and complex fluoroaluminum species in solutions of varying F:Al mole ratios and pH values 125

Table 6-1 Comparison of concentration and mass detection limits between UV absorption and chemiluminescence detection methods 139

List of Figures

Figure 1 Schematic diagram of CE instrumentation 19

Figure 2 CE separation Mechanisms 20

Figure 3 The separation principle of MEKC 21

Figure 2-1-1: Experimental set-up used for the CL detection 33

Figure 2-1-2: CL intensity-time profile of Dns-glycine 34

Figure 2-1-3: HPTLC chromatograms of three dansyl amino acids 35

Figure 2-1-4: HPTLC chromatograms of two dansyl amino acids 36

Figure 2-1-5: Relative CL intensity of three amino acid sample spots 37

Figure 2-2-1. Sectional view of the experimental set-up for the stopped-scan, kinetic system. 53

Figure 2-2-2. Substrate Effect on CL emission. 54

Figure 2-2-3. Silica Effect on CL emission. 55

Figure 2-2-4. Comparison of CL measurements at the origin and the R_f, ... 56

Figure 2-2-5 Concentration dependence of CL emission. 57

Figure 3-1 Chemiluminescence spectrum of bilirubin 74

Figure 3-2 Solvent effect on CL emission 75

Figure 3-3 Quantitative CL measurements of bilirubin: 76

Figure 3-4 Spectrum of bovine serum: 77

Figure 4-1-1 CZE electropherograms of bilirubin, ... 93

Figure 4-1-2 MEKC separation of four bilirubin standards 94

Figure 4-1-3 MEKC separation of rabbit bile 95

Figure 4-1-4 MEKC electropherogram of human serum albumin. 96

Figure 4-1-5 Effect of SDS concentration on the migration time 97

Figure 4-1-6 MEKC separation of patient serum samples 98

Figure 4-2-1 Electropherogram of coproporphyrin III and I 109

Figure 4-2-2 Electropherogram of urinary porphyrins in TDCA-BSA 110

Figure 4-2-3 Electropherograms of BSA and TDCA 111

Figure 4-2-4 Spectrum of coproporphyrin III 112

Figure 4-2-5 Electropherograms of urinary porphyrins in SDS-BSA 113

Figure 4-2-6. Influence of field strength on current 114

Figure 4-2-7. Influence of concentration of TDCA on current 115

Figure 5-1 CZE electropherogram of $Al(NO_3)_3$ 126

Figure 5-2 Measured and predicted concentrations of Al-F 127

Figure 5-3 CZE electropherogram of Al species 128

Figure 5-4. Measured and predicted concentrations of Al-OX 129

Figure 6-1-1 Cross-sectional view of the post-column reactor 140

Figure 6-1-2 Effects of TCPO and H_2O_2 concentration on CL emission 141

Figure 6-1-3 Effect of flow-rate due to dynamic elution on relative peak width 142

Figure 6-1-4 Effect of flow-rate due to dynamic elution on the relative CL intensity . 143

Figure 6-1-5 Comparison of the efficiency between UV and CL detection methods . . 144

Figure 6-2-1 Cross-sectional view of the whole column detection system 150

Figure 6-2-2 Comparision of noise levels of different capillaries and inner diameters: 151

Figure 6-2-3 Isoelectropherogram measured using the capillary scanning device. . . . 152

Figure 7-1 Scattering profiles of TiO_2 particles carried by the argon streams 164

Figure 7-2 Spatial distributions of I_2 molecules under the influence of forced argon . 165

CHAPTER 1 INTRODUCTION

I. *Objectives*

The objectives of my research involve the understanding of the unique features of peroxyoxalate chemiluminescence, capillary electrophoresis and their combined application to solve significant proplems in bioanalytical chemistry. Analytical methodology and instrumentation development are an integral part of this thesis and summarized as follows:

- Investigation of the bioanalytical application of peroxyoxalate chemiluminescence for biological bilirubin determination. This work will study the solvent and base catalytic effects on the chemiluminescence emission of bilirubin. Comparison will be made with those of conventional fluorescence and visible absorption methods.

- Instrumentation development for chemiluminescence monitoring. Thin-layer chromatography (TLC) is an area of great interest for using peroxyoxalate chemiluminescence detection. This work includes design and fabrication of chemiluminescence photometric instrument.. Extensive studies will concentrate on the kinetic effects of the peroxyoxalate chemiluminescence on solid surfaces and the optimum conditions for TLC measurements by chemiluminescence detection.

- Improvement of the detectibility in capillary electrophoresis (CE). This work involves design and fabrication of a second generation whole column detection device for capillary isoelectric focusing. The feasibilty of coupling peroxyoxalate chemiluminescence to CE will also be investigated.

- Improvement of the application of CE technique in the areas which are poorly addressed or insufficient by other separation methods. This work involves the use of

micellar electrokinetic chromatography for the separation of a biologically important class of molecules called tetrapyrroles in clinical samples and inorganic speciation of aluminum with indirect UV detection.

-A short project in the area of graphite furnace atomization is also conducted in which a model system is used to investigate the gas-flow pattern.

II. *Peroxyoxalate Chemiluminescence*

Historical Aspect

Chemiluminescence, the emission of light caused by a chemical reaction, is a phenomenon of great analytical importance with many potential applications. The last 30 years have witnessed fast progress in the elucidation of the reactions and mechanisms underlying light production by non-biological chemiluminescence systems. Together with the advancement of highly sensitive instrumentation a variety of new analytical methods based on chemiluminescence reaction could be developed for sensitive and selective detection of biologically significant molecules for biomedical research and diagnosis. The first example of peroxyoxalate chemiluminescence was reported in 1963 by Chandross [1], who studied the reaction of oxalyl chloride with hydrogen peroxide in presence of fluorescent compound. In the late 1960's there were several reports on chemiluminescence from reactions of hydrogen peroxide with oxalyl chloride [2], oxalic anhydrides [3], oxalic esters [4,5], and oxalic amides [6] in presence of fluorescent organic compounds. These reactions were substantially more efficient than those previously reported classical non-biological chemiluminescence

including lophin (imidazole derivative), lucigenin (biacridinium salt) and luminol (phthalhydrazide derivative) and, since they appeared to constitute a general class of reactions involving peroxyoxalate intermediates, the term "*peroxyoxalate chemiluminescence*" has been used as a generic name.

In luminescence, an external light source is used to raise a molecule to an excited electronic state and light is emitted when the molecule returns to the ground state. In chemiluminescence, the process is identical but the energy necessary for excitation is provided by a chemical reaction. The energy required for visible light emission (400 nm - 800 nm) is in the range 200 - 400 KJ/mol.

An efficient chemical pathway leading to the excited state of the product molecule must be capable of emitting energy as light (direct chemiluminescence) or be able to transfer its energy to another molecule that has this potential(sensitized chemiluminescence). Peroxyoxalate chemiluminescence is sensitized chemiluminescence and decomposition of the 1,2-dioxetane (I) intermediate may provide the chemical energy required for excitation and sensitized chemiluminescence [7, 8], but the mechanism is still not known with certainty for oxalic esters [7-11]. Rauhut and co-workers [3, 4] have first proposed that C_2O_4 (II) is the decomposable intermediate providing the transferrable excitation energy for the fluorophore, producing its excited singlet state and leading to the typical fluorescence emission process. The chemiluminescence efficiencies are in the range 1-23% for several substituted oxalate esters [5]. Lechtken and Turro [12] studied several fluorophores and concluded that

it was possible to generate electronically excited states with an energy of up to 430 KJ/mol. They have also shown that chemiluminescence efficiency decreases steadily with increasing singlet excitation energy.

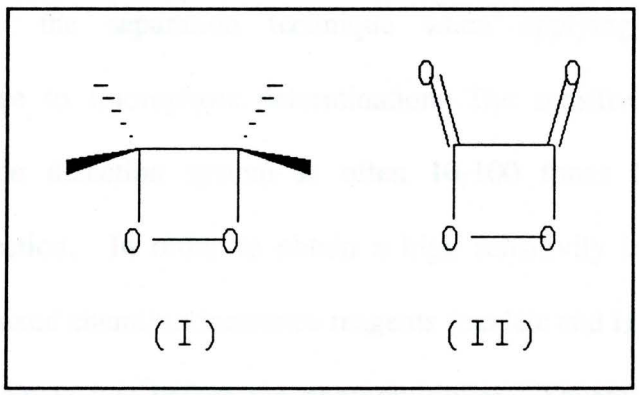

Peroxyoxalate chemiluminescence is a general chemiluminescence system because energy is produced by the reaction of an oxalate derivative with hydrogen peroxide which can excite (and thus serve as a "source") various fluorescent compounds (fluorophores) such as polynuclear aromatics, tetrapyrroles, etc. The reaction with hydrogen peroxide in presence of a fluorophore is very selective and a linear chemiluminescence signal response range of three to four orders of magnitude is usually obtained. The advantage of peroxyoxalate chemiluminescence over luminol chemiluminescence is that the analysis can be done at a wide range of pH. Methods for determination of fluorophores, on the other hand, can not be very selective due to

the peroxyoxalate chemiluminescence, which is capable of exciting any compound with fluorescence in the visible or infrared region of the spectrum, although there is a considerable variation in quantum yield [13].

The Measurement of Peroxyoxalate Chemiluminescence

For the past decade, peroxyoxalate chemiluminescence has been widely used in conjunction with the separation technique when applying the peroxyoxalate chemiluminescence to fluorophore determination. The sensitivity of peroxyoxalate chemiluminescence detection system is often 10-100 times higher than that of fluorescence detection. In order to obtain a high sensitivity in a chromatographic system, the pre-mixed chemiluminescence reagents (oxalate and H_2O_2) should be added into the column eluate just before the photomultiplier. Several oxalates have been investigated for their solubility in column LC solvents and stability in the presence of hydrogen peroxide and chemiluminescence intensity [14,15]. Unfortunately, none of these oxalates combine all the required characteristics and often compromises have to be made. Usually, TCPO (bis(2, 4, 6-trichlorophenyl)oxalate) is used in the concentration range 1 - 10 mM because of its stability in the presence of hydrogen peroxide. DNPO (bis(2, 4-dinitrophenyl)oxalate) is more soluble in common LC solvents, such as acetonitrile and methanol, but has a limited applicability due to its very fast reaction kinetics. The concentration of hydrogen peroxide is usually higher than the oxalate concentration, typically 50 - 500 mM solutions are mixed with oxalate

solution.

Finally, the advantage of chemiluminescence in comparison with fluorescence is that no light source is used, so excitation optics are superfluous. Emission light can be collected more efficiently because stray light is not present. A theoretical calculation by Seitz and Neary [16], based on the assumption that sensitivity of a chemiluminescence method depends only on the light detection, revealed that sub-attomol detection limits could be achieved. The peroxyoxalate chemiluminescence can occur very rapidly (i.e., < 1 s), although the duration is influenced by the reaction conditions. Such a wide range presents a challenge to the development of instrumentation for chemiluminescence monitoring.

Theoretical Aspect

In general, the efficiency (ϕ_{Cl}) of a chemiluminescence reaction can be described by the following equation

$$\phi_{CL} = \phi_R \phi_I \qquad (1\text{-}1)$$

where ϕ_R is the number of molecules in the excited-state per number of molecules reacted and ϕ_I is the number of molecules emitting light per number of excited-state molecules (luminescence efficiency). This means that the emitted light can be used for the determination of low concentrations of one of the reactants (including catalysts) if the chemiluminescence efficiency is high enough. Another interesting possibility is that

an excited molecule transfers its energy to a so-called acceptor molecule with adequate luminescence efficiency. In this case the total chemiluminescence efficiency can be descibed by

$$\phi_{CL} = \phi_R \phi_{ET} \phi_I \qquad (1\text{-}2)$$

where ϕ_{ET} is the number of excited acceptor molecules per number of molecules directly excited by the reaction (donor molecules). This indirect (sensitized) chemiluminescence extends considerably the number of types of molecule that can be determined by chemiluminescence; the chemiluminescence efficiency is dependent on the reaction conditions. This is true not only for ϕ_R but also for ϕ_{ET} and ϕ_I. For example, it is well known that ϕ_I strongly depends on the solvents in which the luminescence process takes place.

If chemiluminescence is measured in a dynamic system, i.e. for FIA (flow injection analysis) or HPLC detection, the kinetics of the reaction are also very important. For the peroxyoxalate chemiluminescence reaction, much more attention has been paid to the half-life of the reaction and its influence on the sensitivity of a detection system based on this reaction. It has been demonstrated that the half-life is dependent on the oxalate structure, the solvent composition, the pH, the water content, the catalyst concentration and the temperature [14,17-20].

The chemiluminescence decomposition of dioxetanes has been studied by several groups [21,22], and Schuster [23,24] introduced the chemically initiated electron

exchange luminescence (CIEEL) mechanism; the chemiluminescence step is the electron back-transfer from intermediate to fluorophore, resulting in its excited state. Peroxyoxalate chemiluminescence is also thought to follow a CIEEL-type mechanism, which means that there should be a good correlation between the oxidation potential of fluorophore and the chemiluminescence efficiency. This was confirmed by Catherall and his co-workers [25] who thoroughly investigated the kinetics and the mechanism of this chemiluminescence reaction. They found that the chemiluminescence intensity was strongly dependent on the electronegativity of the aryl group of the oxalate ester and that a common intermediate (the above mentioned 1, 2-dioxetanedione; C_2O_4) was highly unlikely. A key intermediate was proposed in which one of the aryl groups is still present. Alvarez and his co-workers [26] found a biphasic intensity-time profile for the reaction of hydrogen peroxide with TCPO in ethyl acetate catalysed by triethylamine. A multiple intermediate mechanism was proposed in which more light-producing pathways are possible. However, the real nature of the exciting intermediate is a matter of debate and much research is still needed for better understanding of the peroxyoxalate chemiluminescence process.

Problems in the Analytical Application of Peroxyoxalate Chemiluminescence

A major limitation of coupling peroxyoxalate chemiluminescence with a flow system such as HPLC is the need for an organic solvent, considering solubility, stability and efficiency. It is suggested that the peroxyoxalate chemiluminescence reaction

mechanism probably involves nucleophilic attack of H_2O_2 on the oxalate carbonyl. This means that water or any other nucleophilic solvents can also attack the chemiluminescence reagents and consume it in non-radiative pathways (more detailed discussion in chapter 4). Water in the solvent system increases the rate of the decomposition and decreases the time to reach chemiluminescence maximum intensity (in emission-time profile).

The reaction compatibility in thin-layer chromatography (TLC) is not such a problem since an aqueous phase can be easily removed after chromatography. Attempts were made to use peroxyoxalate chemiluminescence monitoring for TLC by successively spraying the plates with TCPO and because of their proven advantages of rapid and convenient sample processing [27]. Although chemiluminescence can be measured in this way, the experimental design and asynchronous light collection meant a considerable loss of potential sensitivity which would have greatly restricted the application of this technique had it been pursued.

III. *Capillary Electrophoresis*

Historical Aspect

In 1980's, capillary electrophoresis (CE) developed rapidly into a first-class analytical separation technique. Its advances in instrumentation and method development will not only enhance or complement existing mature separation techniques such as liquid chromatography and conventional gel electrophoresis, but also severely challenge these separation methods. In 1980, Mikkers [28] described both isotachophoresis and zone electrophoresis. He reported the separation of 16 organic acids by capillary zone electrophoresis in a PTFE capillary (200 μm i. d). The sample was applied to one end of the capillary and the components migrated to the far end under the influence of an applied potential, where the separated zones were detected by means of a conductivity and UV detector. The separations obtained by Mikkers were excellent, but the peak shapes were poor due to the limitations of the equipment, which had been designed for capillary isotachophoresis. The detector also had insufficient sensitivity, and thus required relative large sample loads. This leads to a potential drop across the separation zones, giving the asymmetrical peak shapes. Jorgenson and Lukacs [29] first introduced the glass capillary column to electrophoresis and demonstrated the high resolution capability of capillary zone electrophoresis in 1981. In contrast to Mikkers, Jorgenson and Lukacs explored electroosmotic flow in electrophoresis when the glass capillary column was used, and with the inherent

sensitivity of a fluorescence detection system, symmetrical peaks were obtained. A simple theory describing the separation was also presented.

Since the fused silica capillary became commercially available, one can deal with capillary tube and capillary electrophoresis with ease. Consequently, the CE research has made remarkable progress in the late 1980's.

Another milestone in the early days of CE was the introduction of surfactant-organized assemblies (micelles) as "pseudo-stationary phase" by Terabe and his co-workers [30] in 1984. This is a new type of separation method in which electrophoresis and chromatography are combined and this CE mode was termed as "micellar electrokinetic capillary chromatography" (MEKC). MEKC uses the CE technique but its separation principle is the same as that of chromatography. MEKC permits the separation of electrically neutral or nonionic compounds by electrophoretic technique on the basis of the differential migration time and differential solute distribution of the micellar phase [31, 32]. Uncharged species could be separated by partition between the hydrocarbonaceous interior of the micelle and aqueous background electrolyte. It is even effective for the separation of ionic compounds [33]. Selectivity and peak shapes are improved without losing CE's high resolution capability.

CE techniques have been applied to a wide variety of ionic types, and with the advent of MEKC, the area of application has been expanded to include uncharged compounds. Electrophoresis has been the separation technique used in biochemistry, but the visualization methods, which are time consuming, did not allow good

quantification of separated species. The development of on-line detection in capillaries was started by Martin and Everaerts [34] in 1958 with isotachophoresis and continuing in the late 1970s and early 1980s with the development of instrumentational zone electrophoresis. It is now becoming a serious rival to the established gas and liquid chromatographic methods of separation.

The Principles of Separation and CE instrumentation

Up until now, the instrumentation in CE has been relatively similar to that used in LC (Figure 1). Simplely stated, in CE the electric field has replaced the pump in driving the separation process.

In free solution electrophoresis, a narrow band of sample is surrounded by a buffer in the electric field, individual ions move at different speeds towards the cathode or anode, neutrals do not move at all, provided that there is no electroosmotic flow. With untreated capillaries, since the velocity of electroosmotic flow easily dominates electrophoretic mobilities, there results an interesting separation mode of CE: anions and cations as well as neutrals will finally pass the detecting point. Their movement in different directions is over-compensated by electroosmosis and neutrals move exactly with the speed of electroosmosis (Figure 2).

MEKC is an interesting separation principle which allows even neutrals to be separated. Free solution electrophoresis (FSE) in combination with electroosmosis (EEO) is usually performed. In addition to FSE, the buffer contains micelles formed

by the ionic detergent in a concentration above the CMC (critical micelle concentration). If micelles are formed by an anionic detergent, the outer negative charges are in neutral to alkaline medium. Therefore these micelles move towards the anode, but EEO more than compensates for this movement and finally they move towards the cathode with reduced speed in comparison to cations and neutrals (Figure 3). Every analyte interacting with these micelles is thus separated from those analytes which do not interact.

Theoretical Aspect

In zone electrophoresis, the velocity of migration of a charged species (ϑ_e) is proportional to the electrophoretic mobility (μ_e) and the potential field strength (E)

$$v_e = \mu_e E = \mu_e \frac{V}{L} \qquad (2\text{-}1)$$

where V is the applied voltage and L is the length of capillary between two reservoirs. The electrophoretic mobility depends on the charge density of solute and thus, the overall valence and size, as well as the viscosity (η) and dielectric constant (ϵ) of the medium. The mobility also varies strongly with temperature, approximately 2% per degree [35]. The time (t) necessary to migrate the distance (l) between the injection and detection points can be determined from the velocity in Eqn.(2-1) as

$$t = \frac{l}{V} = \frac{l}{\mu_e E} = \frac{lL}{\mu_e V} \qquad (2\text{-}2)$$

It should be emphasized that l and L are usually not the same value.

A fundamental process in CE and MEKC is electroosmosis. This bulk movement of solvent is caused by small zeta (ζ) potential at the silica-water interface, which induces the adsorption of a minute excess of anionic species in the static diffuse double-layer [36]

$$\zeta = \frac{4\pi\eta\mu_{eo}}{\epsilon} \qquad (2\text{-}3)$$

where μ_{eo} is the coefficient of electroosmotic flow. The electroosmotic flow creates an apparent mobility which can be directly determined from Eqn (2-1) by measuring the velocity of an uncharged species. The apparent mobility (μ^{α}) of the solute now becomes

$$\mu^{\alpha} = \mu_{eo} - \mu_{e} \qquad (2\text{-}4)$$

or

$$\nu^{\alpha} = \nu_{eo} - \nu_{e} \qquad (2\text{-}5)$$

where the apparent velocity (ϑ^{α}) can be calculated from the effective column length (l) and migration time (t_R)

$$\nu^{\alpha} = \frac{l}{t_R} \qquad (2\text{-}6)$$

and the electroosmotic velocity (ϑ_{eo}) is defined as follows [37]

$$v_{eo} = \left(\frac{\epsilon\zeta}{4\pi\eta}\right) E \qquad (2\text{-}7)$$

The separation efficiency in CE for the case in which the only source of band broadening is diffusion [38] is given by the following equation

$$N = \frac{\mu^{a} El}{2D} = \frac{\mu^{a} V}{2D}\left(\frac{l}{L}\right) = \left(\frac{\mu_{eo}-\mu_{e}}{2D}\right) V\left(\frac{l}{L}\right) \qquad (2\text{-}8)$$

where D is the diffusion coefficiency and can be calculated by the Stokes-Einstein equation [39]

$$D = \frac{RT}{6\pi\eta Na} \qquad (2\text{-}9)$$

where N is the Avogadro's constant and a is the radius of spherical particles.

The Joule heating is the major problem in electrophoresis. The temperature difference (ΔT) from the center to the wall (parabolic temperature profile) can be expressed as [40]

$$\Delta T \sim E^2 \lambda C r_c^2 \qquad (2\text{-}10)$$

where C is the concentration of the electrolyte, λ is the the molar conductivity of the solution and r_c is the tube diameter. This relationship shows clearly that the higher the field, the narrower the tube diameter must be. Typically the diameter of 25 - 100 μm capillaries are employed in order to minimize Joule heating.

With respect to resolution (R_s), we can write that [41]

$$R_s = \frac{1}{4}\left(\frac{\Delta\mu_e}{\mu_e'}\right) N^{\frac{1}{2}} \qquad (2\text{-}11)$$

where $\Delta\mu_e$ is the difference in electrophoretic mobility between two solutes and μ_e' is the mean mobility of those species. In MECC, migration time (t_R), the capacity factor κ' of the solute, can be calculated by following equation [33, 42]

$$t_R = \frac{1+k'}{1+\left(\frac{t_0}{t_{mc}}\right)k'} t_0 \qquad (2\text{-}12)$$

where the κ' is given by

$$k' = \frac{t_R - t_0}{t_0\left(1-\frac{t_R}{t_{mc}}\right)} \qquad (2\text{-}13)$$

or

$$k'' = \frac{v_e^*(s) - v_e(s)}{v_e(mc) - v_e^*(s)} \qquad (2\text{-}14)$$

where, the symbol of each migration time is given in Figure 3 and, $\vartheta_e(s)$, $\vartheta_e^*(s)$ are the electrophoretic velocity of the solute in aqueous buffer solution or micellar phase and $\vartheta_e(mc)$ is the electrophoretic velocity of the micelles. The Eqn. (2-13) and (2-14) are applicable for the neutrals and the ionized solute (more detailed discussion in chapter 4). Thus, the resolution in MECC is given by [31]

$$R_s = \frac{N^{\frac{1}{2}}}{4} \frac{\alpha-1}{\alpha} \frac{k_2'}{1+k_2'} \frac{1-\frac{t_0}{t_{mc}}}{1+\frac{t_0}{t_{mc}} k_1'} \qquad (2\text{-}15)$$

where α is the separation factor given by k_2'/k_1' ($k_2' > k_1'$). The difference between MECC and conventional HPLC is accounted for by the last term of the equation. As t_{mc} becomes infinite, the last term is equal to unity and the resultant equation becomes identical to that of conventional HPLC.

In conclusion, an advantage of CE (including MEKC) over conventional HPLC for separation is its high column efficiency. We can easily obtain ca. 250,000 plate numbers in a relative short time, similar efficiency can be also obtained with capillary LC, but it requires much longer analysis time. Fast and efficient separations in CE or MEKC are due to the following factors:

(i) flat velocity profiles of electroosmotic flow and electrophoretic migration

(ii) fast partition kinetics in micellar solubilization

(iii) minimal thermal effect by efficient heat dissipation of the small diameter of the fused silica capillary column

However, even though capillary electrophoresis provides attractive advantages over HPLC or slab gel electrophoresis in the area of separation technique, it should be noted that CE is not a tool to replace HPLC or slab gel electrophoresis. Each method has its own advantages and disadvantages, the proper perspective is to consider adding CE rather than replacing current methodology.

Problems in Capillary Electrophoresis

As mentioned above, although CE has attractive advantages over HPLC and slab gel electrophoresis in the area of separation technique, further improvements of CE are necessary. In general, UV detection, using a miniaturized HPLC cell, is the most widely applied procedure for detection in CE. Unfortunately, although mass detection with CE is quite low, sample concentrations for CE are generally in the range of 10^{-5} - 10^{-6} M, several orders of magnitude less than those used in HPLC. Therefore, much research is needed to improve the detectibility in CE.

The heat of any chromatographic or electrophoretic system is the column. In CE, column failure may arise from the gradual accumulation of particulate material such as "sticky" proteins or other macromolecules. The capillary used in CE thus needs more attention and improvement. Basically, a hydrophilic, non-ionizable, non-charged and pH 1 - 14 stable coating is required. At the present time commercially available polyacrylamide coating does not fulfill all the requirements. Another alternative is buffer modification which is a very important technique in the separation of compounds by CE. Additives that interact with an analyte component are very useful in altering the electrophoretic mobility of that component, but basic understanding of the separation chemistry has to be extended.

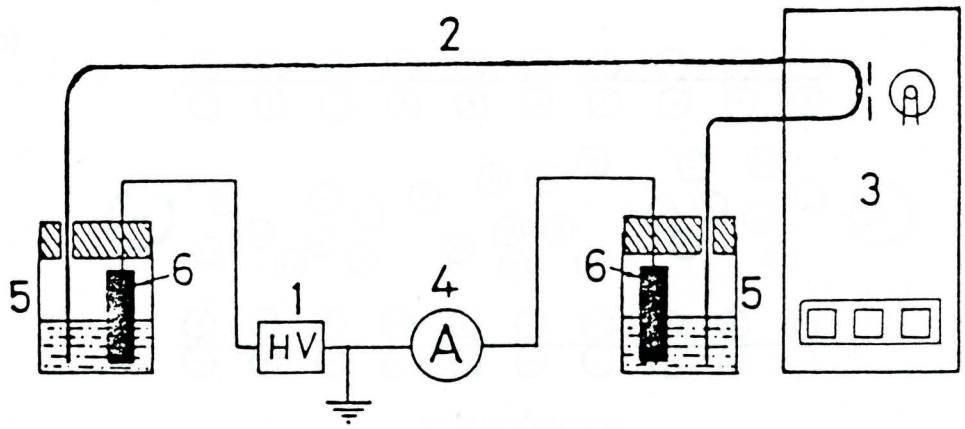

Figure 1. Schematic diagram of CE instrumentation: (1) high-voltage power supply, (2) capillary, (3) detector, (4) ammeter, (5) buffer reservoirs and (6) platinum electrodes.

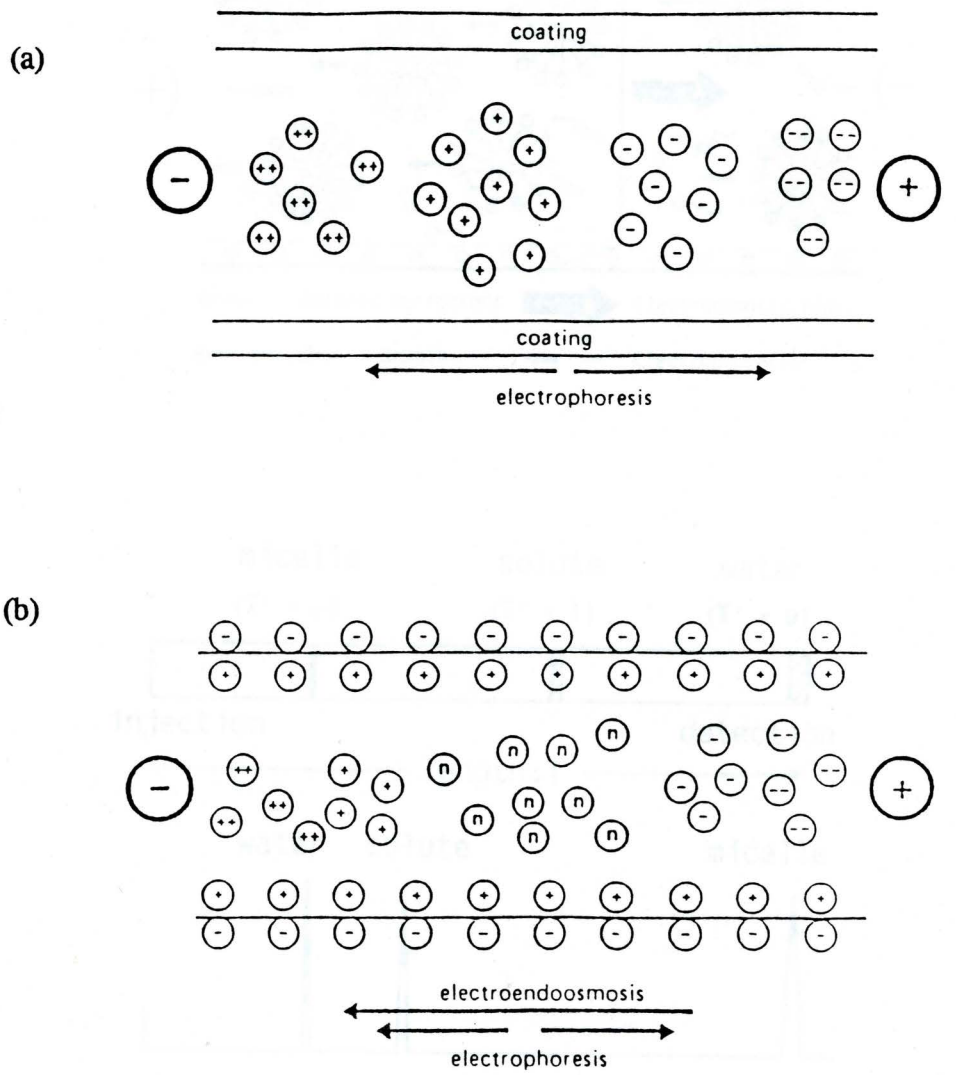

Figure 2 CE separation mechanism: (a) free zone electrophoresis on a coated capillary; (b) on an uncoated capillary in combination with electroosmosis.

(a)

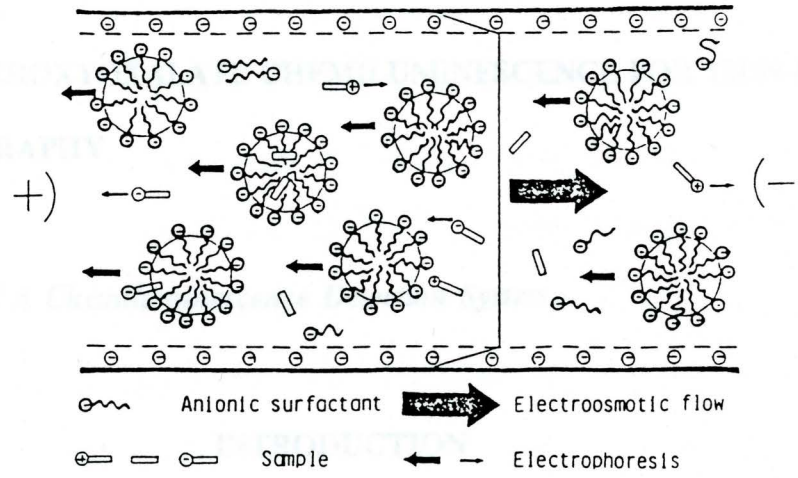

(b)

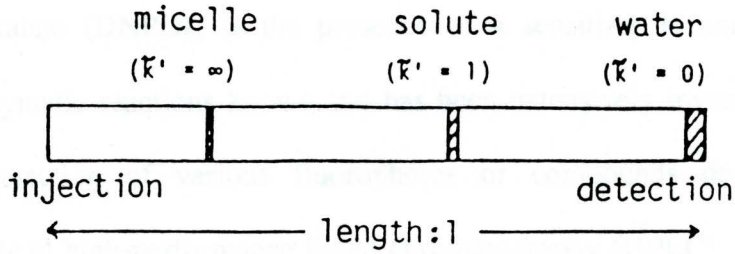

(c)

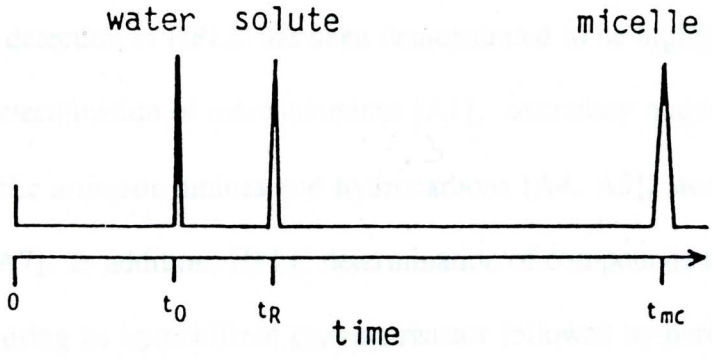

Figure 3 The separation principle of MEKC: (a) micellar EKC: (b) zone separation in a capillary and (c) a chromatogram of a hypothetical mixture of water, solute and micelle.

CHAPTER 2. PEROXYOXALATE CHEMILUMINESCENCE FOR THIN-LAYER CHROMATOGRAPHY

I. *The Design of A Chemiluminescence Detection System*

INTRODUCTION

The peroxyoxalate chemiluminescence (CL) reaction involving the oxidation of oxalate derivatives, typically bis(2,4,6-trichlorophenyl)oxalate (TCPO) or bis(2,4-dinitrophenyl)oxalate (DNPO), in the presence of a sensitizer is among the most efficient nonenzymatic reactions known and has been extensively investigated for the post column detection of various fluorophores or compounds derivatized with fluorescent labels in high-performance liquid chromatography (HPLC). For example, peroxyoxalate CL detection in HPLC has been demonstrated to be highly sensitive and selective for the determination of catecholamines [A1], secondary and tertiary amines [A2, A3], polycyclic aromatic amines and hydrocarbons [A4, A5], steroids [A6] and carboxylic acids [A7]. In addition, HPLC determination of compounds such as choline and acetylcholine using an immobilized enzyme reactor followed by peroxyoxalate CL detection has also been reported [A8]. Recently, a number of dansyl amino acids have been used as a model system for the optimization of CL detection in HPLC based on the oxidation of TCPO or DNPO and the average detection limit and relative standard

deviation on reproducibility were found to be about 200 fmol (0.07 ng) and 4%, respectively [A9]. In contrast, very little work has been reported on the use of CL detection methods for the determination of analytes after separation by thin-layer chromatography (TLC). The reason for this is perhaps in large part related to experimental difficulties encountered in the synchronization of timing between introduction of the CL reagents onto the TLC plates and detection of the rapidly decaying CL emission generated from the analytes adsorbed on the plate surface. This particular timing problem, however, can be overcome with relative ease in HPLC since all experimental parameters can be controlled with good accuracy [A9].

The use of CL detection in TLC was first demonstrated by Curtis and Seitz involving the measurement of various dansyl amino acids by successively spraying the plate with TCPO and H_2O_2 solutions and subsequently collecting the CL emission with an optical fiber-based detection system [A10]. Although in general this CL detection method was shown to be comparable to conventional fluorescence detection, it was found that the CL intensity changed rapidly with time under optimized conditions, leading to loss in sensitivity during a complete scan of the TLC plate. To minimize this problem, CL detection was coupled with a vidicon rapid scanning spectrometer since this detection system is capable of simultaneously measuring CL emission from all areas of the plate, thus reducing errors associated with the measurements of the rapidly changing CL signal [11]. However, this modification introduced complexity and cost to the CL instrumentation, making it difficult, for example, in the application of CL

detection methods for analyses in routine clinical laboratories.

In this study a novel experimental set-up involving the use of a pneumatic nebulizer to provide relatively uniform and reproducible spraying of the pre-mixed peroxyoxalate CL reagents (TCPO and H_2O_2) onto the TLC plates and its coupling with an optical fiber to synchronize the timing between chemical excitation and measurement of CL emission is reported. Experimental parameters such as nebulization conditions, positioning and size of the optical fiber, microenvironment of the sample spot, scan speed and particle size of the TLC plate were optimized to achieve sensitive and reproducible detection of three dansyl amino acids.

EXPERIMENTAL SECTION

Apparatus. Figure 2-1-1 shows a diagram of the experimental set-up. A commercially available TLC scanner (CAMAG) was modified to serve as a precision two-dimensional stage for scanning the TLC plate in the x-y directions. Situated at a fixed position directly above the translational stage was a pneumatic nebulizer mounted in series with an optical fiber along the x-direction using an aluminum plate (dimension: 1.5 x 6 cm^2), which was designed to allow for adjustment of distance between the nebulizer and optical fiber and of their respective heights from the TLC plate. Pneumatic nebulization provides a means by which a steady flow of reactive aerosol is sprayed onto the sample spots that are traveling directly beneath the nebulizer along the x-direction; the optical fiber allows for CL emission generated from the sample spots to be rapidly and reproducibly transported to the detection system in synchronization with

chemical excitation. A concentric pneumatic nebulizer obtained from an atomic absorption spectrophotometer (Model 82-810, Jarrell Ash) was used for the generation of aerosol. As shown in Figure 1, appropriate concentrations of TCPO and H_2O_2 solutions were placed in separate containers and the solutions were forced to move towards the direction of the nebulizer under the influence of pressurized argon gas. A gas flow controller obtained from a gas chromatograph (Model 376000, Varian) and a fine metering valve (Part No. 180502, PGC Scientifics) were placed between the gas flow controller and the CL reagent containers to allow for fine adjustment of the liquid flow rates of TCPO and H_2O_2. These two CL reagents were mixed within a stainless steel tee (1/16" Swagelok) and this premixed solution was then delivered to the nebulizer via a 50-cm long x 75-μm inner diameter fused silica capillary (Cat. No. Tsy-075375, Polymicro Tech.). After the premixed solution entered the nebulizer, an argon gas stream (nebulizing gas) with flow rate controlled by another gas-flow controller interacted with the liquid stream of premixed CL solutions, resulting in the formation of aerosol which was sprayed onto the TLC plate. It should be noted that one or more reactive intermediates may be formed due to reaction of TCPO with H_2O_2 [A12].

Two types of optical fibers were evaluated for the transport of CL emission to the detection system: an optical fiber bundle, 61-cm long x 1.6-mm diameter with a numerical aperture of 0.55 and an acceptance angle of 68° (Part No. 77520, Oriel), and a single optical fiber, 50-cm long x 0.4-mm diameter with a numerical aperture of 0.22 and an acceptance angle of 47.2° (Superguide G, Fiberguide). One end of the optical

fiber was placed adjacent to the nebulizer as shown in Figure 1 and the other end was interfaced to the detection system. The CL emission was isolated by a 10-nm bandpass filter centered at 520 nm (Corion) and was then detected by a photomultiplier tube (Model 9558B, EMI) operated at a voltage between 700 to 800 V. The photocurrent was fed to a picoammeter (Model 7080, Oriel) and the signal was recorded on an integrator (Chromjet, Spectra-Physics).

Optimization of Detection Sensitivity. A TLC plate was sprayed successively with a diluted dye solution of rhodamine B to completely wet the plate surface. The dye molecules adsorbed on the silica gel surface were then excited chemically using the aerosol aspirated from the nebulizer to determine the optimum flow rates for the CL reagent solutions and the nebulizing argon gas stream by adjusting the corresponding gas flow controllers and/or fine metering valve and monitoring the characteristics of the CL emission. It was found that at a pressure reading of 20 psi (flow rate: 6 L/min) and 3 psi (flow rate: 0.03 ml/min) for the nebulizing argon gas and CL reagent solution flows, respectively, the aerosol aspirated from the nebulizer appeared to produce a relatively strong and steady electronic signal. This CL emission can also be observed visually from the plate surface as very well-defined luminescence zones. Using this set of optimized flow conditions, the optimum distance between the nebulizer and optical fiber and their respective heights from the plate surface which give the highest CL intensity while maintaining good chromatographic resolution were also briefly investigated. It was found that for the CL detection of three dansyl amino acids

separated on HPTLC plates, *vide infra*, the optimum distances between these experimental components were as follows: nebulizer and optical fiber = 8 mm; optical fiber and plate surface = 4 mm; tip of nebulizer and plate surface = 5 mm (corresponding to 15 mm from the aerosol exit orifice).

Procedures. Development was carried out in either an acid solvent system of chloroform-ethyl acetate-methanol-acetic acid (9:15:4.5:0.2) or a basic solvent system of methyl acetate-2 propanol-aqueous ammonia (9:7:2). The plates were air dried for a few minutes at room temperature after development. If added, CL enhancers, i.e., various organic solvents, were pre-sprayed onto the sample spots using a compressed gas sprayer (Cat. No. 14654, Alltech) prior to CL measurements. A hand-held uv lamp was used to generate visible fluorescence from the sample spots to aid in the alignment of the sample spots separated on the plate along the x-direction with respect to the position of the nebulizer and optical fiber. Afterward, the plate was sprayed with the aerosol while scanned along the x-direction at an optimum scan speed of 2 mm/s.

Chemicals and Materials. TCPO was prepared by the procedure described by Mohan and Turro [A13]. Dansyl-glycine, dansyl-L-arginine and dansyl-L-leucine were purchased from Sigma. Hydrogen peroxide (30%) and all other chemicals were obtained from Aldrich. The dansyl amino acids were dissolved in 20% 0.4 M Li_2CO_3-HCL buffer of acetonitrile and kept at below 0° C. Stock solutions of TCPO and H_2O_2 with concentrations of 3 - 5 mmol/L in ethylacetate and 0.88 - 1.2 M/L in acetonitrile, respectively, were used. Separations were performed on either conventional silica gel

TLC plates (Whatman LK6) or 5-μm silica gel HPTLC plates (Whatman LHP-K) which were purchased from Alltech.

RESULTS AND DISCUSSION

Figure 2-1-2(a) shows a CL emission intensity-time profile of dansyl-glycine spotted on a HPTLC plate. It can be seen that the CL intensity reached its maximum within ~ 5 s after the sample spot has been sprayed with the aerosol, followed by a rapid decay of the CL signal. This observation is consistent with those obtained by Curtis and Seitz who investigated the effects of TCPO and H_2O_2 concentrations on the CL intensity of dansyl-glycine adsorbed on silica gel TLC surfaces and found that at high peroxide concentrations, i.e., 0.8 to 1.2 M, the CL intensity was the highest but lifetime was very short, and the converse was true for low peroxide concentrations [A10]. However, variation in TCPO concentration in the range above 10^{-3} M appeared to have little effect on the CL intensity-time behavior.

Using the present experimental set-up, rapid and reproducible measurements of the CL emission at the peak maximum region as shown in Figure 2-1-2(a) is possible, thus allowing for significant enhancement in sensitivity and precision for the quantitation of analytes using the peroxyoxalate CL reaction in TLC. At a distance of 8 mm between the nebulizer and optical fiber, a scan speed of 2 mm/s was found to produce the best sensitivity while maintaining good resolution for the detection of three dansyl amino acids separated on a HPTLC plate using an acid solvent system as shown in Figure 2-1-3(a). At this scan speed, each sample spot travels past the light collection

zone of the optical fiber at ~ 4 s after it has been sprayed with the aerosol, which happens to fall within the time period at which the peak maximum of CL emission occurs as shown in Figure 2-1-2(a). The average limit of detection (LOD) based on a signal-to-noise ratio (S/N) of 3 for the three dansyl amino acids was found to be ~ 0.45 ng, which is about an order of magnitude lower than that reported by Curtis and Seitz (LOD for dansyl-glycine ~ 7 ng) using their optical fiber based detection system [A10]. Relative standard deviation (n = 6) for dansyl-glycine (3.1 ng per spot) was found to be ~ 6%, which could arise from inconsistency in the manual spotting of small volume (0.10 to 0.50 μL) of samples onto the HPTLC plates using a 1-μL syringe and/or variations related to chemical excitation, e.g., CL efficiency. Calibration plots of dansyl-glycine indicated linear response from LODs up to 0.1 μg (r = 0.995). Figure 2-1-3(b) shows a HPTLC chromatogram of the three dansyl amino acids obtained under the same experimental conditions as in Figure 2-1-3(a) except using a basic solvent system for development. It can be seen that significant peak overlap occurs between dansyl-glycine and dansyl-L-arginine. To minimize the extent of this overlap, higher resolution was obtained by employing an optical fiber with significantly smaller core diameter as the light guide while keeping other experimental conditions the same. Figures 2-1-4(a) and (b) compare the resolution and sensitivity of the two dansyl amino acids separated on the same HPTLC plate using an optical fiber bundle and a single optical fiber, respectively. It is clear that significant enhancement in resolution was achieved by employing the optical fiber with smaller core diameter but this gain in

resolution was accompanied by a loss in sensitivity.

It has been demonstrated that luminescence intensity of certain amino acid derivatives generated by conventional TLC fluorescence detection methods can be enhanced by ~ 100 fold after the plate has been sprayed with a viscous and non-volatile organic solvent system containing liquid paraffin or Triton X-100 [A14]. Thus, it seems that further gain in sensitivity for the CL detection of dansyl amino acids separated on TLC plates may be achieved by exploiting the capabilities of the present experimental set-up to detect CL signals enhanced by pre-spraying the sample spots with organic solvent systems having appropriate physical properties. Interestingly, Figures 2-1-2(a) and (b) indicate that the CL intensity of dansyl-glycine was slightly higher when the sample spot has been pre-sprayed with ethyl acetate; however, when compared to Figure 2-1-2(c) which shows the effect of pre-spraying dioxane onto the sample spot, enhancement in CL intensity is even higher. This observation was surprising since it is well known that CL intensity is greatest in ester and ether solvents. A similar observation has also been reported by Curtis and Seitz, who suggested that when compared to ethyl acetate, the stronger interaction of dioxane with the TLC plate may play an important role in providing greater CL intensity for the dansyl amino acids [A10]. Perhaps more interestingly, Figures 2-1-2(d) and (e) show that a CL intensity-time profile of dansyl-glycine changed significantly, i.e., increased in peak intensity and lifetime, after the sample spots were pre-sprayed with two different viscous and non-volatile organic solvent systems.

To evaluate the gain in detectability of dansyl-glycine after treatment with the viscous and non-volatile organic solvent systems, Figures 2-1-5(a-c) show the relative CL intensity of three equal amounts of dansyl-glycine samples eluted simultaneously on the same HPTLC plate and detected with the present experimental system at identical R_f values. It can be seen that the Triton X-100:chloroform and liquid paraffin:chloroform solvent systems enhanced the CL intensity ~ 5- and 7-fold, respectively, which yield a corresponding average LODs (S/N = 3) of about 0.10 ng and 0.08 ng, respectively. The average relative standard deviation (n=6) on reproducibility using both solvent systems was ~ 4% (3.1 ng per spot). Lastly, the detectability of dansyl amino acids separated on HPTLC plates as compared to conventional TLC plates were also briefly investigated. It was found that without the influence of any organic enhancers, the average LOD (S/N = 3) obtained for the CL detection of the three dansyl amino acids separated on TLC plates was ~ 0.80 ng, which is only slightly higher than that found on HPTLC plates (~ 0.45 ng).

CONCLUSION

More detailed studies are necessary for the further optimization of various experimental parameters to achieve better analytical figures of merit. To this end, a better understanding of the fundamental processes involved in the chemical excitation of analytes adsorbed on the plate surface and of the physico-chemical basis for the increase in CL observed when using plates treated with a viscous and non-volatile

solvent is essential; of particular interest would be a comparison study of CL intensity-time behavior of analyte and background signals generated from the plate surface since the kinetics of these signals have been shown to be different when performing CL detection in HPLC, which leads to significant improvement of detection limits of the analytes [A15].

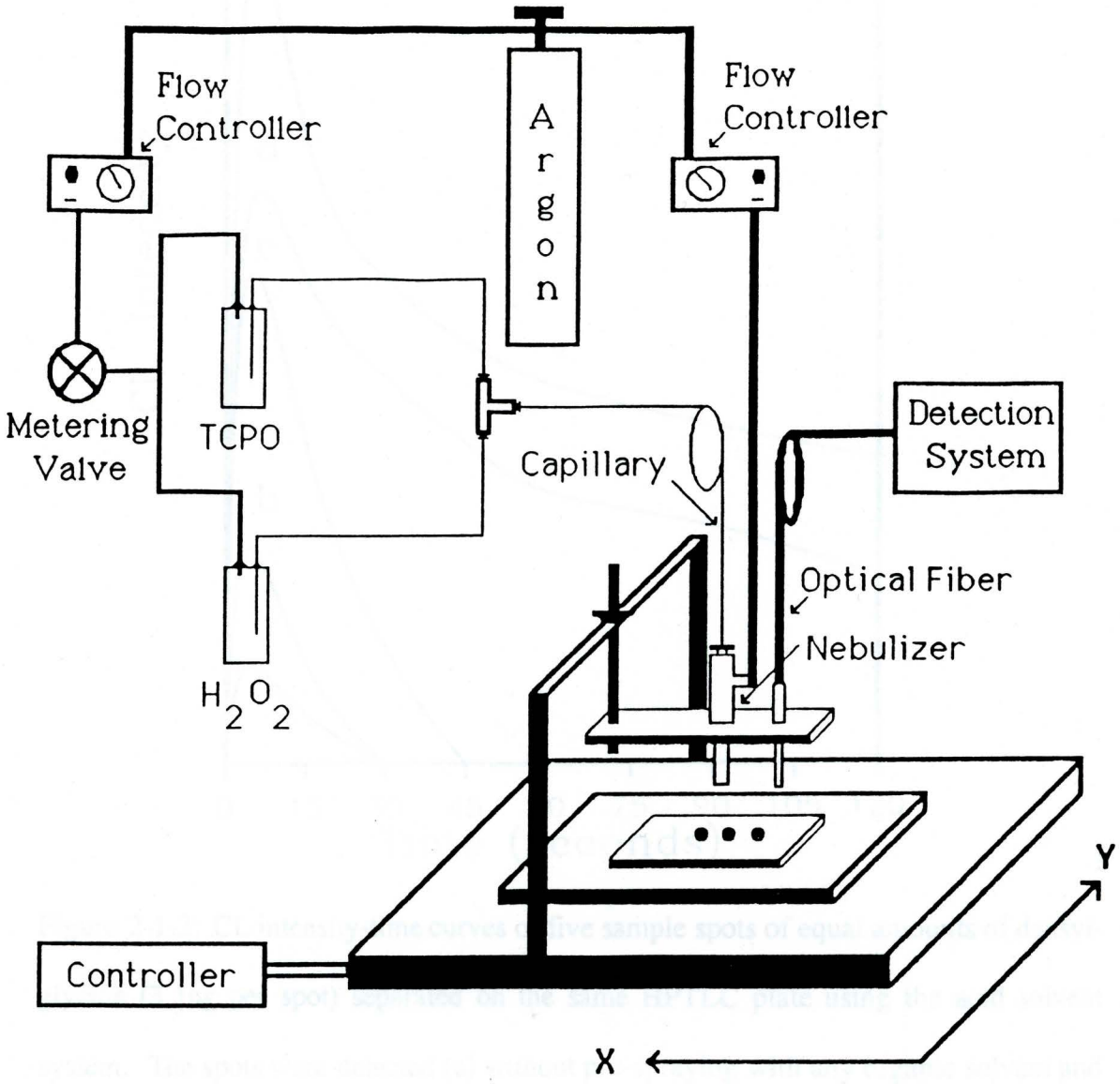

Figure 2-1-1: Experimental set-up used for the CL detection of dansyl amino acids separated on HPTLC or TLC plates.

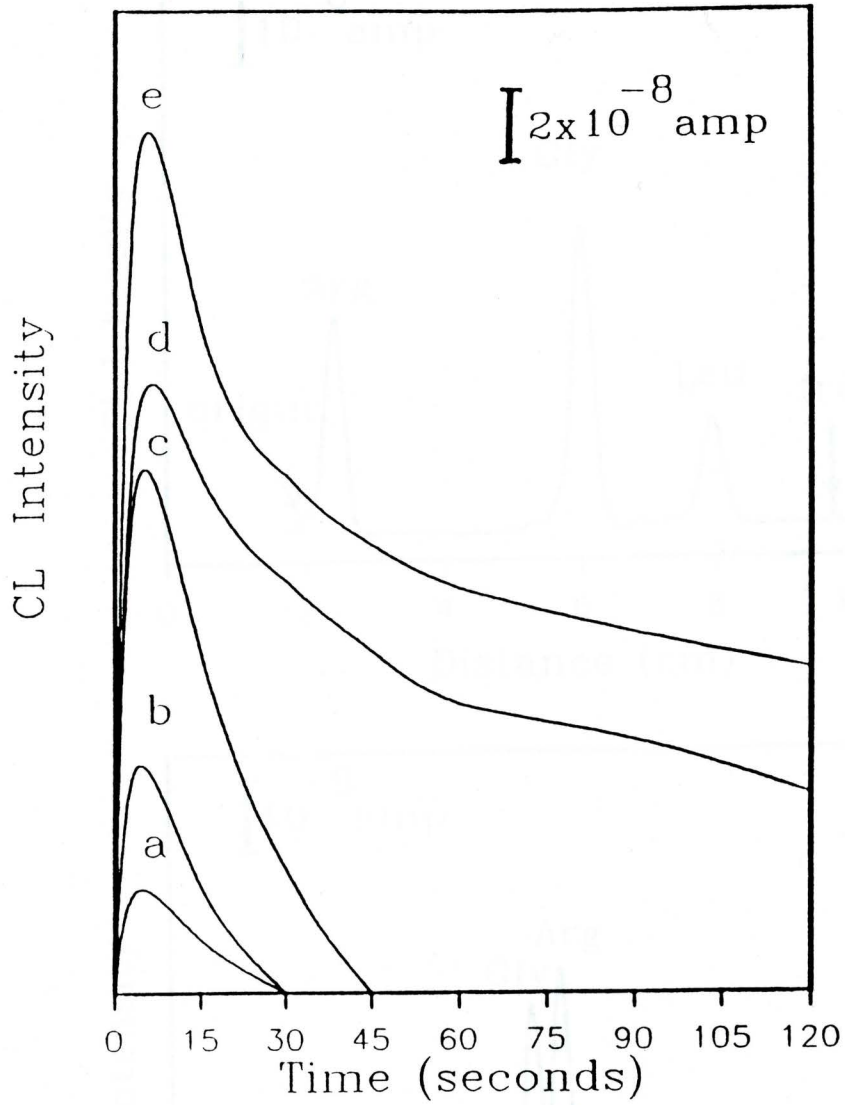

Figure 2-1-2: CL intensity-time curves of five sample spots of equal amounts of dansyl-glycine (3.1ng per spot) separated on the same HPTLC plate using the acid solvent system. The spots were detected (a) without pre-spraying with any organic solvent and after pre-spraying with (b) ethylacetate, (c) dioxane, (d) Triton X-100/chloroform mixture (1:4 v/v), and (e) liquid paraffin/chloroform mixture (3:2 v/v). TCPO and H_2O_2 concentrations were 3 mM and 0.88 M, respectively.

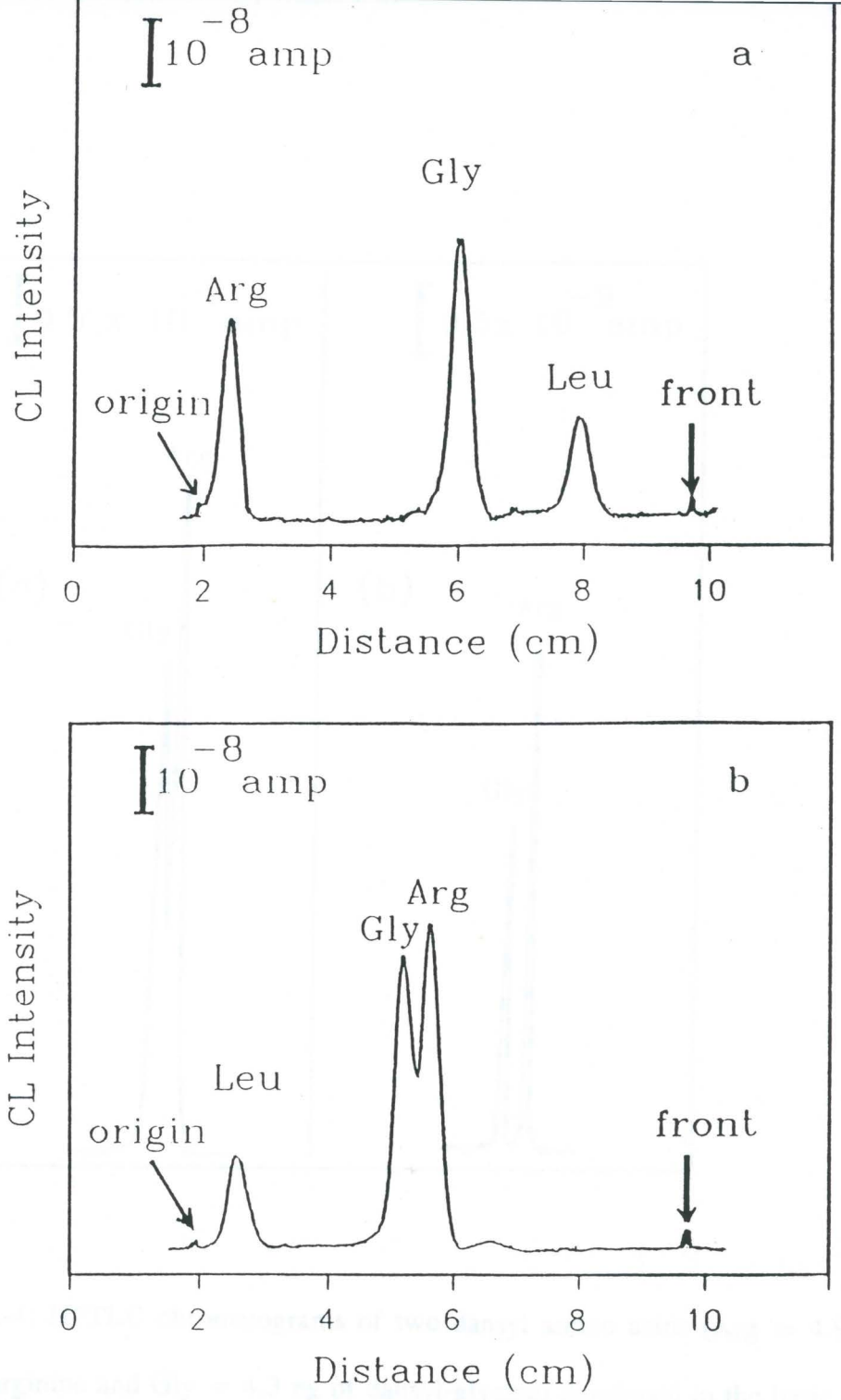

Figure 2-1-3: HPTLC chromatograms of three dansyl amino acids (Arg = 4.9 ng of dansyl-L- arginine, Gly = 4.3 ng of dansyl-glycine and Leu = 3.8 ng of dansyl-L-leucine) developed in (a) the acid solvent system and (b) the basic solvent system. TCPO and H_2O_2 concentrations were 3 mM and 0.88 M, respectively.

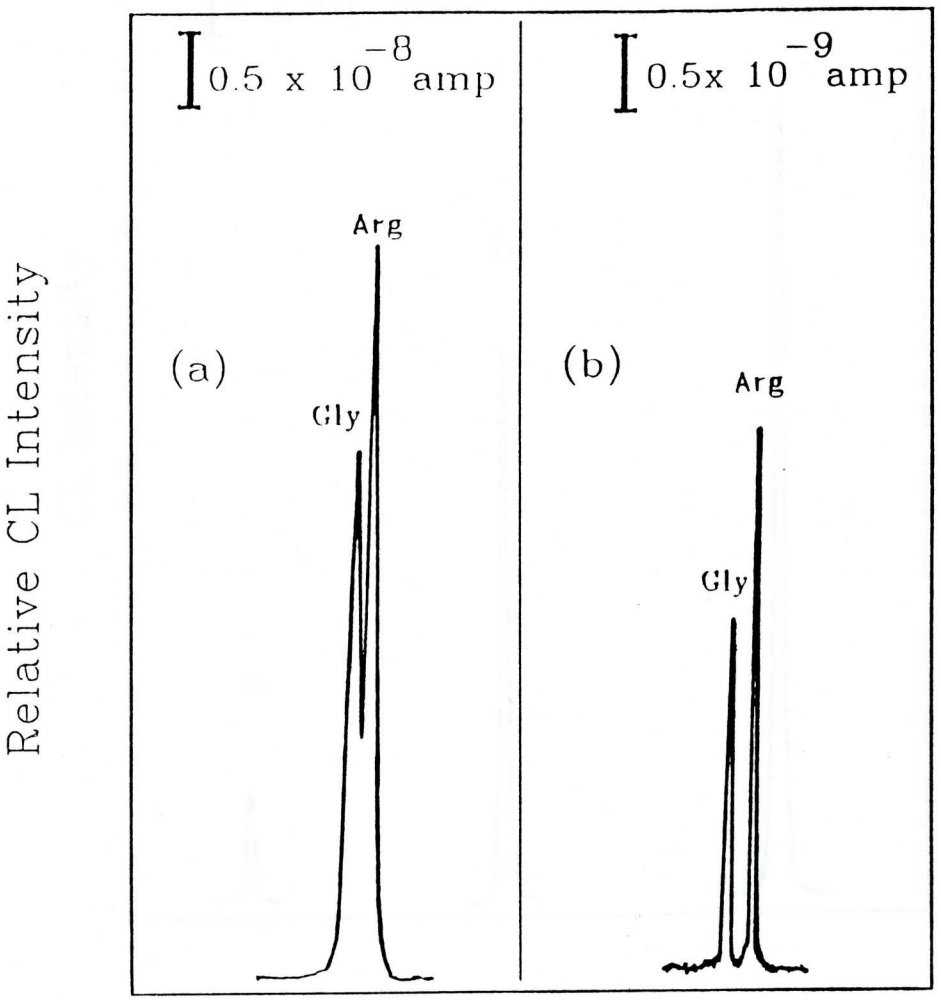

Figure 2-1-4: HPTLC chromatograms of two dansyl amino acids (Arg = 4.9 ng of dansyl-L-arginine and Gly = 4.3 ng of dansyl-glycine) developed in the basic solvent system and detected using (a) an optical fiber bundle and (b) a single optical fiber. TCPO and H_2O_2 concentrations were 3 mM and 0.88 M, respectively.

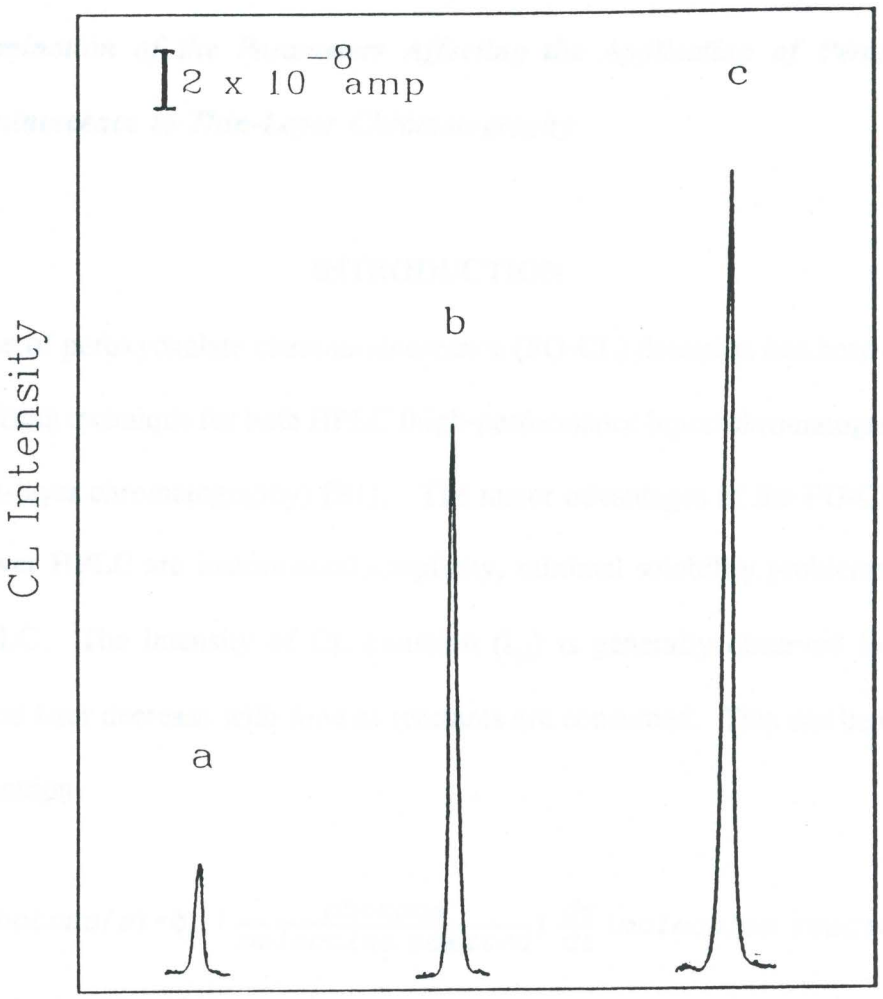

Figure 2-1-5: Relative CL intensity of three sample spots of equal amounts of dansyl-glycine (3.1 ng per spot) separated on the same HPTLC plate using the acid solvent system. The spots were detected (a) without pre-spraying with any organic solvent and after pre-spraying with (b) Triton X-100/chloroform mixture (1:4 v/v), and (c) liquid paraffin/chloroform (3:2 v/v). TCPO and H_2O_2 concentrations were 5 mM and 1.2 M, respectively.

II. *Determination of the Parameters Affecting the Application of Peroxyoxalate Chemiluminescence to Thin-Layer Chromatography*

INTRODUCTION

The use of peroxyoxalate chemiluminescence (PO-CL) detection has been shown to be a promising technique for both HPLC (high-performance liquid chromatography) and TLC (thin-layer chromatography) [B1]. The major advantages of the PO-CL method in TLC over HPLC are instrumental simplicity, minimal solubility problems and low cost of TLC. The intensity of CL emission (I_{cl}) is generally observed to increase initially and later decrease with time as reactants are consumed. This can be described by the equation:

$$I_{cl}(photons/s) = \Phi_{cl}\left(\frac{photons}{molecules\ reacted}\right)\frac{dc}{dt}(molecules\ reacted/s)$$

where Φ_{cl} is the CL efficiency of production of excited states (probability of excited-state molecules) times the emission efficiency (number photons emitted per number of excited-state molecules), dc/dt is the rate of the chemical reaction; the number of molecules reaction per unit of time. Because the emission intensity is determined by the rate of the chemical reaction, measurement of emission intensity can be used as the basis of quantitation for any species whose concentration determines the rate of the chemical reaction.

In recent years considerable efforts have been made in the areas of kinetic study and optimization of the PO-CL reaction for the analytical applications [B2-B5]. Most of these studies dealt with solution phase-CL. The PO-CL has not been an acceptable technique for TLC until recently [B1]. In this work we have adapted some of those procedures which have been sucessfully used in solution phase-CL studies [B4, B5] for the CL reaction on solid surfaces. Although the information on the mechanism of CL reaction is absent, the factors which may affect the chemiluminescence efficiency in a gas stream or on a solid surface can be used to optimize the conditions for the PO-Cl detection. In this paper, the effects on the CL background emission and the influence of CL production on various substrate surfaces, catalyst and enhancers are measured with a stopped-scan, kinetic system. From data on both CL intensity and lifetime, some important insights into surface effects and enhancer selection for CL-TLC may be gained. Other potentially important experimental variables such as flow rate and the influence of fluorophors on CL efficiency are also investigated.

EXPERIMENTAL

Apparatus

The CL spectrodensitometer has been previously described in detail (1). A change was made by using a Sage syringe pump (model 341, Orion) instead of the gas pressure system to deliver the CL reagents. The syringe pump provides a simple and precise control of the flow rates of CL reagents. An aluminum box (8 x 5 x 6 cm) was

installed to isolate air from the measurement region of the densitometer (Figure 2-2-1).

Materials and Reagents

Pure standards of meso-, copro-, penta-, hexa-, hepta- and uro-porphyrin were purchased from Porphyrin Products (Logan, UT). High purity bis (2, 4, 6 - trichlorophenyl)oxalate (TCPO) was purchased from Fluka (Ronkonkoma, NY) and recrystallized in benzene. Hydrogen peroxide (30%) was purchased from Fisher. Dansyl-glycine, dansyl-L-arginine, dansyl-L-leucine and perylene were purchased from Sigma. All other reagents were of analytical grade from Fisher and Aldrich. The dansyl amino acids were dissolved in a 20% 0.4 M Li_2CO_3-HCL buffer of acetonitrile. The porphyrin standards were dissolved in a small amount of 1 M NaOH and were then diluted with a 20 % 0.05 M phosphate buffer (pH=7.0) in acetonitrile. Both standard solutions were kept at below 0°C. Stock solutions of TCPO and H_2O_2 with concentrations of 0.05 - 5 mmol/L in ethyl acetate and 0.01 - 0.8 M/L in acetonitrile were used, respectively. The Cl measurements were performed on 250 μm silica gel HPTLC plates (Whatman, LHP-K), 250 μm reversed phase C-18 HPLC plates (Alltech, Unibond), 250 μm alumina TLC plates (EM, 60 G, neutral) and 200 μm chromatography papers (Whatman) which were purchased from Alltech and Fisher.

Methods

Kinetic study of Chemiluminescence Emission: 10 μl TCPO was applied on the thin-layers, all data were measured on silica gel HPTLC plates except where otherwise

specified. The H_2O_2 was sprayed onto the plates through a nebulizer of the CL densitometer for 4 seconds (~ 10 μl at a flow rate of 150 μl/min). TCPO was stable on the thin-layer in the dark for about 10 minutes, approximately a loss of 10% was found after 20 minutes. If needed, a purge gas of argon was set at a flow rate of 100 ml/min. Imidazole (50 mM) was prepared in 30% 0.05 mM phosphate buffer in acetonitrile. Appropriate amounts of imidazole were added to the H_2O_2 solution and the water component was adjusted *ca.* 5% of the H_2O_2 solution (v/v) with the phosphate buffer. Fumed silica (0.014 μm) was suspended in acetonitrile (5%, w/v), 1 ml of the suspension was mixed with an appropriate amount of perylene or directly applied to the chromatography paper.

Quantitative chemiluminescence measurements: CL emission from sample spots was isolated using an optical fiber bundle (1.6 x 610 mm, Oriel) and a 10 nm bandpass filter (Corion) centered at 520 nm for the dansyl amino acids and 620 nm for the porphyrins. The output signal was recorded on an integrator (Chromajet, Spectra-Physics).

Esterification of porphyrins: Briefly, the porphyrin standards were converted into their methyl esters by direct treatment with 5% sulphuric acid in methanol and extracted with chloroform. The extracts were washed with 10% $NaHCO_3$ and distilled water before evaporating to dryness under reduced pressure [B6].

Standard Solution: Individual standards were diluted with 20% 0.05 M phosphate buffer of acetonitrile. Typically 0.5 μl of standard solutions were applied to the origin

on the plates. For comparison purposes, the same sample volumes with different concentrations of each standard were applied.

Development of the chromatograms: Development was carried out in an ethanol-dioxane (1:1, v/v) solvent system for the porphyrins, and a chloroform-ethyl acetate-methanol (9:15:4.5) system for the amino acids. The plates were dried in an argon stream for a few minutes at room temperature. If added, CL enhancers were pre-sprayed onto the sample spots using a compressed gas sprayer (Cat. No. 14654, Alltech) prior to CL measurements. A hand-held UV lamp was used to generate visible fluorescence from the sample spots to aid in the alignment of the sample spots separated on the plate along the x-direction with respect to the position of the nebulizer and optical fiber. Afterward, the plate was sprayed with the aerosol while scanned along the x-direction at an optimum scan speed of 2 mm/s. Typically 3 mM TCPO and 0.1 M H_2O_2 were used with a 6 L/min of nebulization gas flow rate.

RESULTS AND DISCUSSION

On occasion, it will be observed that the PO-CL response for a substance in TLC will be less than expected from measurements made in solution. Two phenomena, CL quenching and catalytic degration of the CL reagents or the fluorphors, may be responsible for this. The first is largely physical and generally reversible. The most common CL quenching agent is oxygen. Fortunately it is generally small and can be masked by displacing air with an inert gas in the measurement region of the densitomenter. A similar method for fluorescence detection is described in the

literature [B7]. The extent of CL quenching often depends on the sorbent medium and it is frequently more severe for silica gel than for bonded-phase sorbents due to the fact that the relative non-polar PO-CL solvents have a poor permeation to the relatively polar silica layer [B8]. Figure 2-2-2 shows the intensity-time profiles of the PO-CL on varying surface materials. The mechanism of quenching is not known with certainty, but it is generally assumed that adsorption onto silica gel provides additional non-radiative pathways for dissipation of the excition energy. Figure 2-2-3 shows a change in the CL intensity-time profile when perylene was mixed with fumed silica as compared to where the fluorophor was on top of the silica-layer. The CL signal was significantly diminished when the fluorophore was covered with the silica- layer due to the energy loss to the silica sorbents. Similarly, the maximum CL emission was significantly different before and after developing sample spots (Figure 2-2-4) on silica gel plates. Thus the reactive aerosol may only reach a very finite depth in the plates, the most efficient CL reaction should happen on the surface. Inorganic and organic catalytic oxidatants are the most common chemical substrates which can cause an unstable CL response or less efficient CL processes since trace impurities can not be avoided during the preparation of TLC plates. Catalytic substances may decrease the time to reach maximum intensity (in the emission *vs.* time profile) and can also attack the CL reagent and consume it in non-CL side reactions. Tables 2-1 and 2-2 show the concentration dependance of the CL reagents on lifetime of the CL background emission. Although it is difficult to compare the kinetic effects of the CL reaction on

a solid surface with the CL reaction in solution, the rate of the chemical reaction was much faster in the presence of imidazole (Table 2-3). The life time of the PO-CL reaction may be shorter than it is in solution due to the quick evaporation of organic solvents from the TLC plates [B8]. The silica sorbents may also degrade the intermediate of the PO-CL reaction. This may be the case that in the presence of oxygen, the lifetime of a volatile intermediate [B9] which formed in the gas stream may be shorter. Therefore the maximum CL enhancement of imidazole by the catalytic effect in solution phase does not apply to a semi-solution phase reaction on solid surface due to a very short intermediate life time. Table 2-4 shows that the maximum CL intensity was increased in an argon atmosphere, the half-life time was decreased since the argon may speed up the evaporation of the solvents. The half-life time remained almost the same when spraying the plates with a non-volatile solvent, i.e., paraffin or triton X-100.

In our earlier work [B1], viscous liquids were employed to enhance the CL signal. Viscous liquid may provide a microenvironment which improves the PO-CL efficiency by reducing the effects of quenching agents such as oxygen or the rate of solvent evaporating from the surfaces. In favorable cases, application of the enhancers can increase the signal response as much as 2 to 10 fold (Table 2-5). The maximum CL intensity was decreased as the percent component of triton X-100 increased (Table 2-5). This may be due to the influence of the surfactant on the rate of the chemical reaction since the half-life time was approximately 12 x longer in 50 % triton X-100-dioxane

(~4.8 min) than it is in dioxane (~0.4 min).

Since the PO-CL involves an energy transfer process, the CL effeciency is highly dependent on the fluorophore [B10]. Therefore, the use of the PO-CL method for polar fluorophores such as urinary porphyrin is not practically favorable. The mass limits of detection (MLOD) are reported to be ~0.4 fmol in capillary electrophoresis [B11], 20-25 fmol in HPLC [B11, B12] and 10 fmol in TLC [B13] with conventional fluorescence detection. But the MLOD was approximately 2 oreders of magnitude higher in the PO-CL-TLC (Table 2-6). A significant improvement in the MLOD was found to be ~ 70 fmol when the porphyrin free acids were converted into their methyl esters.

Table 2-7 shows that in the range of 0.03 - 0.15 ml/min flow rate of the CL reagents, no significant influence on sensitivity was observed. The respoducibility of peak areas was much better at a relatively lower flow rate, because at a higher flow rate diffusion-induced zone broadening of the sample may increase in the wet layer during the time of spraying and scanning the samples on the plate.

The maximum CL intensity increased as the concentration of TCPO increased, and the maximum CL response was found at ~ 0.3 M of H_2O_2 (Figure 2-2-5). Considering lifetime of the chemical reaction (Table 2-1, 2-2) and to avoid high concentration of the CL reagents, optimally 3 mM for TCPO and 0.1 M for H_2O_2, were used, respectively.

The experimental conditions of pH and types of solvents or the water component can be easily adjusted by post-chromatographic treatments. The problems are typical of

CL-HPLC but are minimal for CL-TLC. Although the strongest CL response was found on chromatography paper due to relatively efficient permeation of the CL solvent in the paper layer than in the solid adsorbent, the reproduciblity was also the worst among the test substrates (Table 2-8) since the sample zone is more easily spread on paper during the spraying of the CL reagents. If equal sample volume was applied, linear signal response was over a range of 2 - 3 order of magnitude (Table 2-9), in this case the variation caused by irregular spot shapes can be minimized.

CONCLUSION

PO-CL is a useful technique when coupled with TLC. Since TLC is the most widely used method for routine chemical analysis, further development in the area of CL-TLC for biomedical studies is of particular interest. The sensitivity of the newer CL densitometry makes it possible to use the PO-CL detection method for a chemical analysis at a femtomole level.

Table 2-1. Effect of TCPO concentration on background intensity*

	TCPO (mM)							
	0.05	0.1	0.25	0.5	1.0	2.0	3.0	5.0
$\tau_{1/2}$(s)	4.3	5.4	6.1	6.3	6.7	7.2	7.5	7.9
I (nA)	10.1	15.2	16.9	20.4	26.6	38.1	45.8	48.3

* H_2O_2 was 10 mM and flow rate was set at 0.07 ml/min for 4 s.

Table 2-2. Effect of H_2O_2 concentration on background intensity**

	H2O2 (mM)						
	1	5	10	20	30	50	100
$\tau_{1/2}$(s)	13.5	9.8	6.8	5.3	4.8	4.3	3.2
I (nA)	15.7	21.2	25.7	32.6	44.7	69.1	58.8

** TCPO was 0.5 mM and flow rate was set at 0.07 ml/min for 4 s.

Table 2-3. Effect of imidazole concentration on background intensity***

	imidazole (mM)					
	0.5	1.0	2.0	5.0	10	25
$\tau_{1/2}$(s)	6.2	4.5	2.4	1.9	1.3	1.1
I (nA)	30.8	39.5	68.6	53.5	46.8	26.9

*** Experimental conditions as in Table 2-2, various concentrations of imidazole were made in 10 mM H_2O_2.

Table 2-4. Environmental effects on the CL emission.*

	dioxane		paraffin/dioxane (3:2)	
	in air	in argon	in air	in argon
$\tau_{1/2}$(min)	0.29	0.19	5.30	5.28
I (μA)	0.34	0.65	2.76	3.17
I_{air}/I_{arg}	1.9		1.2	

* [TCPO] = 3 mM; [H_2O_2] = 0.1 M, flow rate = 0.07 ml/min. The CL emission with 5 ng of Dnsglycine was measured at its R_f.

Table 2-5 Maximum CL Enhancement (fold)**

Spray reagent	maximum CL enhancement (fold)
Liqid paraffin/dioxane (3:2)	9.8
(2:1)	7.8
liquid paraffin/chloroform (3:2)	8.0
Triton x-100/dioxane (1:4)	5.7
(2:3)	4.3
(2:1)	2.7
Dioxane	5.1
Ethyl Acetate	2.3

** Experimental conditions were as in Table2- 4

Table 2-6 Effects of flow-rate on the CL emission***

mL/min	Relative CL intensity	RSD $^{\alpha}$(n=5)
0.02	4.0 (0.28)	6%
0.03	11.0 (0.79)	6%
0.05	12.5 (0.89)	7%
0.07	14.0 (1.00)	7%
0.10	13.8 (0.98)	9%
0.12	12.5 (0.91)	13%
0.15	11.5 (0.82)	14%

*** Experimental conditions were as in Table 2-4. $^{\alpha}$ Relative standard deviation on the peak areas.

Table 2-7 Comparison of the Mass Limits of Detection Between Porphyrin Free Acids and Their Methyl Esters****

Porphyrin	MLOD (S/N = 3) free acid (pmol)	ester (fmol)
meso	0.82	63
copro	0.80	58
penta	1.08	60
hexa	1.15	64
hepta	2.20	78
uro	3.09	97

****Experimental conditions were as in Table2-4

Table2-8 Substrate Effect on Maximum CL Emission and Reproducibility*.

Dns-glycine (ng)	chromatogr. paper I_{cl} (%)	RSD	HPTLC-RP18 I_{cl} (%)	RSD	HPTLC I_{cl} (%)	RSD	alumina I_{cl} (%)	RSD
80	94	7.6	78	5.8	33	3.5	20	5.1
40	32	7.3	29	5.6	7.5	4.4	4.8	4.1
20	6.3	10.8	5.6	6.6	2.0	5.9	1.3	6.2
10	1.3	12.3	1.1	6.7	0.9	6.3	0.7	7.4

* I_{cl} - relative CL intensity corrected from the CL background; RSD (%) - relative standard deviation (n=4) on peak areas. Experimental conditions were as in Table 2-4.

Table 2-9 Linear regression analysis of the CL measurements**.

sample	LDR	log-log slope	correction coefficient (n=6)	LOD (ng)
Dns-L-leucine	225	0.54	0.995	0.53
Dns-glycine	285	0.65	0.993	0.42
Dns-L-arginine	310	0.61	0.993	0.39

**Experimental Conditions were as in the table 2-4 Evaluated on HPTLC plate; LDR = linear dynamic range, corresponding to the ratio of the upper concentration limmit of linearity (within 3%) and LOD, for the log-log plot; LOD = limits of detection (S/N = 3).

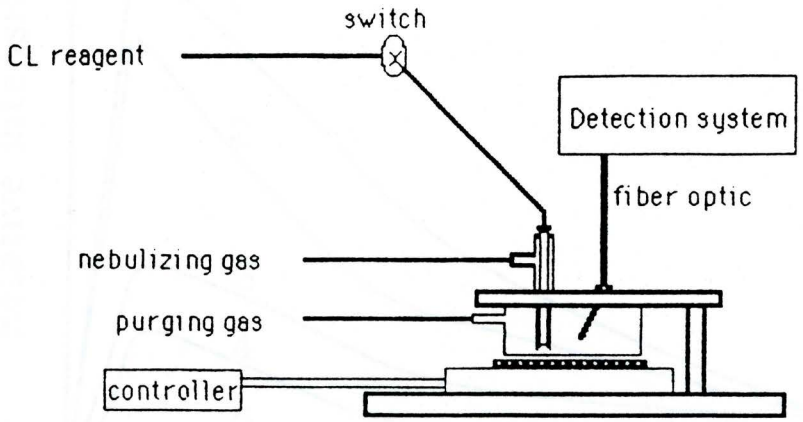

Figure 2-2-1. Cross-sectional view of the experimental set-up for the stopped scan, kinetic system.

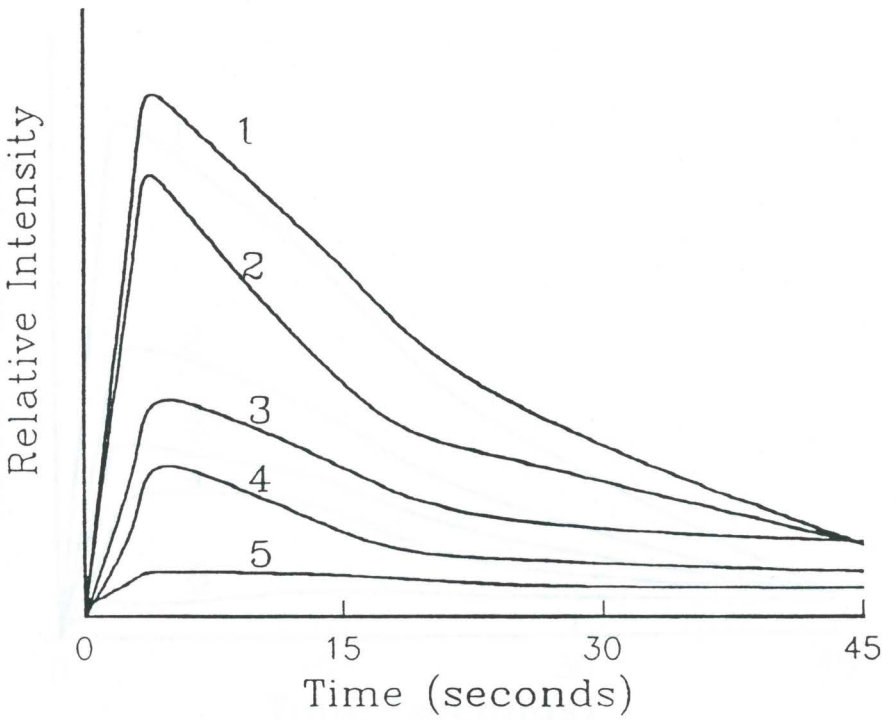

Figure 2-2-2. Substrate effect on CL emission. 1-chromatography paper; 2-HPTLC-RP18; 3-Silica gel HPTLC; 4-Alumina; 5-blank. [TCPO]= 3 mM; $[H_2O_2]$= 0.1 M; [perylene]= 10^{-6} M. Flow rate = 0.1 ml/min for 10 s.

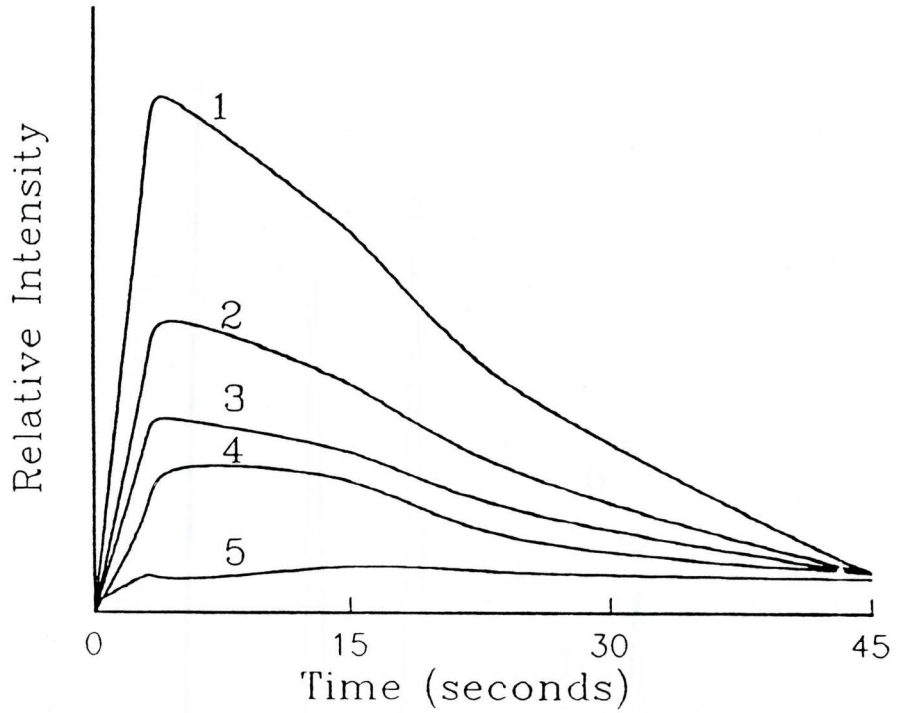

Figure 2-2-3. Silica effect on CL emission. 10^{-6} M perylene on: 1-chromatography paper; 2-top of 0.014 μm fumed silica; 3-mixed with 0.014 μm fumed silica; 4-covered with 0.014 μm fumed. Experimental conditions were as Figure 2-2-2.

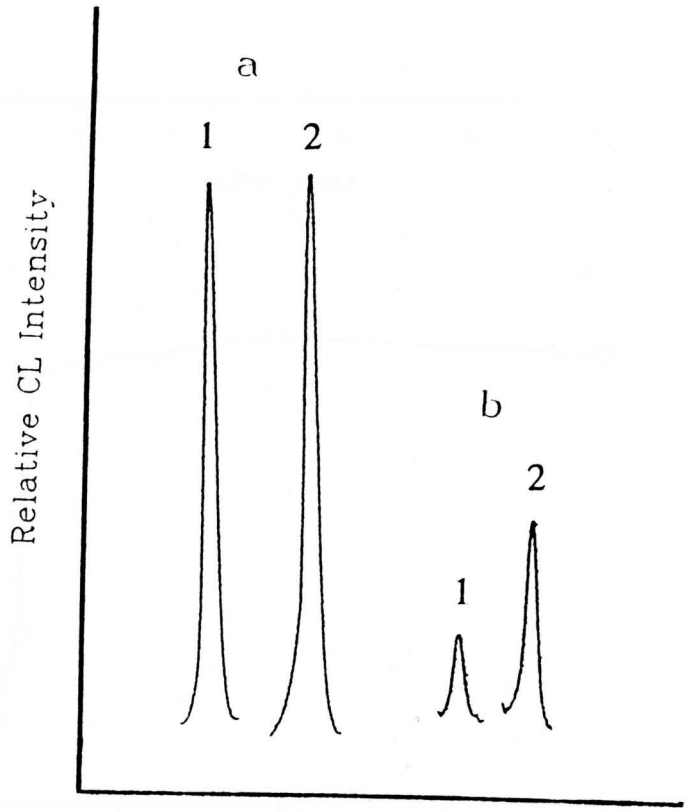

Figure 2-2-4. Comparison of Cl measurements at the origin and the R_f, a) on chromatography paper; b) on silica gel HPTLC. 1-measured at origin; 2-measured at R_f. Concentrations of TCPO and H_2O_2 were as in Figure 2. 40 ng of Dns-glycine was used as the fluorophore, scanning speed was set at 2 mm/s.

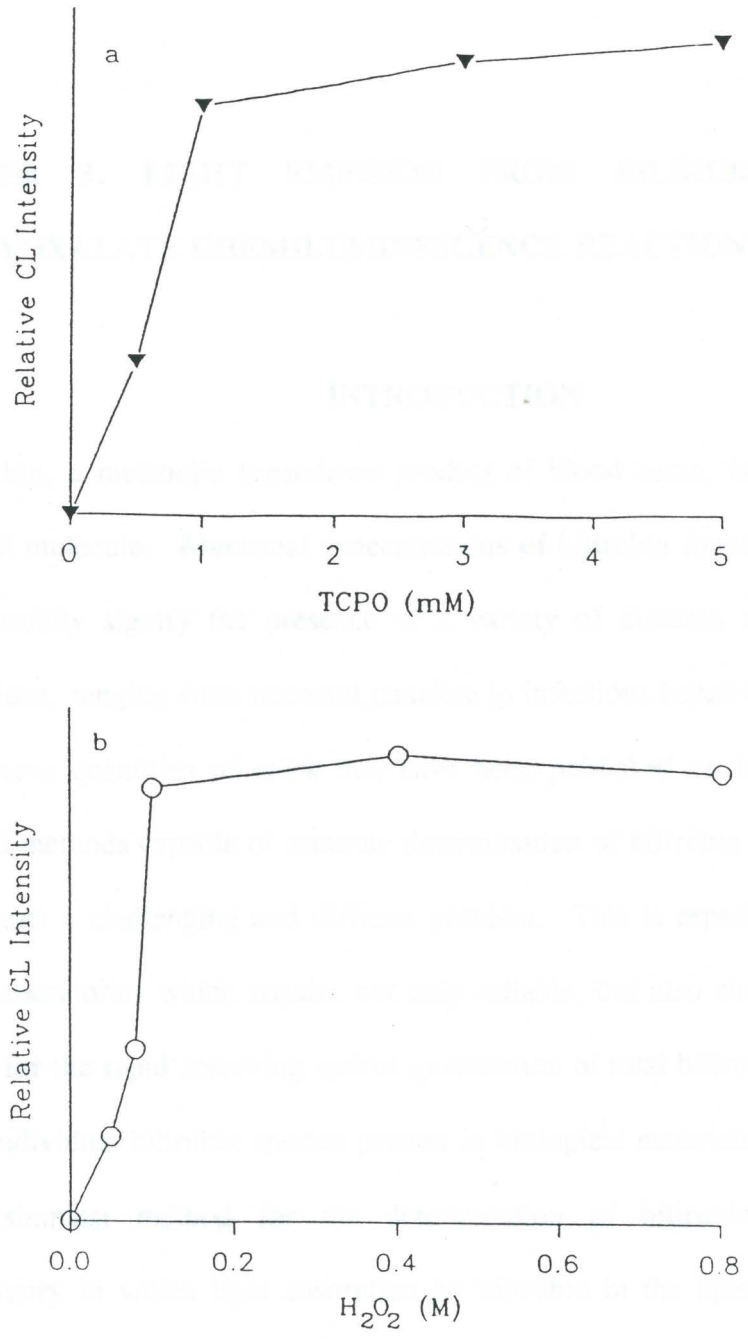

Figure 2-2-5. Concentration dependence of CL emission. (a) TCPO; (b) H_2O_2. CL was measured at the R_f, on silica gel HPTLC plates. $[H_2O_2]$= 0.1 M in (a); [TCPO]= 3 mM in (b); 40 ng of Dns-glycine was used as the fluorophore, scanning speed was set at 2 mm/s.

CHAPTER 3. LIGHT EMISSION FROM BILIRUBIN FROM THE PEROXYOXALATE CHEMILUMINESCENCE REACTION

INTRODUCTION

Bilirubin, a metabolic breakdown product of blood heme, is a highly significant biological molecule. Abnormal concentrations of bilirubin found in human serum or plasma usually signify the presence of a variety of diseases associated with liver dysfunctions, ranging from neonatal jaundice to infectious hepatitis [C1, C2]. In spite of enormous quantities of work that have been published on bilirubin, the lack of analytical methods capable of accurate determination of bilirubin and/or its conjugates still remains a challenging and difficult problem. This is especially true for routine clinical laboratories which require not only reliable, but also simple and inexpensive methods for the rapid screening and/or quantitation of total bilirubin concentrations as well as individual bilirubin species present in biological materials.

The simplest method for the determination of bilirubin is perhaps direct absorptimetry in which light absorption by bilirubin in the blue-green region of the visible spectrum is monitored [C3]. However, this method is not very sensitive and is prone to interference problems. To increase sensitivity and selectivity, the most widely used approach has been the coupling of bilirubin with suitable diazonium salts to form colored azo derivatives. A large number of papers have been published based on this

approach for the absorption measurement of the derivatized bilirubin [C1, C2]. Unfortunately, all these methods still lack the simplicity and reliability required for routine analysis in clinical laboratories. It has been known for a long time that fluorescence of free bilirubin is difficult to detect due to very efficient radiationless decay paths that return the excited bilirubin rapidly to the ground electronic state [C4]. However, it has been clearly established that relatively strong fluorescence from bilirubin can be detected when bilirubin is bound to albumin or micelles [C5, C6]. In fact, standard fluorometric methods have been developed for the determination of bilirubin in the presence of albumin [C2, C7]. However, these methods are not very popular in routine clinical laboratories, perhaps in part due to the complexities and expensive instrumentation associated with fluorometric techniques.

In recent years chemiluminescence has shown great promise to be a powerful analytical technique for routine usage in clinical laboratories due to its outstanding analytical advantages in terms of detectability, speed, simplicity and linear dynamic range [C8, C9]. The peroxyoxalate chemiluminescence reaction, which is based on the oxidation of aryl oxalate esters by hydrogen peroxide in the presence of a suitable fluorescent species (sensitizer), has been successfully exploited for the detection of a number of highly fluorescent sensitizers, e.g., polyaromatic hydrocarbons and urinary porphyrins [C10, C11]. To the best of our knowledge, the fluorescent emission of bilirubin generated by chemical excitation via a chemiluminescence reaction has never been reported. This is perhaps not surprising since the fluorescent quantum yield (f_{FL})

of bilirubin is extremely low near room temperature ($\leq 10^{-5}$ in water or chloroform). Indeed, whether free bilirubin fluoresces or whether the fluorescence can be detected via excitation at ~430 nm has been a subject of controversy [C12].

In this chapter the observation of light emission from bilirubin dissolved in an organic solvent as a result of the peroxyoxalate chemiluminescence system involving the reaction of bis(2,4,6-trichlorophenyl)oxalate and hydrogen peroxide is reported for the first time. The effects of various solvents on the chemiluminescence intensity were briefly investigated. To evaluate the analytical potential of the present chemiluminescence method for the determination of bilirubin, the limit of detection (LOD), selectivity, and linear dynamic range were examined. Furthermore, the total bilirubin contents in a real biological sample (bovine serum) was determined using the present chemiluminescence method and were compared with those obtained from absorption and fluorescence techniques.

EXPERIMENTAL

Materials

Bis(2,4,6-trichlorophenyl)oxalate (TCPO) was synthesized and purified according to the procedure of Mohan and Turro [C13]. Hydrogen peroxide (30%) was obtained from Fisher. HPLC grade ethylacetate and acetonitrile were used as the solvents for TCPO and H_2O_2, respectively. Hemoglobin, protoporphyrin, b-carotene, riboflavin,

bovine serum, benzo[a]pyrene and phosphoric acid were all purchased from Sigma.

Bilirubin (unconjugated bilirubin IX) and its conjugate, bilirubin ditaurite, were obtained from U. S. Biochemical and were used as received since their extinction coefficients were in agreement with the accepted values for pure pigments and, furthermore, the thin-layer chromatography on silica gel showed bilirubin and bilirubin ditaurite to migrate as single spots without the presence of any detectable impurities [C14]. *N,N'*-dimethylformamide, pyridine, chloroform and dimethylsulfoxide were purchased from Fisher and used as solvents for bilirubin or bilirubin ditaurite. Stock solutions were made up just before each experiment and used immediately.

Methods

Absorption Spectra. Direct absorptimetry of bovine serum samples were carried out using a 8451A diode-array spectrophotometer (Hewlett Packard). Sample preparation procedures for the extraction of total bilirubin from bovine serum were as follows: 200 mL of bovine serum was placed in a centrifuge tube containing 4 ml of the solvent system: ethylacetate-DMF-pyridine 15.00:84.99:0.01 (v/v/v) and was shaken vigorously for 30 s. The tube was then placed in a centrifuge and run at 2500 rpm for 2 min. The supernatant (3 ml) was then transferred to a 1-cm cell and the absorbance spectrum was measured.

Fluorescence and chemiluminescence spectra. Fluorescence spectra were recorded using an SLM-Aminco 8000 photon-counting spectrofluorometer. Excitation wavelength was set at 435 nm and the bandpass was set at 16 nm. For the

measurement of fluorescence spectra of benzo[a]pyrene appropriate amounts of benzo[a]pyrene were dissolved in the various solvents studied and placed in a 1-cm quartz cell. For the measurement of bilirubin spectra from bovine serum, sample preparation and measurement procedures were adopted from a standard fluorescence method [C2]. In a 1-cm quartz cell, 50 mL of bovine serum was added and mixed with 0.5 ml of phosphoric acid. After 5 min, 3 ml of water was added to the cell and mixed. Procedures for obtaining the spectra of the blank were the same except that 50 mL of water was added instead of bovine serum.

Chemiluminescence spectra were also recorded using the SLM-Aminco 8000 photon-counting spectrofluorometer but with the light source turned off. Emission slit was set for a bandpass of 16 nm. A spectrum was obtained for a single scan by photon-counting for 0.5 s at intervals of 5 nm. Five scans were averaged for each spectrum reported. For the measurement of the chemiluminescence spectra, appropriate amounts of benzo[a]pyrene, bilirubin or bilirubin ditaurite standards dissolved in a particular solvent were mixed with 1 ml of 1 to 5 mM TCPO in a 1-cm quartz cell; 3 to 5% H_2O_2 (1 ml) was then added to generate chemiluminescence emission. For the measurement of chemiluminescence spectra of total bilirubin from bovine serum, procedures used in the absorption experiment for the extraction of total bilirubin from 100 mL bovine serum was performed. Afterward, 1 ml of 2 mM TCPO was added to 2 ml of the supernatant in a 1-cm quartz cell. A spectrum was recorded by the addition of 1 ml of 5% H_2O_2. chemiluminescence spectra of the blanks were also obtained

using similar procedures but without the presence of bilirubin standards or bovine serum.

Quantitative chemiluminescence measurements. A home-built luminometer was used for the recording of chemiluminescence intensity as a function of time. Basically, it consists of a 5 ml glass test tube (sample cell) housed within a light-tight compartment. Chemiluminescence emission from the sample cell passed through a filter and a series of focusing lenses before reaching a photomultiplier tube (R928, Hamamatsu). A 10-nm bandpass filter centered at 520 nm (Corion) was used to isolate chemiluminescence emission from bilirubin. The photocurrent was fed to a picoammeter (Oriel) and the output signal was filtered through a 1.0 s time constant before recording on a strip-chart recorder. To make measurements of chemiluminescence intensity of bilirubin, 1 ml of the bovine serum extract or bilirubin standards dissolved in DMF-pyridine was mixed with 1 ml of 2 mM TCPO in the sample cell and was stirred continuously with a magnetic stir bar; 1 ml of 3% H_2O_2 was then added to the sample cell to generate chemiluminescence emission

RESULTS AND DISCUSSION

Figure 3-1 shows the chemiluminescence spectrum of bilirubin dissolved in *N,N*-dimethylformamide (DMF). It is important to note that the spectral distribution of chemiluminescence is similar to the fluorescence spectra of bilirubin reported in the literature [C5, C6], suggesting that the chemiluminescence emission may also be a

result of radiative transition of electrons from the first singlet excited electronic state to the ground state of bilirubin. It can be seen that the chemiluminescence maximum of bilirubin is centered at ~512 nm, which is within the 505 - 545 nm range reported for the fluorescence maxima of bilirubin bound to micelles or albumin. It has been suggested that the variation in the fluorescence maximum may be due to differences in conformation and/or ionization of bilirubin in these different environments [C12].

The relative fluorescence intensity of bilirubin was measured for a number of organic solvents and the results were as follows: pyridine > dimethylsulfoxide (DMSO) > DMF > chloroform ($CHCl_3$). It was observed that the fluorescence of bilirubin in chloroform ($f_{FL} \sim 10^{-5}$), for which an intramolecularly hydrogen bonded form of bilirubin is known to predominate [C15], was barely detectable above the Raman scattering of the solvent. The fluorescence intensity increased slightly when bilirubin was dissolved in the other three organic solvents ($f_{FL} \sim 10^{-4}$). These results are similar with those reported in the literature [C16], which indicated that fluorescence of bilirubin usually increases with increasing polarity, dielectric constant, and basicity of the solvent, probably due to more effective disruption of the intramolecular hydrogen bonding and/or ionization of bilirubin. The same solvent series was employed for the observation of chemiluminescence from bilirubin. It was surprising to find that chemiluminescence was detected in DMF and not in the other solvents studied. In order to understand this phenomenon, it is important to remember that in the peroxyoxalate chemiluminescence reaction the luminescence intensity is directly

proportional to the product of the efficiency of chemiluminescence (f_{CL}) and rate of the reaction, and f_{CL} is the product of the efficiency of chemical excitation (f_{CE}) and f_{FL} [C17]. Thus, it is possible that a relatively large f_{FL} of bilirubin in a particular solvent may be offset by a low f_{CE} and/or slow kinetics, leading to an undetectable luminescence intensity. To investigate this possibility, we have studied the effects of this solvent series on the relative fluorescence and chemiluminescence intensity of benzo[a]pyrene because this probe molecule gave comparable relative fluorescence intensity over the above range of solvents and thus allowed for a qualitative evaluation of solvent effects on f_{CE} and/or rate of the reaction.

The relative fluorescence intensity of benzo[a]pyrene (normalized intensity) has the following trend: DMSO (1.00) > DMF (0.60) > $CHCl_3$ (0.35) > pyridine (0.25), while the trend for the relative chemiluminescence intensity was very different: $CHCl_3$ (1.00) > DMF (0.40) > DMSO (0.08) > pyridine (0.06). These results suggest that DMSO and pyridine could be more effectively quenching the f_{CE} and/or slowing down the kinetics of the peroxyoxalate chemiluminescence reaction relative to DMF or $CHCl_3$. Further evidence of this postulation are shown in Figure 3-2(a) which shows that the chemiluminescence intensity of benzo[a]pyrene in $CHCl_3$ increased slightly with the presence of small amounts of DMF (probably due to an increase in the f_{FL}) but began to decrease significantly after a certain threshold concentration of DMF ($\sim 8\%$) was exceeded. With the presence of DMSO or pyridine in $CHCl_3$ it can be seen that the chemiluminescence intensity decreased dramatically as the percentage of $CHCl_3$ in the

solution became smaller, suggesting that pyridine and DMSO severely quench the f_{CE} and/or decrease the rate of the reaction. It has been suggested that peroxyoxalate reaction mechanisms probably involve nucleophilic attack of hydrogen peroxide on the oxalate carbonyl [C17]. Thus, it is possible that nucleophilic solvents such as DMF, DMSO and pyridine could also attack the chemiluminescence reagent and consume it in non-chemiluminescence side reactions. However, other factors such as interference of donor-acceptor complex formation and/or inhibition of electron transfer due to solvent effects are also possible [C17-C19].

The question of why chemiluminescence of bilirubin can only be detected in DMF among the solvent series studied can be partly addressed in terms of the balance between efficiency and kinetic parameters for this system. For bilirubin in $CHCl_3$ it is possible that the f_{FL} of bilirubin ($\sim 10^{-5}$) is too low to yield any detectable chemiluminescence signals. On the other hand, bilirubin in DMSO and pyridine may reduce the f_{CE} and/or rate of the reaction to such an extent which rendered the luminescence intensity undetectable. However, it appears that bilirubin in DMF provides an optimum balance between f_{FL}, f_{CE} and/or kinetics among the solvent series studied, allowing the chemiluminescence of bilirubin to be detected. It should be noted that under the present experimental conditions, no chemiluminescence emission was detectable from the mixing of chemiluminescence reagents with the solvents studied without the presence of bilirubin (blanks); however, at higher detection sensitivity, a small amount of background chemiluminescence signal can be detected from the blanks,

which has been shown to occur for a variety of aryl oxalate esters [C20].

Figure 3-2(b) shows that the chemiluminescence intensity of bilirubin in DMF increased in the presence of small amounts of pyridine but not with the addition of DMSO. The addition of small amounts of pyridine may catalyze the peroxyoxalate chemiluminescence reaction [C17] and/or cause an increase in the chemiluminescence intensity by effectively slowing down the twisting motion of bilirubin and thereby increasing its f_{FL} [C6, C16, C21]. Furthermore, it has been suggested that exciplex formation may occur between bilirubin and the solvent molecule in the presence of pyridine, leading to possible enhancement in the rate of excitation of the peroxyoxalate chemiluminescence reaction [C16, C21]. With further increases in the pyridine concentration above $\sim 0.01\%$ in DMF, however, it can be seen that the chemiluminescence intensity of bilirubin begins to decrease, probably due to the negative effect of pyridine on the f_{CE} and/or rate of the reaction.

Figure 3-3(a) shows that chemiluminescence signal of bilirubin near the LOD in the solvent system of DMF-pyridine 99.99:0.01 (v/v). The solvents chosen for TCPO and H_2O_2 were ethylacetate and acetonitrile, respectively, since these solvents have been shown to provide the optimum experimental performances in terms of solubility, stability, chemiluminescence intensity and lifetime for the measurement of a number of fluorophores in static systems [C18, C23]. Based on a signal-to-noise ratio (S/N) of three, the absolute and relative LOD's calculated from calibration plots using peak heights as shown in Figure 3(a) were found to be 5.0 ng and 8.5 nM, respectively.

Calibration plots drawn for a series of bilirubin standards exhibited linearity from the LOD up to 20 mM and the corresponding linear regression constant was 0.997.

Considering the relatively low f_{FL} of bilirubin in DMF and pyridine ($\sim 10^{-4}$) and the effects of solvents on f_{CE} and/or rate of the reaction, the LOD's that can be achieved using the present chemiluminescence methods are quite good. For comparison an absolute LOD of 134 pg has been reported for albumin-bound bilirubin using a laser-based fluorometric technique [C6]; using a laser-based photothermal technique for the detection of free bilirubin adsorbed on thin-layer chromatographic plates, an absolute LOD of 2.5 ng was obtained [C24]. It should be noted that the normal concentrations of bilirubin present in human serum or plasma are relatively high, which falls in the range of 6 to 17 mM [C2]. Figure 3-3(b) shows that with a bilirubin concentration of 6.0 mM spiked into the DMF-pyridine solvent system, the chemiluminescence signal is significantly higher than the background level, suggesting that the sensitivity of the present chemiluminescence method should be more than sufficient for the detection of elevated level of bilirubin in human serum or plasma.

The selectivity of this chemiluminescence method for the detection of bilirubin in the presence of a number of common interference species in serum or plasma was examined. Figure 3(c) shows the chemiluminescence signal of 6 mM of bilirubin in the presence of a mixture of hemoglobin, protoporphyrin, b-carotene and riboflavin. The concentrations of these interference species as shown in Figure 3-3(c) are representative of the normal concentrations usually found in human serum or plasma [C25]. It can

be seen that the chemiluminescence signal of bilirubin with and without the presence of these common interference species as shown in Figures 3(b) and (c) were about the same, suggesting these particular species present in normal concentrations in serum should have negligible effects on the chemiluminescence detection of bilirubin using the present approach.

The threshold concentrations at which the above interference substances could cause a noticeable variation in the chemiluminescence intensity ($\pm$ 3%) of bilirubin were determined by spiking these species individually into the solvent system. Hemoglobin and b-carotene are known to cause interference problems when using direct absorptimetry for the determination of bilirubin in plasma [C2]. Fortunately, it was found that hemoglobin is highly insoluble in DMF and there was no noticeable change in the chemiluminescence intensity of bilirubin even when concentrations of hemoglobin ten times larger than the normal concentration was present. However, b-carotene in large excess (4000 mg/L) did consistently cause a decrease in the maximum chemiluminescence intensity of 6.0 mM of bilirubin. This is not surprising since there is an overlap between the emission band of bilirubin and absorption band of b-carotene at $\sim$ 510 nm. On the other hand, it is interesting to note that protoporphyrin and riboflavin present in relatively large concentrations (440 mg/L and 900 mg/L, respectively), as compared to their normal concentrations in human serum, were shown to cause an increasing signal interference in the chemiluminescence intensity of bilirubin. This is, again, not surprising since these are highly fluorescent species

capable of emitting relatively intense radiation in the yellow-red region of the visible spectrum. In fact, chemiluminescence emission from urinary porphyrins generated from the peroxyoxalate chemiluminescence system has already been demonstrated to be a sensitive and selective technique for the screening of various forms of porphyrias in clinical laboratories [C11].

Comparisons were made between the present chemiluminescence method and absorption and fluorescence methods for the determination of total bilirubin concentration, i.e., bilirubin and its conjugate, in bovine serum. It should be noted that the normal total bilirubin concentration in bovine serum falls in the range of 1 to 5 mg/L, consisting mostly of bilirubin (unconjugated form) [C26]. Figure 3-4(a) shows an absorption spectrum of a bovine serum sample. It can be seen that a fairly diffuse band barely detectable from the background was observed between 400 to 500 nm. Although it is known that bilirubin absorbs in the 420 to 460 nm, it is difficult to tell whether or not this weak absorption band as shown in Figure 3-4(a) was due to absorption by bilirubin and/or interference species present in the serum. This result is consistent with those reported in the literature which stated the lack of sensitivity of direct absorptimetry for the determination of bilirubin in human serum at the borderline level ($\sim$ 4 mg/L) [C2].

To increase the detection sensitivity, a standard fluorescence method [C2] was employed for the measurement of fluorescence spectrum of bovine serum as shown in Figure 3-4(b). For comparison, Figure 3-4(c) shows the chemiluminescence spectrum

of the bovine serum sample dissolved in a solvent system of ethylacetate-DMF-pyridine 15.00:84.99:0.01 (v/v/v). Ethylacetate was added to accelerate the precipitation of the proteins present in the serum. It is interesting to see that the chemiluminescence spectrum of the bovine serum is very similar to that obtained from the bilirubin standard as shown in Figure 3-1, suggesting that the chemiluminescence emission from the bovine serum was likely due to bilirubin and it conjugate present in the sample. It should be noted that chemiluminescence spectrum of conjugated bilirubin (bilirubin ditaurite) has also been obtained using the present chemiluminescence method and it was found that the chemiluminescence intensity and spectral distribution were similar to those obtained from bilirubin (unconjugated), except there was a slight red shift in the peak maximum for conjugated bilirubin of about 20 nm. Similar shift in peak maxima can also observed for fluorescence spectra of bilirubin and bilirubin ditaurite, which has been proposed as a mean for the differential determination of these two forms of bilirubin in serum [C27]. By measuring the chemiluminescence intensity of the bovine serum sample and a series of bilirubin standards at ~ 520 nm, the total bilirubin concentration in bovine serum was calculated to be 2.7 mg/L, which is consistent with the total bilirubin concentration range normally found in bovine serum (1 to 5 mg/L).

In comparing the fluorescence and chemiluminescence spectra of the bovine serum sample as shown in Figures 3-4(b) and (c), respectively, it can be seen that the location of the peak maxima was about the same for both methods and the magnitudes of the

fluorescence and chemiluminescence signals were comparable. However, an important difference is that in the fluorescence method a relatively large background signal was obtained from the blank, i.e., phosphoric acid and water, probably due to the combination of emission from fluorescent impurities and Raman scattering from the blank. To obtain a fluorescence spectrum as shown in Figure 3-4(b), subtraction of background from the sample spectra was necessary. It is interesting to note that the bandwidth of the fluorescence spectrum was slightly broader then that of the chemiluminescence spectrum, suggesting that there could be fluorescence contributions from fluorescent interference species present in the bovine serum sample such as riboflavin and flavin-type compounds, which are capable of emitting relatively intense radiation in the spectral region between 450 and 600 nm [C28].

CONCLUSION

In summary, the present study shows for the first time that chemiluminescence of bilirubin can be detected in an organic solvent system using the peroxyoxalate chemiluminescence reaction. The effects of solvents on the f_{FL}, f_{CE} and/or rate of the reaction appear to play an important role in the optimization of the chemiluminescence intensity of bilirubin. Although the sensitivity of the present chemiluminescence method does not appear to be significantly better than the standard fluorescence method, it should be more than adequate for the determination of elevated levels of total bilirubin concentrations in human serum or plasma. When compared to fluorescence

methods, the major advantages of the present chemiluminescence method are simplicity, wide linear dynamic range, less expensive instrumentation and perhaps better selectivity, which are important criteria for routine usage in clinical laboratories. Further investigations of the selectivity of the present chemiluminescence method for the detection of bilirubin should be performed. It may be possible to modify the present chemiluminescence detection scheme for the rapid screening of total bilirubin concentration in human serum or plasma by direct injection of samples into a flow injection analysis system. If quantitation of individual bilirubin species is required, the use of high-performance liquid chromatography in conjunction with chemiluminescence detection could potentially offer a number of unique analytical advantages [C29].

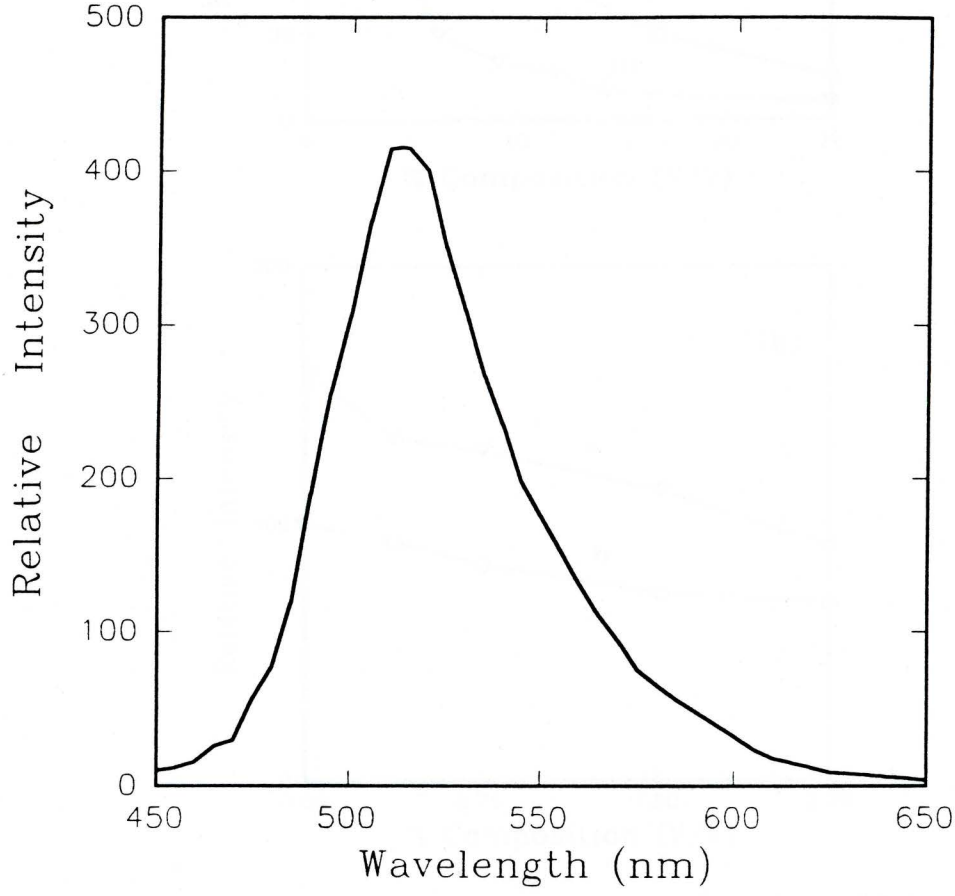

Figure 3-1 Chemiluminescence spectrum of 4.5×10^{-4} M bilirubin in DMF. Concentrations of TCPO and H_2O_2 were 5×10^{-3} M and 5% (v/v), respectively.

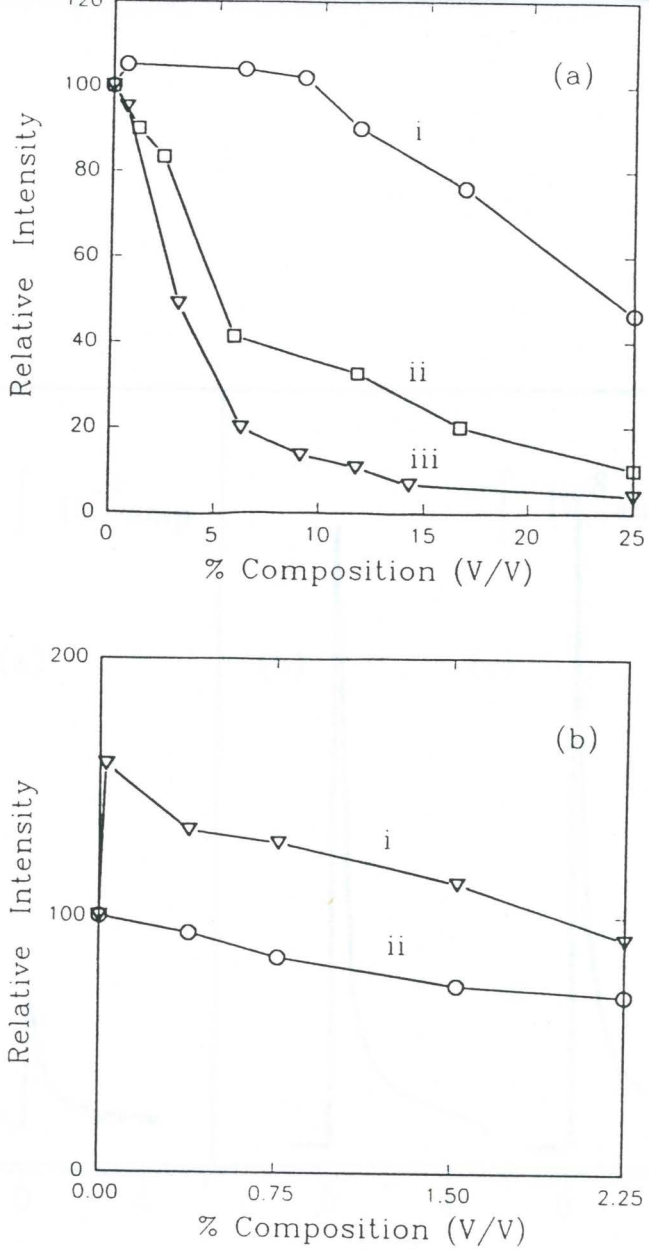

Figure 3-2 (a) Chemiluminescence intensity of 2.4 x 10^{-6} M benzo[a]pyrene as a function of percentage of (i) DMF, (ii) DMSO and (iii) pyridine present in chloroform. Concentrations of TCPO and H_2O_2 were 1 x 10^{-3} M and 3% (v/v), respectively, and (b) chemiluminescence intensity of 4.0 x 10^{-5} M bilirubin as a function of percentage of (i) pyridine and (ii) DMSO present in DMF. Concentrations of TCPO and H_2O_2 were 5 x 10^{-3} M and 5% (v/v), respectively.

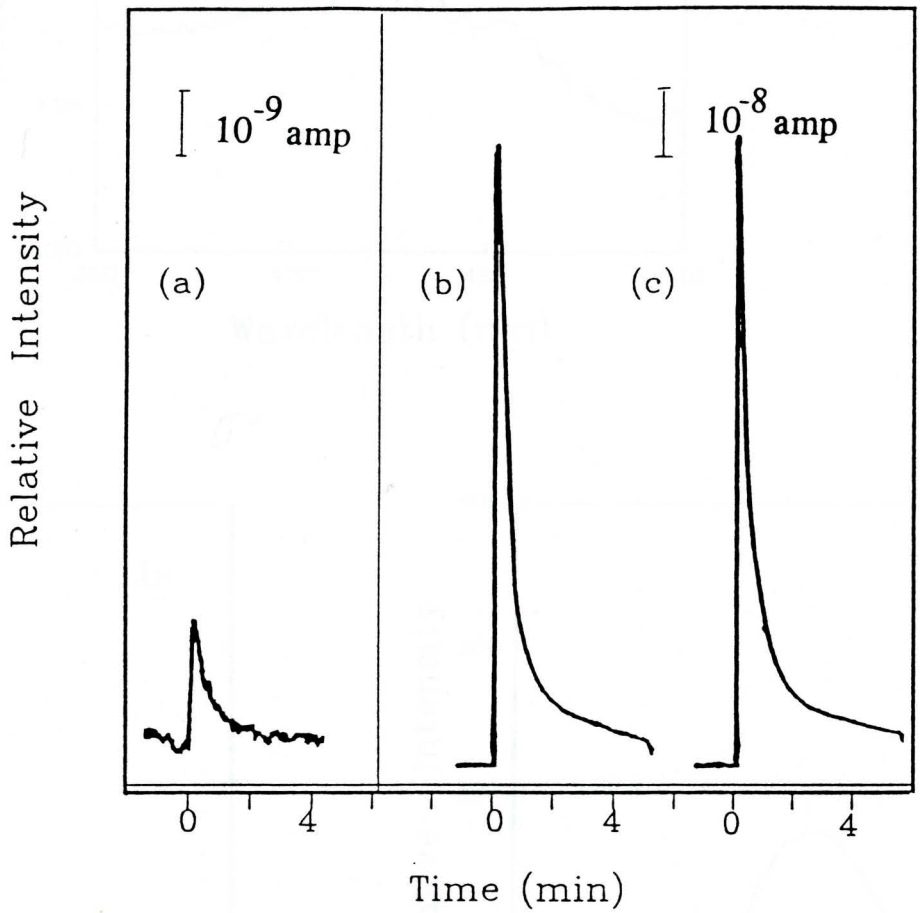

Figure 3-3 Chemiluminescence intensity as a function of time: (a) 25 nM bilirubin, (b) 6.0 mM bilirubin and (c) 6.0 mM bilirubin mixed with 20 mg/L hemoglobin, 600 mg/L b-carotene, 35 mg/L protoporphyrin and 20 mg/L riboflavin in 99.99:0.01 (v/v) of the solvent system:DMF-pyridine. Concentrations of TCPO and H_2O_2 were 2 x 10^{-3} M and 3% (v/v), respectively.

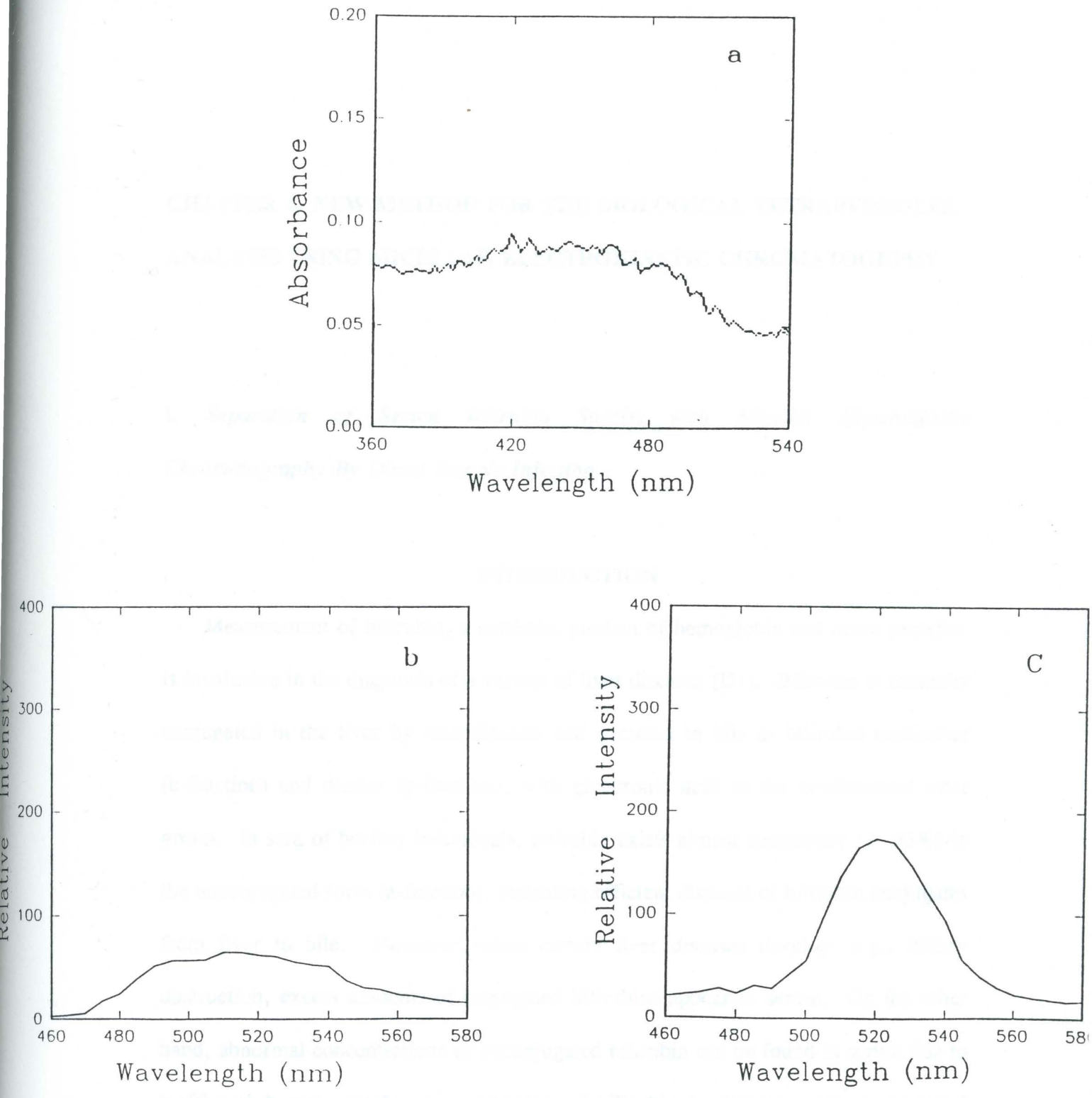

Figure 3-4 Spectrum of bovine serum: (a) absorption, (b) fluorescence, and (c) chemiluminescence.

CHAPTER 4. NEW METHOD FOR THE BIOLOGICAL TETRAPYRROLES ANALYSIS USING MICELLAR ELECTROKINETIC CHROMATOGRPHY

I. *Separation of Serum Bilirubin Species with Micellar Electrokinetic Chromatography By Direct Sample Injection*

INTRODUCTION

Measurement of bilirubin, a catabolic product of hemoglobin and heme proteins, is invaluable in the diagnosis of a variety of liver diseases [D1]. Bilirubin is normally conjugated in the liver by esterification and excreted in bile as bilirubin monoester (b-fraction) and diester (g-fraction), with glucuronic acid as the predominant ester group. In sera of healthy individuals, bilirubin exists almost completely (> 95%) in the unconjugated form (a-fraction), indicating efficient disposal of bilirubin conjugates from liver to bile. However, when certain liver diseases develop, e.g., biliary obstruction, excess amounts of conjugated bilirubins appear in serum. On the other hand, abnormal concentrations of unconjugated bilirubin can be found in serum due to inefficient hepatic uptake or conjugation of bilirubin in diseases such as neonatal jaundice. In addition to the three major chemical forms of bilirubin (a-, b- and

g-fractions), there exists a fourth form of bilirubin that is covalently bound to albumin (d-fraction) in human serum [D2]. Interestingly, it has been recently reported that concentration profiles of delta (d) and conjugated bilirubins in serum could be used for identifying rejection in patients undergoing orthotropic liver transplant [D3].

Most clinical laboratories utilize methods based on modifications of the traditional Jendrassik-Gróf diazo reaction for fractionation of "direct" reacting (b- and g-fractions) and "indirect" reacting (a-fraction) bilirubins. However, since 10% to 15% of the a-fraction may be direct reacting, the direct diazo reaction could overestimate the level of conjugated bililrubin. Moreover, the albumin-bound fraction (d) of serum also exhibits a direct diazo reaction, resulting in a possible overestimation of b- and g-fractions [D1].

To overcome some of these limitations of diazo methods, a number of high-performance liquid chromatographic (HPLC) techniques have been developed in recent years that are capable of accurate quantitation of individual bilirubin species in human serum [D4-D9]. However, HPLC methods for bilirubin analyses are currently too expensive and, since these methods always require some types of sample preparation procedures to remove serum proteins prior to chromatographic analyses, they are too elaborate and time-consuming for use in most routine clinical laboratories.

Capillary zone electrophoresis (CZE) has proved to be a highly efficient technique for the separation and determination of ionized substances with short analysis time and at low cost. By the introduction of surfactants above their critical micelle

concentrations (CMC) in the run buffer while maintaining the same equipment design of CZE, i.e., in an open-tubular capillary of very small internal diameter, a new type of separation method based on micellar partitioning of the solute and electrophoretic migration of the micelle - micellar electrokinetic chromatography (MEKC) - has been shown to be a powerful technique for the separation of electrically neutral molecules. Interestingly, the selectivity and peak shapes were found to be even better for the MEKC separation of some ionic substances as compared to CZE. Using MEKC, for example, separation of porphyrins [D10], phenols [D11], some amino acid derivatives [D12, D13], nucleosides [D14] and drugs [D15] have been reported. Importantly it has been demonstrated that plasma or serum proteins, which must be at least partially removed prior to HPLC analyses, were solubilized by the surfactants employed in MEKC, thus allowing for the determination of drugs in plasma by direct sample injection methods [D16].

In this paper we describe the application of a MEKC method for the determination of serum bilirubin using the anionic surfactant-sodium dodecyl sulfate (SDS) in the run buffer to solubilize serum proteins. Using this method, a direct sample injection analysis of four bilirubin fractions can be performed without the use of any deproteinization or extraction procedures. Separation performances and detectabilities for the measurement of these individual bilirubin species were investigated using spiked model serum and pathological human serum samples.

EXPERIMENTAL

Apparatus

A commercially available CE instrument (Model SpectraPHORESIS 1000, Spectraphysics, San Jose, CA, USA) was used to perform both CZE and MEKC experiments with absorption detection at 450 nm or 280 nm. An untreated 50-cm x 75-mm I.D. fused-silica capillary tube (Polymicro Technologies, Phoenix, AZ, USA) was used for all separations and an integrator (Chromjet, Spectraphysics, San Jose, CA, USA) interfaced to the CE instrument was used for data processing.

Chemicals and Buffers

SDS, Woodward's reagent K and essentially fatty acid-free human serum albumin were purchased from Sigma (St. Louis, MO, USA) and all other chemicals (except for bilirubin standards) were of analytical grade and purchased from Aldrich (Milwaukee, WI, USA) or Fisher (Springfield, NJ, USA). Buffer solutions used for performing CZE experiments were prepared by mixing appropriate volumes of 0.02 M sodium tetraborate (borax) and 0.1 M boric acid to give buffer solutions of appropriate pH values. Afterward, methanol was added to the run buffer to prepare working buffer solutions of appropriate concentrations. To prepare run buffer for MEKC experiments, appropriate amounts of SDS were added to the CZE run buffer solutions and filtered through an 0.2-mm membrane before methanol was added to give the buffer solutions of the desired concentration.

Bilirubin Standards

Unconjugated bilirubin (bilirubin IXa) and diconjugated bilirubin (bilirubin ditaurite·Na) were obtained from U.S. Biochemical (Cleveland, OH, USA). Unconjugated bilirubin was used as received since its extinction coefficient was in agreement with accepted value for pure pigment and its separation using high-performance thin-layer chromatograph (HPTLC) and MEKC showed no detectable impurity. However, diconjugated bilirubin was purified using HPTLC according to previously described procedures [D17] since the electropherogram showed ~ 5% impurity. Monoconjugated bilirubin was extracted from rabbit bile using Eberlein's method [D18] and further purified on HPTLC plates. Covalent complex of bilirubin and albumin (biliprotein) was synthesized from unconjugated bilirubin and Woodward's reagent K (*N*-ethylphenylisoxazolium-3'-sulfonate) according to the method of Kuenzle *et al.* [D19]. To prepare spiked model serum samples, appropriate amounts of a mixture of the four bilirubin standards were dissolved in 0.02 M borax buffer solutions containing 6% human serum albumin. Before direct injection of the model serum sample, a 1:1 (v/v) dilution with the run buffer was made for each sample.

Rabbit Bile and Human Serum Samples

Fresh bile from young rabbits was purchased from PEL-Freez Biologicals (Rogers, AR, USA) and pathological serum samples were obtained from six patients in Moses Taylor Hospital (Scranton, PA, USA). These bile and serum samples were kept frozen

and stored in the dark before the experiments. Before direct injection of the samples, a 1:2 or 1:3 (v/v) dilution with the run buffer was made for each sample.

Capillary Conditions

New capillaries were treated by purging with 0.5-M NaOH for about 1.5 h and then filling capillary with the run buffer for 12 h before use.

CE Instrument Conditions

The parameters employed for operation of the SpectraPHORESIS 1000 instrument were as follows: the detector was set for 450 nm or 280 nm with a rise time of 0.3 s, injection was set for vacuum at 2.0 s injection time, column temperature was maintained at 20° C, voltage was at 16 kV and polarity +. The run time was 15 min and the current draw was 45 mA using 25-mM SDS and 20-mM borax buffer solutions. Between runs washing of the capillary was performed with 0.1-M NaOH for 2 min and then with the run buffer for another 2 min.

RESULTS AND DISCUSSION

CZE of Bilirubin Standards

Figures 4-1-1 (a) and (b) show the electropherograms of unconjugated and diconjugated bilirubin standards, respectively, obtained by free solution, counter migration capillary electrophoresis. It is important to note that the run buffer used for

obtaining these two electropherograms contained 5% methanol. Without the methanol, asymmetric peaks were found for both unconjugated and diconjugated bilirubins. Interestingly, similar observations have also been reported for the CZE separation of hydrophobic porphyrin standards [D10], i.e., coproporphyrin and mesoporphyrin (cyclic tetrapyrroles), which possess similar structures as bilirubin ("linear" tetrapyrroles). It was suggested that poor solubilities of these hydrophobic porphyrins in the run buffer without the presence of methanol contribute to asymmetric peak shapes and, furthermore, may mediate the adsorption of these porphyrins onto the capillary wall [D10].

The diconjugated bilirubin standard appears in Figure 4-1-1 (b) is a synthetic ditaurine derivative of unconjugated bilirubin. The chemical and physical properties of this compound, e.g., diazo reactivity and chromatographic behaviors, have been shown to be very similar to those of the bilirubin diglucuronide - the predominant bilirubin diester excreted in human bile [D20,D21]. More importantly, since the molecular size and charge of this compound are also comparable to those of bilirubin diglucuronide, the electrophoretic mobilities of these two forms of diconjugated bilirubin should be quite similar, suggesting that bilirubin ditaurite should be suitable for use as a diconjugated bilirubin standard in CZE and MEKC analyses of serum bilirubins.

As shown in Figures 4-1-1 (a) and (b), the diconjugated bilirubin migrated slightly slower than the unconjugated bilirubin towards the detector under identical

electrophoretic conditions. This elution order could be explained in terms of charge and perhaps hydrophobicity and conformational differences between these two molecules. In CZE the electroosmotic flow directs the bulk flow of the buffer solution in the direction of the negative electrode towards the detector while the electrophoretic mobility directs the negatively charged solutes towards the positive electrode away from the detector. Thus, in general, the least negative charged solute will elute first, followed by solutes with increasing negatively charge when the velocity of electroosmosis is larger than electrophoretic velocities of the solutes (counter migration mechanism).

In Figures 4-1-1 (a) and (b) the least negative charge solute appears to be the unconjugated bilirubin, which is not surprising since it is well known that this molecule is highly non-polar and water insoluble in aqueous solution at pH below 8.0 [D22,D23]. Its non-polar characteristic has been explained in terms of the intramolecular hydrogen bonding that twist the bilirubin molecule in such a way that all the polar head groups are buried inside the hydrophobic core of the molecule. At pH 8.5, the molecule becomes more polar and water soluble, indicating that the two carboxylic side groups within the molecule should be at least partially ionized and increasing its electrophoretic mobility. However, the hydrophobicity and conformation of unconjugated bilirubin may have a negative impact on its electrophoretic mobility, possibly counteracting the effect of increasing negative charge on the migration of this molecule towards the positive electrode away from the detector [D24]. On the other hand, diconjugated

bilirubin (in the form of ditaurite or diglucuronide) is polar and water soluble over a wide range of pH due to lack of intrahydrogen bonding and the possession of two highly acidic moieties on the ditaurine or diglucuronic functional groups (doubly negative charge at pH 8.5), thus resulting in higher electrophoretic mobility towards the positive electrode but longer migration time towards the detector when compared to unconjugated bilirubin.

Although the difference in migration time between unconjugated and conjugated bilirubin was not significant as shown in Figures 4-1-1 (a) and (b), it appears that the separation of a mixture of approximately equal amounts of these bilirubin species into two well-resolved peaks with relatively good efficiency and peak shape using CZE should be feasible. Surprisingly, Figure 4-1-1 (c) shows that this is not the case. The injection of a mixture of unconjugated and conjugated bilirubins into the CE instrument resulted in longer migration times and significant peak broadening and distortion for both bilirubin species. In an attempt to explain this phenomenon, it is helpful to note that rapid and reversible dimerization of bilirubin is known to occur at high concentrations [D1]. Therefore, it is possible that under the influence of high electric field, there may exist strong interaction between unconjugated and diconjugated bilirubins in the run buffer, perhaps due to intermolecular hydrogen bonding between these two molecules. This aggregation effect may lead to an increase in the electrophoretic mobilities and decrease in the solubilities of the bilirubin species, resulting in longer migration times and perhaps in enhanced interactions of these species

with the capillary wall, respectively.

MEKC of Spiked Model Serum

Figure 4-1-2 shows the separation of a model serum sample consisting of a mixture of the four bilirubin standards using run buffer containing SDS. It can be seen that the resolution and peak shape obtained for the separation of unconjugated and diconjugated bilirubins (peaks 1 and 3) are significantly improved over those obtained by CZE as shown in Figure 4-1-1 (c). Also, the migration times of these peaks were found to be identical to those obtained from injecting model serum spiked with the individual bilirubin standard into the CE system. These results suggest that SDS was quite effective in minimizing aggregation that occurred between unconjugated and diconjugated bilirubins and possibly also reducing adsorption of bilirubins onto the capillary wall due to solubilization of the bilirubin molecules with the SDS micelles [D25] and binding of SDS onto electrostatic and hydrophobic sites on the capillary wall [D10]. The solubilization or interaction of SDS micelles with bilirubin could explain the increase in migration times found for both unconjugated and diconjugated bilirubins due to an increase in the negative charge of these micelle-bound bilirubin species and consequently retarding the counter migration of these species towards the detector. However, a larger change in migration time was obtained for diconjugated bilirubin as shown in Figure 4-1-2. This may be due to the presence of a larger hydrophobic region (additional ditaurine functional groups) for interactions with SDS, thus increasing

the negative charge and resulting in higher electrophoretic mobility when compared to unconjugated bilirubin.

As shown in Figure 4-1-2, a relatively large difference in migration times between unconjugated and diconjugated bilirubin was obtained as a result of the use of SDS in the run buffer, allowing for another bilirubin species (peak 2) to be separated in this migration window. This particular bilirubin species was obtained from the bile of rabbit because it has been shown that monoconjugated bilirubin (b-fraction) in bile predominates in lower animals such as rabbit and decomposition profiles of this particular bilirubin fraction, along with g- and a-fractions, were consistent with hydrolysis of esters [D26,D27]. Figure 4-1-3 shows an electropherogram of a rabbit bile sample using MEKC. It is clear that the predominant peak (peak 2) appears at a migration time of ~ 7.5 min and was, therefore, isolated for use as the monoconjugated bilirubin standard as shown in Figure 4-1-2. Peaks 1, 3 and 4 in Figure 4-1-3 were tentatively assigned as the a-, g-, and d-fractions, respectively, since their migration times correlate with those obtained from the corresponding bilirubin standards as shown in Figure 4-1-2. Also, the identities of these species were also previously assigned as such in the reversed-phase HPLC separation of rabbit bile [D27].

Peak 4 in Figure 4-1-2 was identified as the bilirubin species covalently bound to human serum albumin (biliprotein), which was synthesized from standard procedures [D19]. It can be seen that biliprotein has the highest electrophoretic mobility and eluted the latest among the four bilirubin standards separated by MEKC. This is reasonably

concentrations of unconjugated bilirubin in human sera are in the range of 6 - 17 mM and for conjugated bilirubin, in the range of 0.1 - 0.2 mM [D22], the detectabilities that can be achieved using the present method are adequate for the diagnosis of mild to acute cases of certain types of unconjugated and conjugated hyperbilirubinemia. Table 4-1-2 presents the relative standard deviation (RSD) calculated for migration times and peak areas of the four bilirubin standards spiked in model serum and bilirubin species found in pathological human serum samples. These data show that the precision of this method is comparable to those obtained in other MEKC methods developed for the determinations of analytes in plasma or serum samples [D16].

Recovery tests were performed by adding various bilirubin standards (20 - 100 mg/ml) into healthy adult sera and the individual bilirubin concentrations were determined by employing MEKC. The average recovery (R) calculated for each bilirubin standard was as follows: unconjugated bilirubin (R = 101%, n = 5); diconjugated bilirubin (R = 98.6% n = 5); and biliprotein (R = 94.3% n = 4). These results indicate that good recovery can be obtained for unconjugated and conjugated bilirubins using the present method.

Patient Samples

Figures 4-1-6 (a) and (b) show two MEKC electropherograms of serum samples obtained from patients with bone cancer and jaundice, respectively. Importantly, the migration times of peaks 1 to 4 in these electropherograms show good correlation with those of unconjugated and conjugated bilirubin standards spiked in model serum as

shown in Figure 4-1-2. Using calibration plots obtained from measuring peak areas of unconjugated bilirubin, diconjugated bilirubin and biliprotein standards, the concentrations of peaks 1 to 4 as appeared in Figure 4-1-6 (a) were calculated to be 46.7 mM, 69.2 mM, 14.5 mM and 8.1 mM, respectively, and in Figure 4-1-6 (b) the concentrations were 63.1 mM, 132.2 mM, 27.1 mM and 5.8 mM, respectively (concentrations of peak 2 in Figures 4-1-6 (a) and (b) were calculated using calibration plots of diconjugated bilirubin). These values are significantly higher than those found in normal human serum [D2], indicating that these patients may be suffering from some type of hemolytic disorders and/or hepatic dysfunction. An unknown asymmetric peak (peak 5) appears in both electropherograms at a migration time of ~ 12 min, which may be due to binding of small amounts of various bilirubin species adsorbed to serum proteins and/or the presence of some other protein-bound pigments which absorb at 450 nm.

CONCLUSION

In summary, we have demonstrated that MEKC can be successfully used for the separation of major bilirubin species present in serum with good selectivity and reproducibility. The major advantages over conventional HPLC methods are direct sample injection capability, instrumental simplicity, minimal sample usage, and lower cost of MEKC, suggesting it could be a practical method for the fractionation and measurement of serum bilirubin species in routine clinical laboratories. Further

improvement in detectability of this method is necessary, which may be accomplished by employing multireflection absorption [D28] or laser-induced fluorescence detection techniques [D29].

Table 4-1-1 Detection Limits and Linearity

Bilirubin	Detection limit [α]	Linearity	
	(μM)	upper limit (μM)	linear regression constant[β]
Unconjugated	6.0	170	0.995
Diconjugated	5.8	284	0.993
Biliprotein	6.5	162	0.998

[a]Detection limits based on S/N = 3 according to peak heights.

[b]Linear regression constants determined from detection limits up to the amounts listed for the upper limits.

Table 4-1-2 Reproducibility of Migration Times and Peak Areas*

Bilirubin	R.S.D. (%) Migration time (n=4)		Peak area (n=4)	
	Model serum	Patient serum	Model serum	Patient serum
Unconjugated	0.23	0.16	3.04	4.20
Monoconjugated	0.25	0.28	2.66	3.20
Diconjugated	0.18	0.25	2.48	3.50
Biliprotein	0.32	0.38	2.73	2.80

*Determined by sequential injections over *ca.* 1.5 h time period for n = 4.

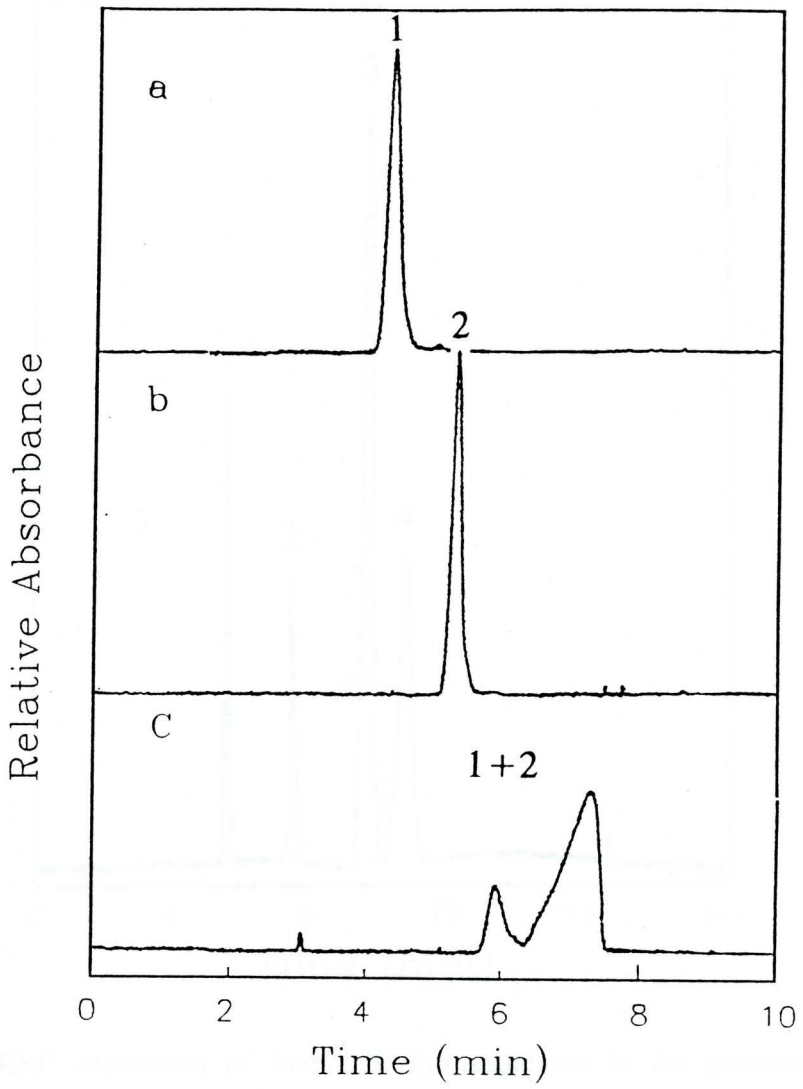

Figure 4-1-1 CZE electropherograms of (a) 35 mM unconjugated bilirubin, (b) 39 mM diconjugated bilirubin , and (c) a mixture of 35 mM unconjugated bilirubin (peak 1) and 39 mM diconjugated bilirubin (peak 2). Buffer: 20 mM borax buffer of pH 8.5 with 5% methanol. Absorbance detection at 450 nm.

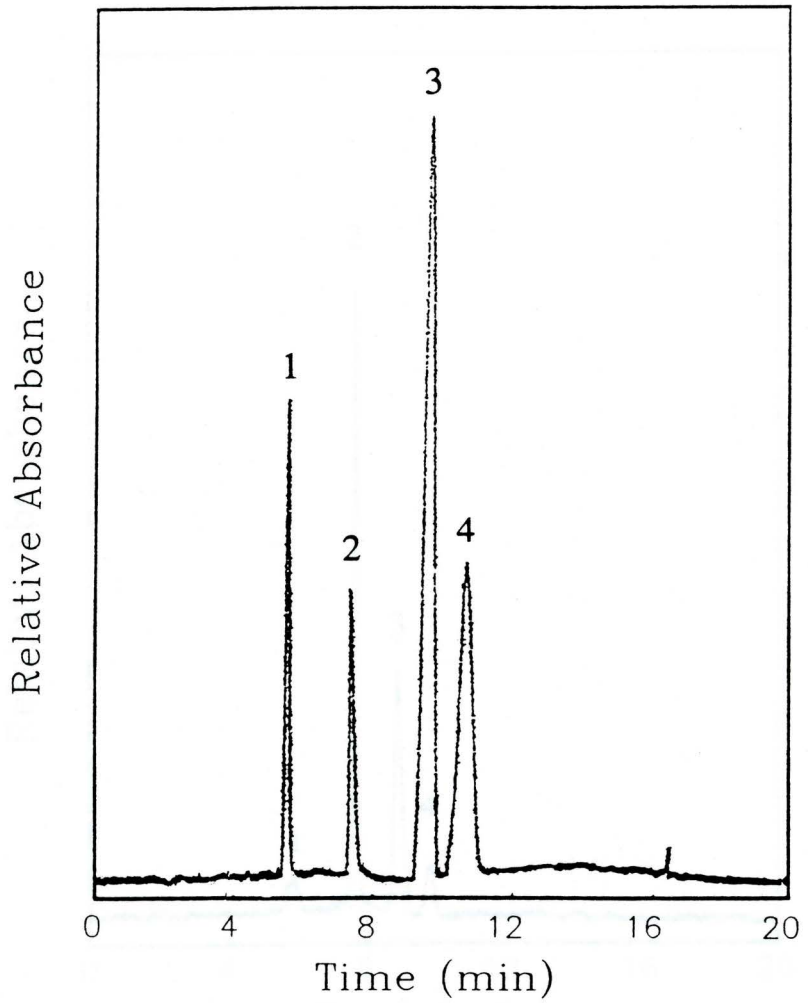

Figure 4-1-2 MEKC separation of four bilirubin standards in the presence of 3% human serum albumin. Buffer: 25 mM SDS in 20 mM borax buffer of pH = 8.5 with 3% methanol. Absorbance detection at 450 nm. Peaks: 1 = 41 mM unconjugated bilirubin; 2 = 25 mM monoconjugated bilirubin, 3 = 57 mM diconjugated bilirubin and 4 = 36 mM biliprotein.

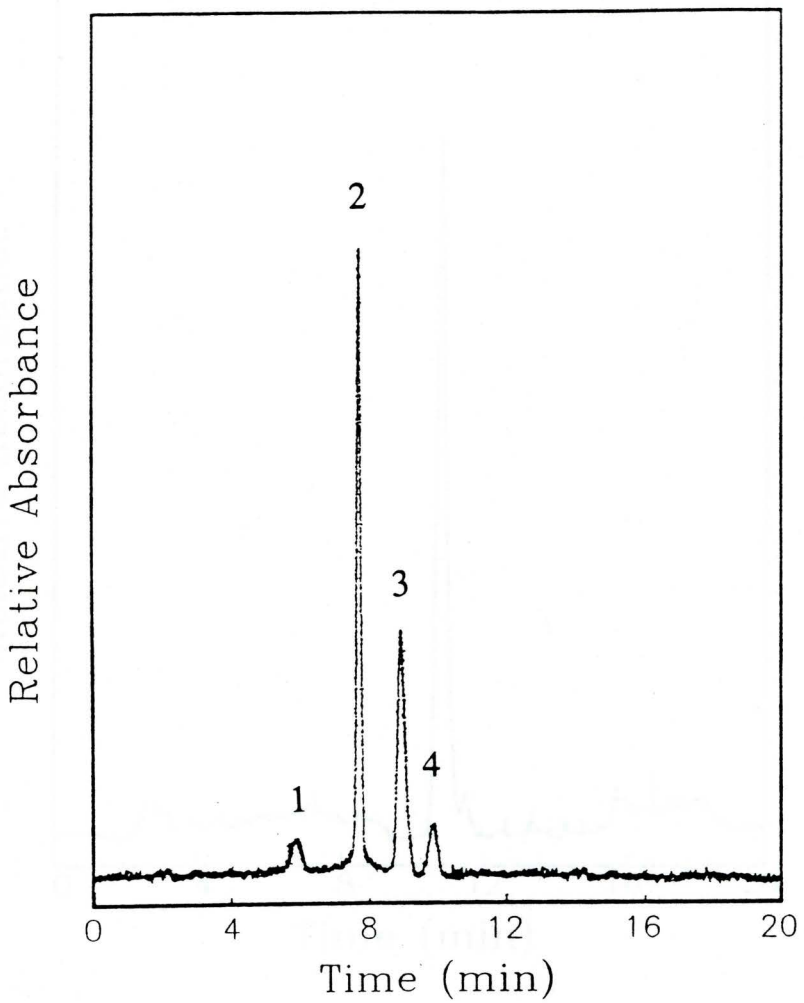

Figure 4-1-3 MEKC separation of rabbit bile (1:3, v/v dilution). Buffer and detection conditions same as Figure 4-1-2. Peaks: 1 = a-fraction, 2 = b-fraction, 3 = g-fraction, 4 = d-fraction.

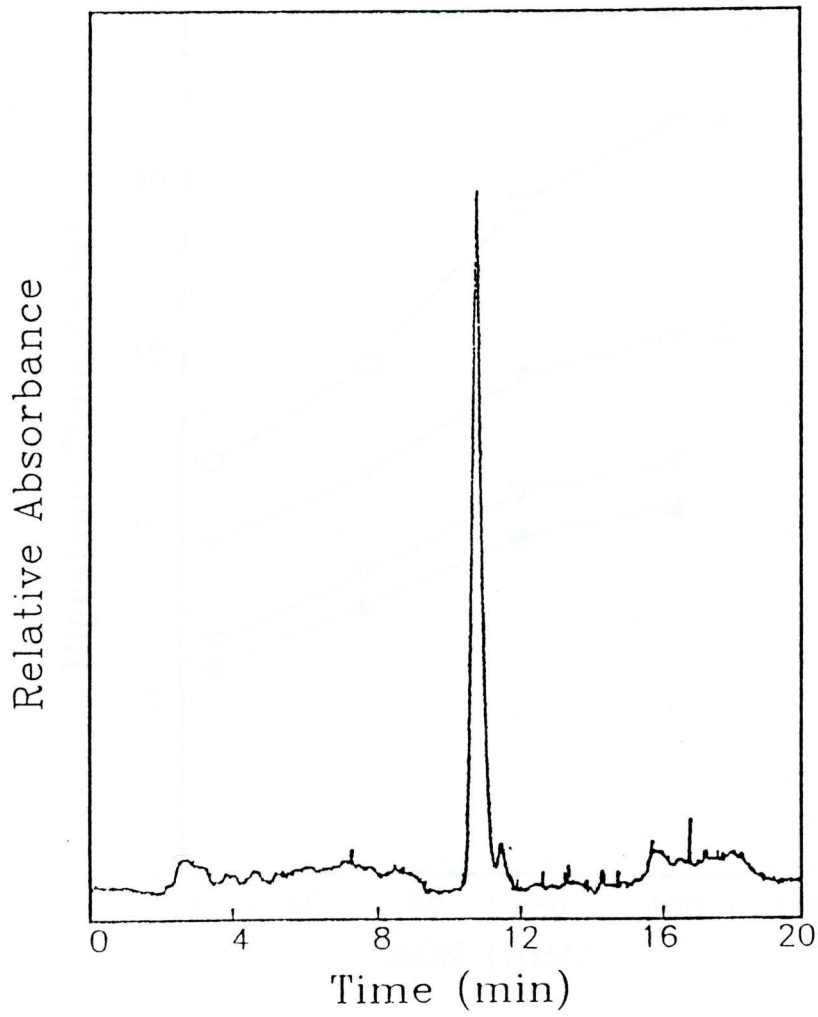

Figure 4-1-4 MEKC electropherogram of 3% human serum albumin. Buffer conditions same as Figure 4-1-2. Absorbance detection at 280 nm.

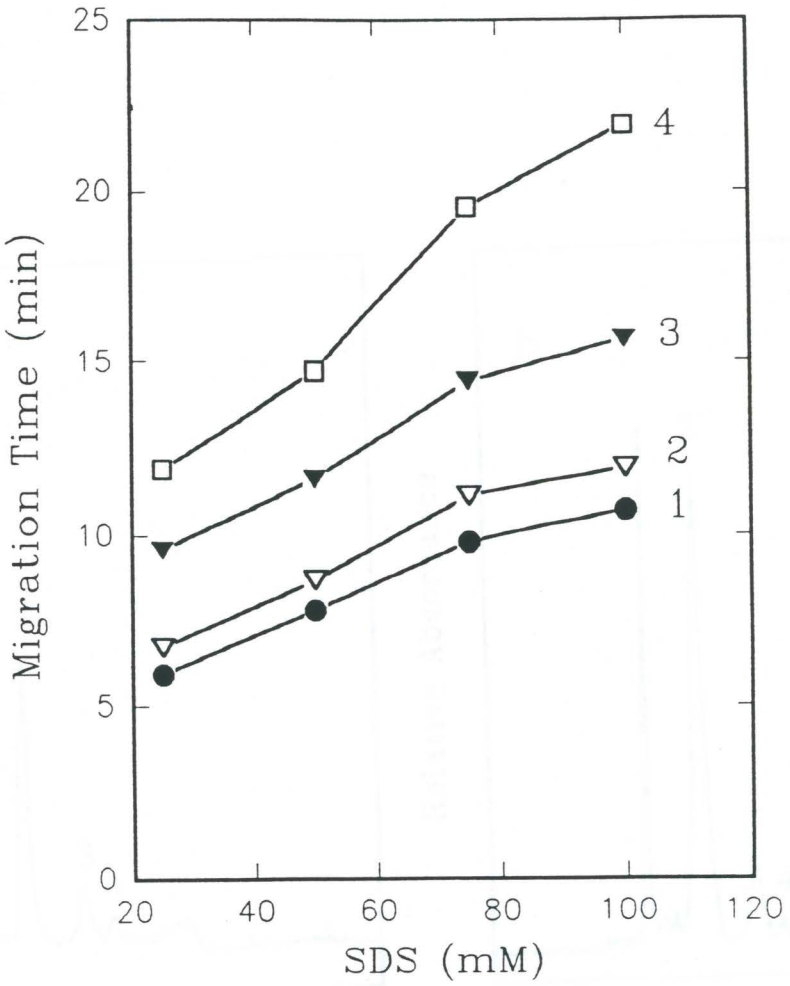

Figure 4-1-5 Effect of SDS concentration on the migration time of four bilirubin standards: 1 = 41 mM unconjugated bilirubin, 2 = 25 mM monoconjugated bilirubin, 3 = 57 mM diconjugated bilirubin and 4 = 36 mM biliprotein. Buffer: 20 mM borax buffer of pH = 8.5 with 3% methanol. Absorbance detection at 450 nm.

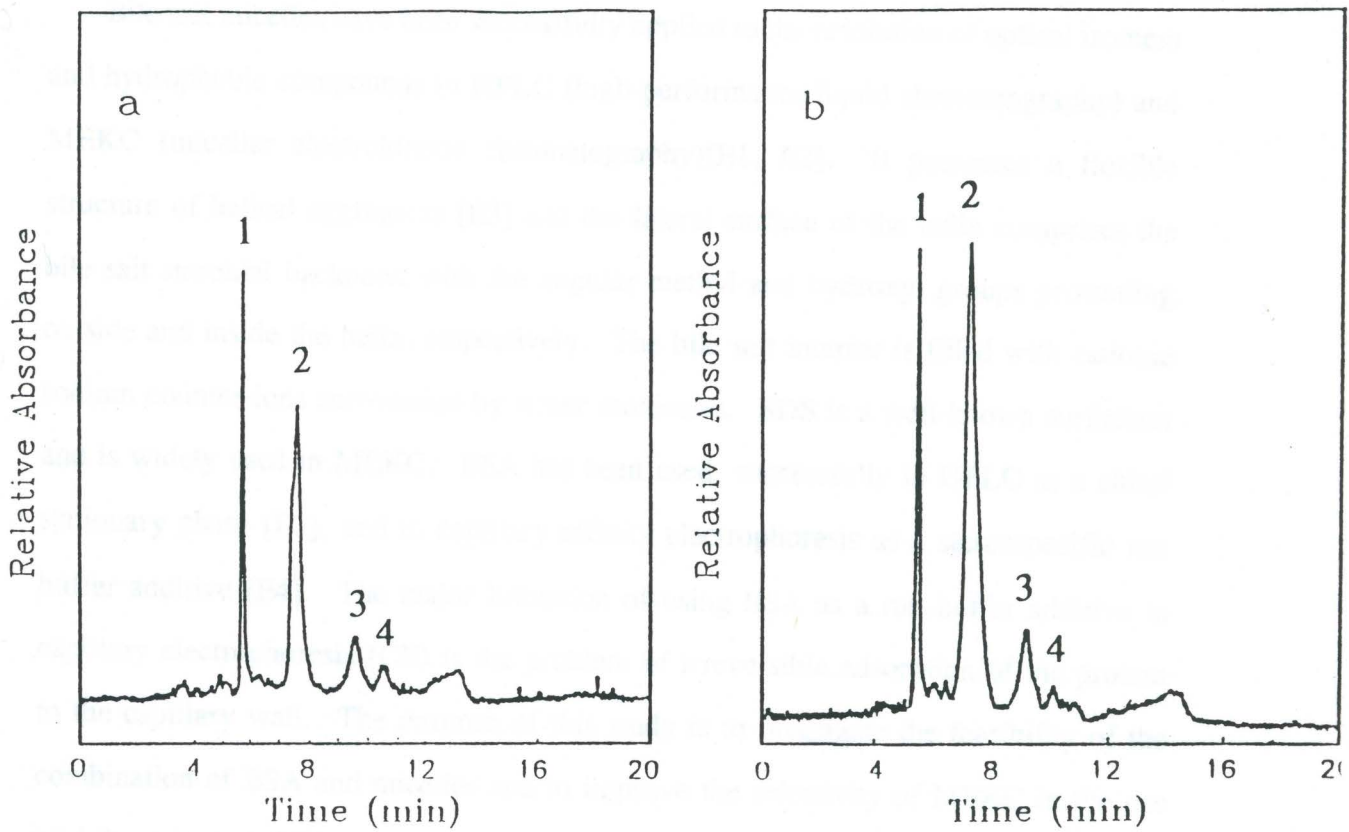

Figure 4-1-6 MEKC separation of patient serum samples (a) bone cancer (1:2, v/v dilution) and (b) jaundice (1:3, v/v dilution). Buffer and detection conditions same as Figure 4-1-2.

II. *Enhanced Separation of Urinary Porphyrins in Miceelar Electrokinetic Chromatography with Bovine Serum Albumin as a Buffer Additive*

INTRODUCTION

Bile salt micelles have been successfully applied to the resolution of optical isomers and hydrophobic compounds in HPLC (high-performance liquid chromatography) and MEKC (micellar electrokinetic chromatography)[E1, E2]. It possesses a flexible structure of helical aggregates [E3] and the lateral surface of the helix comprises the bile salt steroidal backbone with the angular methyl and hydroxyl groups protruding outside and inside the helix, respectively. The bile salt interior is filled with cationic sodium counter-ions surrounded by water molecules. SDS is a well-known surfactant and is widely used in MEKC. BSA has been used successfully in HPLC as a chiral stationary phase [E1], and in capillary affinity electrophoresis as a stereospecific run buffer additive [E4]. The major limitation of using BSA as a run buffer additive in capillary electrophoresis (CE) is the problem of irreversible adsorption of the protein to the capillary wall. The purpose of this study is to invesigate the feasibility of the combination of BSA and micelles and to improve the selectivity of MEKC in the use of bile salt and SDS micelles while minimizing the phenomena of protein-wall-adsorption. The urinary porphyrin was chosen as a model molecule to evaluate the BSA-bile salt micelle system since the bile salt micelles were shown to be incapable of separating negatively charged or high polar racemic compounds in previous reports [E5]. The porphyrins can be separated by MEKC using a SDS-CAPS (3-cyclohexylamino-1-propanesulfonic acid) run buffer with relatively large percentages

of methanol added under rigorous pH conditions, whereas the SDS acts more to compete with the samples for wall sites than as a means of enhancing the selectivity of the system [E6].

EXPERIMENTAL

Chemicals The pure stardards of copro- (I and III), penta-, meso-, hexa-, hepta-, and uro- (I and III) porphyrin were purchased from Porphyrin Products (Logan, Utah). TDCA (taurodeoxycholic acid, sodium salt), SDS, CAPS and essentially fatty-acid free BSA were purchased from Sigma (St. Louis, MO). All other chemicals were of analytical grade from Fisher (Springfield, NJ) or Aldrich (Milwaukee, WI). The run buffer solutions were prepared in doubly deionized water and filtered through a 0.4 μm membrance.

Apparatus A commercially available automative CE instrument (model spectra PHORESIS 1000, Spectra Physics, Freemont, CA) connected to an integrator (Chromjet, Spectra Physics) was used to obtain the data. The wavelength spectra were obtained from the output signal using the data software supplied with the CE instrument on an IBM model 70 computer. The MEKC experiments were performed in untreated fused silica capillaries (Polymicro Technologies, Phoenix, AZ) with dimensions 375 μm x 75 μm and a length of 55 cm.

Procedures New capillaries were conditioned with 20 mM borate-H_3PO_4 buffer for 12 h. before use. The capillary was cleaned between runs with 20 mM borate-H_3PO_4 buffer. The sample injection was set for vaccum ($\sim$ 78 mmHg below) at 2 s injection time and detection was measured at 400 nm. Column temperature was maintained at 35^0C.

RESULTS AND DISCUSSION

Coproporphyrin isomers of type I and III were well resolved in 22 minutes using a sodium taurodexyocholate solution with butanol and methanol as organic run buffer modifiers on a bare silica capillary (Figure 4-2-1). The attempt to separate uroporphyrin isomers of type I and III was unsuccessful using this buffer system, since the hydrophobicity of the bile salt micelle has poor retentivity for hydrophilic molecules such as uroporphyrin. The mixture of six urinary porphyrins was separated in the bile salt micelle solution with relatively poor efficiency, while the efficiency was unacceptable when using the BSA solution. The separation of the urinary porphyrins was achieved with good efficiency using the mobile phase containing BSA and sodium taurodexyocholate at pH 7.4 (Figure 4-2-2). To evaluate the separation efficiency the retention behavior in the bile salt micellar-BSA (BS-BSA) solution must be investigated..

Since the major interactions between bile salt and BSA are thought to be the Van der Waals forces acting through the hydrophobic face of the bile salt molecule and hydrophobic amino acid residues of the protein, commonly referred to as a "steroidal backbone -to-steroidal backbone" association [E7], it is also suggested that the hydrophobic lateral external surface of the bile salt micelle can be adsorbed onto the BSA phase by hydrophobic interactions while maintaning its micellar structure. Figure 4-2-3 (c) represents an electropherogram showing the net electrophoretic mobility of the BS-BSA complex formed in a 10 mM sodium borate-phosphate solution (pH=7.4) with 50 mM sodium taurodexyocholate and 0.015 mM BSA. The UV spectrum obtained for the micelle-BSA solution shows a single peak (Figure 4-2-2c). This suggests that the

the micelle-BSA solution shows a single peak (Figure 4-2-2c). This suggests that the mixed micelle-BSA solution formed in the system is electrophoretically monodispere. The retention behavior characteristics of electrokinetic chromatography for ionized species has been described in literature [E8], here we use the similar assumption to express the velocity of the negative charged species, $v^*(s)$, as follows:

$$v^*(s) = \frac{n_{aq}}{n_T} v(aq) + \frac{n_{BSA}}{n_T} v(BSA) + \frac{n_{Ms}}{n_T} v(Ms) + \frac{n_{Mc}}{n_T} v(Mc) \quad (1)$$

where v(aq), v(BSA), v(Ms), and v(Mc) are the electrophoretic velocities of the solute in aqueous buffer, BSA solution, the bile salt micelle bonded to BSA, and the bile salt micelle (free), respectively. The n term is the molar fraction of the solute in the above phases denoted by subscripts aq, BSA, Ms, Mc, and n_T is the total molar concentration. Equation 1. is true only if v(BSA), v(Ms), and v(Mc) remain constant when incorporating the solute. Since the mixed BS-BSA complex is electrophoretic monodispere, v(BSA) must be equal to v(Ms), and therefore v(BSA) = v(Ms) = v(BSA-Ms) and it is reasonable to assume that all bile salts are bonded to BSA when using a relatively high concentration of BSA, forcing n_{mc} to approach zero and consequently the last term in equation 1. can be dropped:

$$v^*(s) = \frac{n_{aq}}{n_T} v(aq) + \frac{n_{BSA} + n_{Ms}}{n_T} v(BSA\text{-}Ms) \quad (2)$$

The capacity factor of the solute is defined in the usual way as:

$$k' = \frac{n_{BSA} + n_M}{n_{aq}} \quad (3)$$

and substitution of equation 3. into equation 2. yields the following expression for the

capacity factor:

$$k' = \frac{\nu*(s) - \nu(aq)}{\nu(BSA\text{-}Ms) - \nu*(s)} \qquad (4)$$

By using equation 4, the capacity factor of the solutes and separation factor of the isomers, α ($\alpha = k'_1 / k'_2$; for $k'_1 > k'_2$) can be calculated as shown in the table 4-2-1.

BSA is throught to have a molecular dimension of ~ 42Å x 141Å [E9] and the micellar radius of taurodexyocholate is approximately 20 to 24 Å [E3]. At the optimum experimental conditions the molar ratio of the bile salt to BSA is greater than 3000, and it is presumed the bile salt micelle incorporates the BSA and a secondary micelle is formed on the BSA psuedostationary phase [E3]. The UV spectrum of the micelle - BSA solution shows an enhancement of absorption at approximately 280 nm which indicates that a strong interaction between the micelle and BSA occurs (Figure 4-2-2(d)). It was found that coproporphyrin experienced a wavelength "red" shift at its maximum absorption band in the BSA run buffer while remaining essentially constant in the micelle - BSA solution when compared to the micellar run buffer (Figure 4-2-4). In an attempt to explain the retention behavior of the solutes in the micelle - BSA system, it is proposed that the solutes are incorporated into the micelle and the micelle complexed with BSA, since the electrophoresed protein has a substantially higher mobility than the uncomplexed solute-micelle. The electrophoretic mobility (μ) of a protein-ligand complex is dependent on the charge of Protein (Z) and ligand (z), and the mass of protein (M) and ligand (m) as shown by equation 5 [E10]

Since the change in charge is large in comparison with the change in mass, the

$$\mu = \frac{(Z \pm z)}{(M+m)^{2/3}} \qquad (5)$$

protein-ligand complex will migrate at a different rate than an uncomplexed protein. Since the electroosmotic flow is the dominate driving force in a bare capillary, the solute with the greater anionic charge will migrate slower (counter-migration), but the more negatively charged anion will spend more time in the micellar phase (either inside or outside of the micelle). The reason that only one pair of the isomers can be separated using BSA in a bare capillary may be due to the fact that the solutes exhibit a minimal difference in charge density (stereo-selectivity is independent of the charge density and electroosmotic flow is the dominate driving force in this system). Previous work shows that a mixture of both isomers of coproporphyrin and uroporphyrin can be separated in a single run using BSA as the run buffer additive with inner treated capillaries, since the electrophoretic mobility is the dominate driving force and the negative charge on uroporphyrin molecule is two times that of the coprophyrin molecule [E11]. However, the separation of a mixture of the six urinary porphyrins was unsuccessful. In a micelle-BSA run buffer, if the equilibrium between the aqueous phase and BSA is neligible when compared to the equilibrium between the aqueous phase and the micelle, the retention mechanism is partly dependent on the behavior of the solute in the micellar solution. The rate of exchange between the micelle and BSA is fast enough to enhance the retentivity of the bile salt micelle to incorporate the hydrophilic molecules, while still limiting the resolution of the more hydrophilic uro-isomers. The resolution (R_s) between the two adjacent peaks of copro- and hexa-porphyrin isomers is given by the traditional MEKC equation [E8]

where t_0 is measured with acetone and $t_{Mc\text{-}BSA}$ is measured with Sudan III, the ratio

$$R_s = \frac{N^{1/2}}{4} \left(\frac{\alpha - 1}{\alpha}\right) \left(\frac{k_2'}{k_2'+1}\right) \left(\frac{1 - t_0/t_{mc}}{1 + (t_0/t_{mc})\, k_1'}\right) \qquad (6)$$

of t_0 to $t_{Ms\text{-}BSA}$ is approximately 0.35. Thus, the R_s for coproporphyrin isomers is calculated to be approximately 1.52 and approximately 1.57 for hexaporphyrin isomers.

Similar results were obtained for the SDS-BSA run buffer (Figure 4-2-4). The peak shapes remained nearly the same as compared with the SDS run buffer, selectivity improved, and more importantly, solubility of the solutes increased as a result of the SDS-BSA run buffer exhibiting a pH 4 units lower than the SDS run buffer. The efficiency of the separation decreased with increasing concentrations of BSA. BSA was found to be extremely stable in a taurodexyocholate run buffer for a period of several weeks but was found to precipitate in an SDS run buffer in only a week. This is not suprising since SDS is an efficient detergent for denaturing BSA, whereby the tertiary structure or folding structure of BSA is destroyed [E12].

The major limitation of the system is that at a fixed molar ratio of the micelle to BSA, the resolution can be improved by increasing the concentration of the run buffer and the column temperature, but at the expense of increasing current caused by increasing ionic strength. Figure 4-2-6 and 4-2-7 show the influence of field and concentration of TDCA or TDCA-BSA on the current. Similarly, a direct relationship between current and temperature is found at a rate of $\sim 5\ \mu A/10C^{o}$ in the range of 25 - 55C°. Although the terteriary structure of the protein may not be an important factor in the retention mechanism due to BSA acting primarily as a supporting medium (in the case of SDS), the performance of separation is still influenced by pH. The optimum pH was determined to be in the range of 7.2 to 7.6 and is dictated by the nature of the protein, which is similar to a previous study using BSA affinity CE [E4]. At a pH

greater than 8.5, precipitation occurs in the SDS-BSA run buffer, while the protein is quite stable in the TDAC-BSA run buffer below pH = 10. Table 4-2-2 shows that the average limit of detection was found to be approximately 1.7 μM ($\sim$ 5 fmol, S/N=3) in the bile salt micelle-BSA buffer system which was about 8% higher than in the SDS-BSA buffer system ($\sim$ 1.1 μmol/or $\sim$ 4 fmol). It is because the "baseline" appeared to be more noisy in the bile salt micelle -BSA buffer system as mentioned above. The reproducibility of migration time and peak areas was very similar in both the buffer systems (Table 4-2-2).

CONCLUSION

It has been demonstrated that a mixed miceller and BSA buffer is very useful system, and although the characteristics of the MEKC system have been preserved, the electrophoretic performance of the system has been improved via modification of the run buffer with BSA. Using BSA as a run buffer modifier in micellar electrokinetic chromatography can significantly improve separation efficiency, and increase sample solubilization via pH changes of a run buffer.

Table 4-2-1 The k' values in different systems.

Porphyrin	k'(1)	k"(2)	k'''(3)
Copro III	3.40	----	----
Copro I	2.39	3.43	1.35
Meso	0.32	0.12	1.37
Penta	1.65	0.91	0.56
Hexa III	1.32	0.88	0.38
Hexa I	1.13	0.78	0.29
Hepta	1.09	0.74	0.27
Uro	1.03	0.72	0.26

(1) in 6 mM sodium borate-phosphoric acid (SBP) buffer (pH=7.4) containing 40 mM sodium taurodeoxycholate-0.013 mM BSA.

(2) in 10 mM SBP buffer (pH=7.4) containing 50 mM SDS-0.015 mM BSA.

(3) in 15% methanol of 20 mM CAPS buffer (pH=11.0) containing 100 mM SDS.

Table 4-2-2 The Relative Standardard Deviation (%) on the Reproducibility of Migration Time and Peak Areas.*

Porphyrin	(1) n=5		(2) n=5	
	Migration time	Peak area	Migration time	Peak area
Copro III	0.29	2.91	----	----
Copro I	0.30	2.87	0.35	2.13
Meso	0.16	3.19	0.28	3.10
Penta	0.31	2.54	0.11	2.07
Hexa III	0.21	3.21	0.15	2.42
Hexa I	0.22	3.52	0.14	2.38
Hepta	0.35	3.83	0.25	2.93
Uro	0.38	4.15	0.27	2.86

* Measured on sequential injections over ca. 2h period for n=5.

(1) Buffer condition was the same as in Table 4-2-1 (1); (2) Buffer condition was the same as in Table 4-2-1 (2).

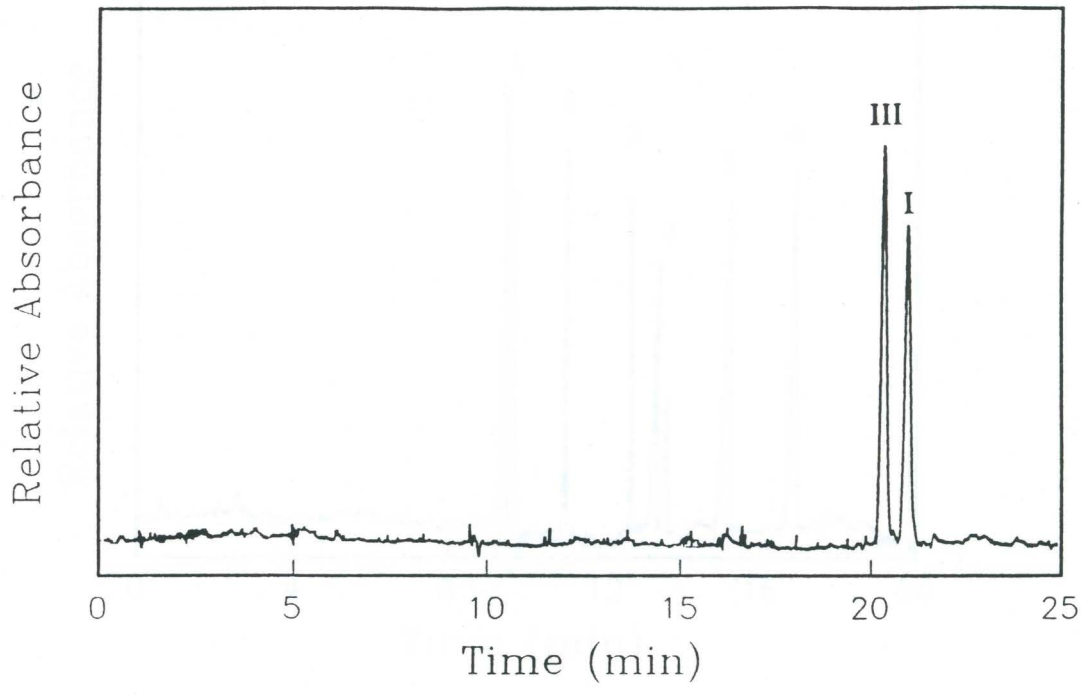

Figure 4-2-1 Electropherogram of coproporphyrin III (12.5 μM) and I (10μM) in 50mM TDCA-6 mM borate-H_3PO_4, pH = 8.0, 5% butanol and 10% methanol (v/v) added. 18 kv.

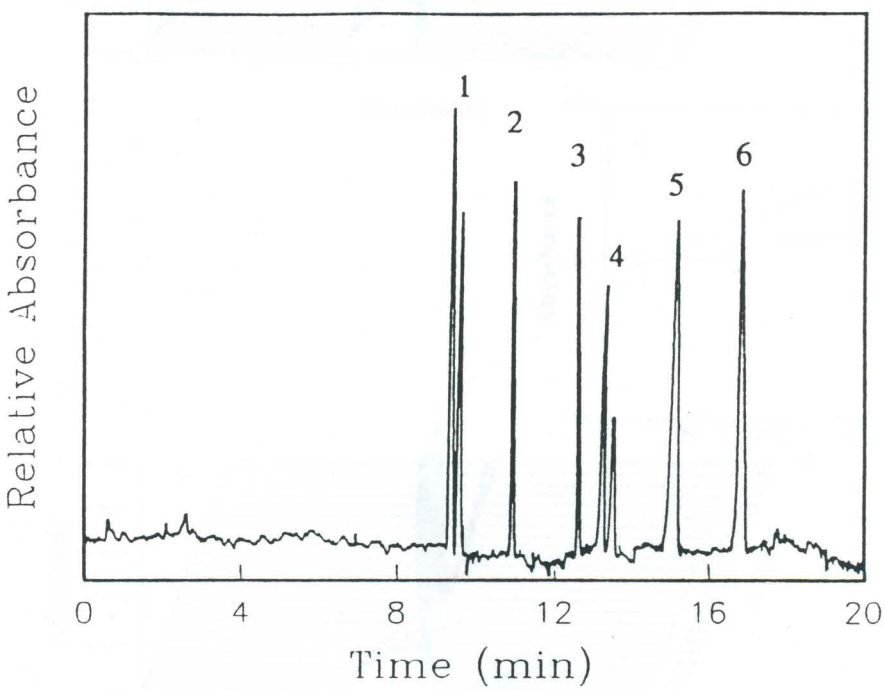

Figure 4-2-2 Electropherogram of urinary porphyrins: 1. copro (III and I)-, 2. penta-, meso-, 4. hexa (isomers)-, 5. hepta- and 6. uro-porphyrin (10 μM) in 40 mM TDCA-0.012 mM BSA and 6 mM borate-H_3PO_4 , pH= 7.4. 18 kv.

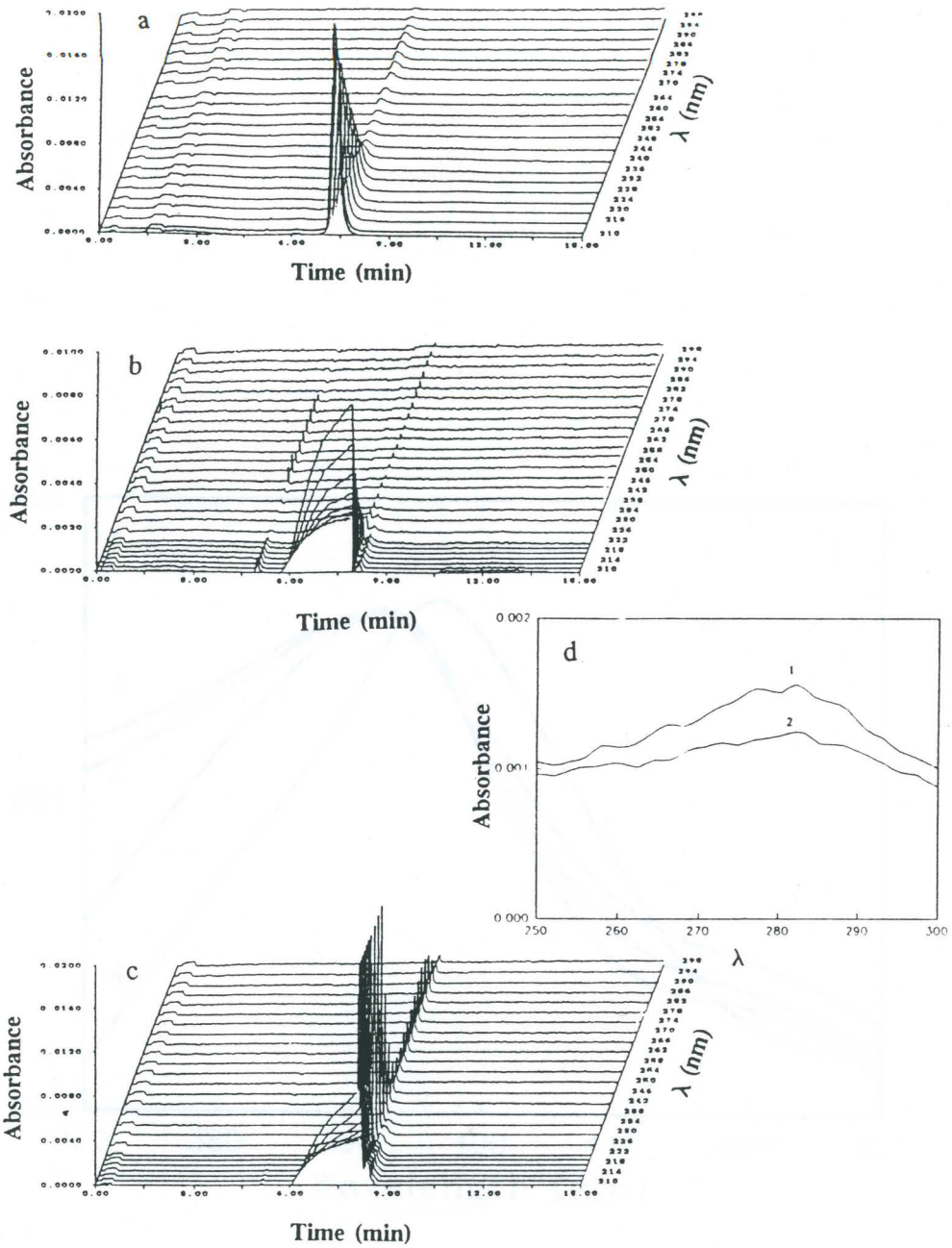

Figure 4-2-3 Electropherograms of (a) 0.015 mM BSA, (b) 50 mM TDCA, (C) a mixture of 50 mM TDCA-0.015 mM BSA and (D) UV spectra of (a) as (1) and (c) as (2) in 10 mM borate-H_3PO_4 , pH= 7.4. 16.5 kv.

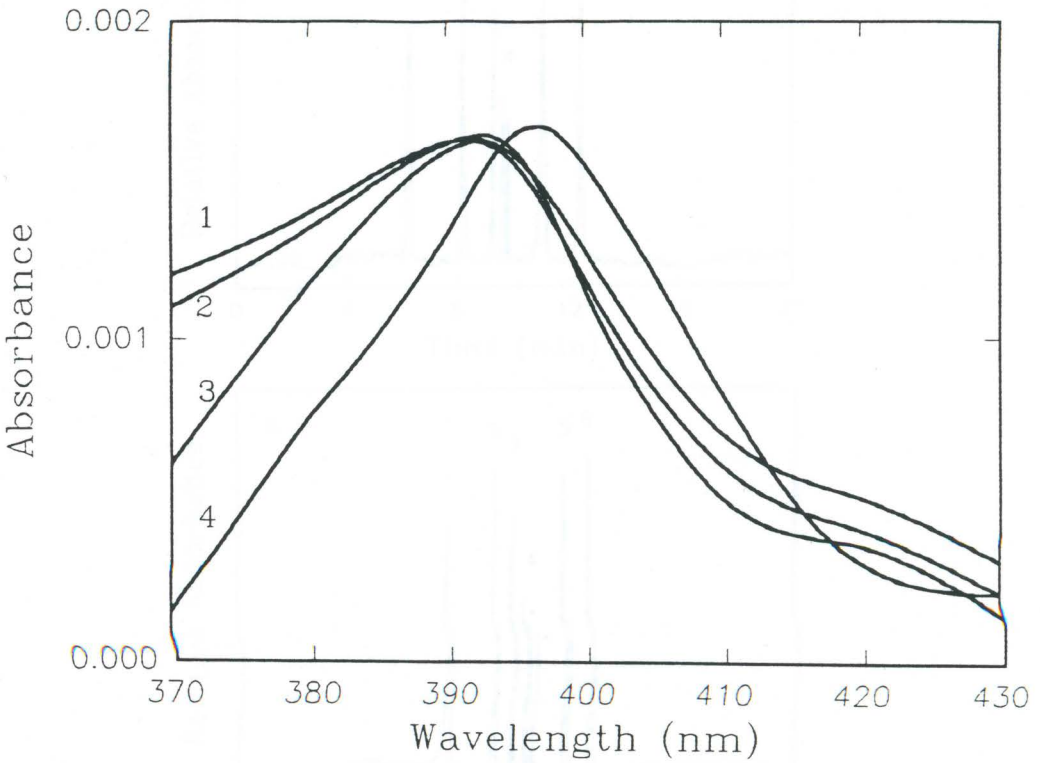

Figure 4-2-4 Spectrum of coproporphyrin III in (1) 50 mM TDCA, (2) 10 mM borate-H_3PO_4 , (3) 50 mM TDCA-0.015 mM BSA and (4) 0.015 mM BSA, pH= 7.4.

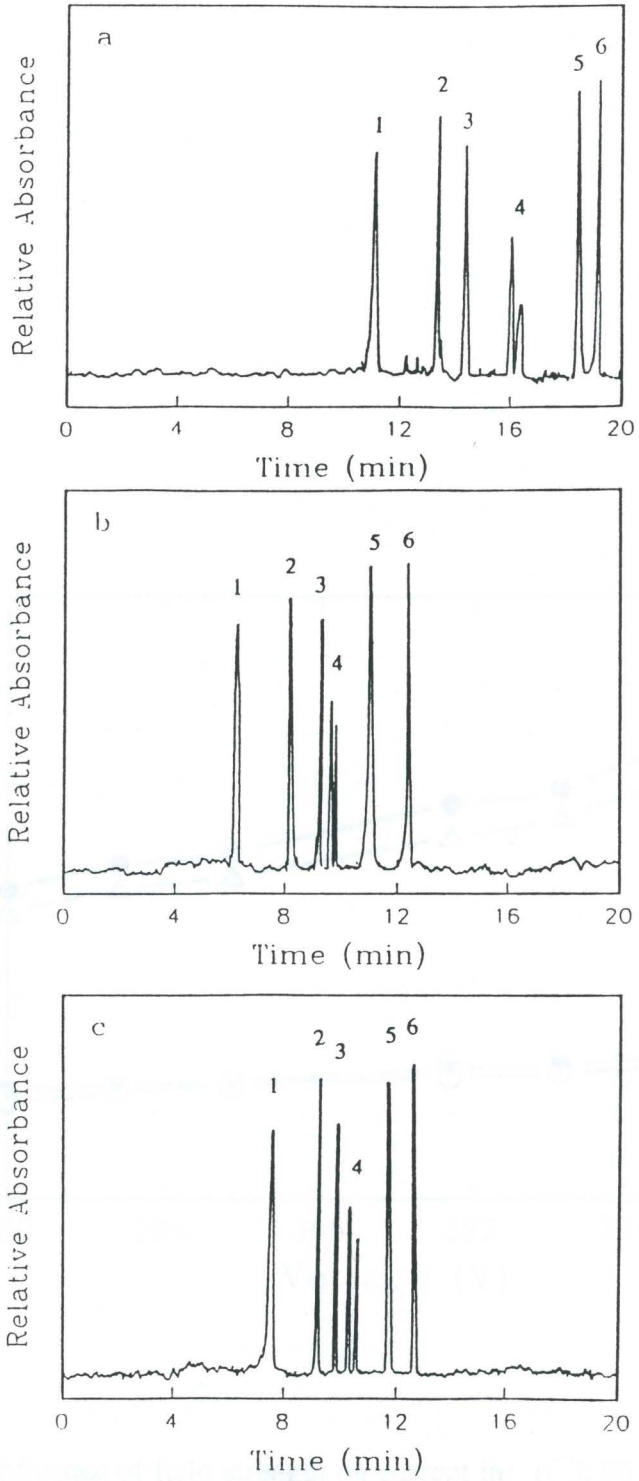

Figure 4-2-5 Electropherograms of urinary porphyrins in (a) 100 mM SDS-20 mM CAPS, 15% methanol (v/v) added, pH= 11, (b) 25 mM SDS-30 mM TADC in 6 mM borate-H_3PO_4, pH= 7.8, 3% butanol added and (c) 50 mM SDS-0.015 mM BSA in 10 mM borate-H_3PO_4, pH=7.4. 18 kv.

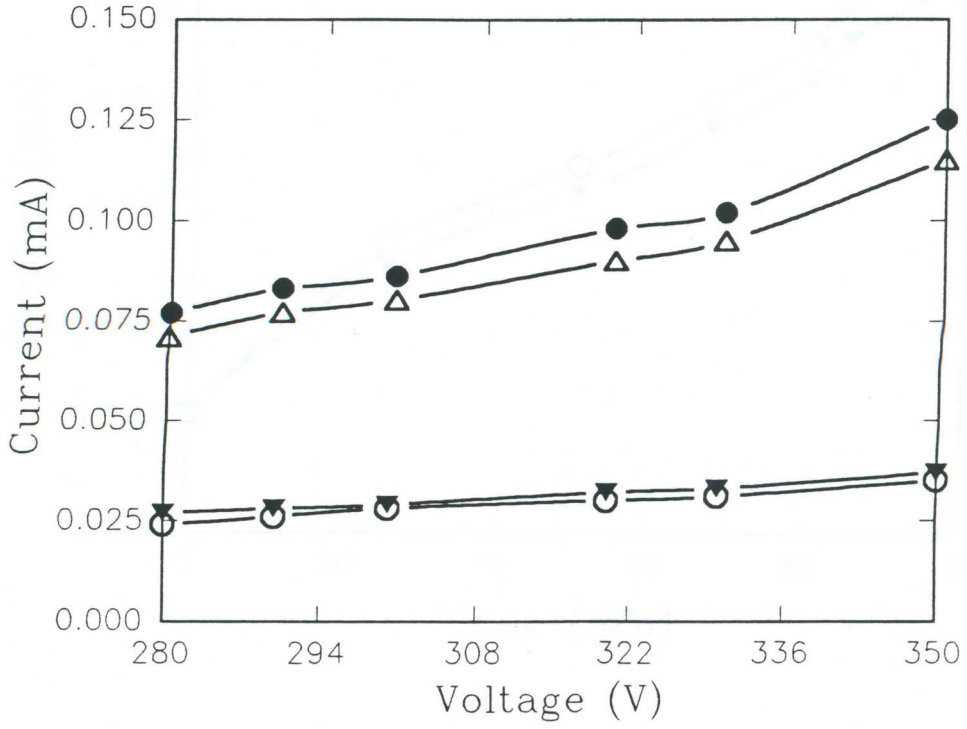

Figure 4-2-6. Influence of field strength on current in: (◯) 50 mM TDCA in 10 mM borate-H_3PO_4 , (▵) 50 mM TDCA-0.015 mM BSA in 10 mM borate-H_3PO_4 , (▾) 0.015 mM BSA in 10 mM borate-H_3PO_4 and (◯) 10 mM borate-H_3PO_4 , pH= 7.4..

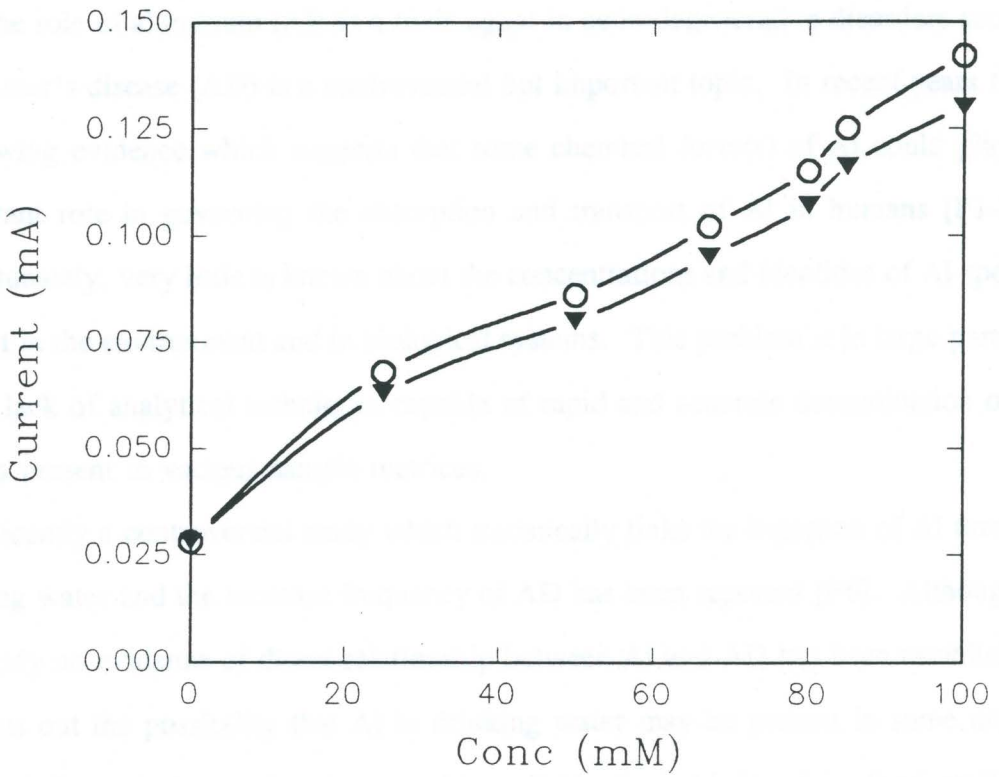

Figure 4-2-7. Influence of concentration of TDCA on current in: (◯) TDCA only and (▾) with 0.015 mM BSA in 10 mM borate-H_3PO_4 buffer, pH= 7.4. Field strength: 300v/cm.

CHAPTER 5 SPECIATION OF ALUMINUM USING CAPILLARY ZONE ELECTROPHORESIS WITH INDIRECT UV DETECTION

INTRODUCTION

The role of aluminum (Al) as a toxic agent in neurodegenerative disorders such as Alzheimer's disease (AD) is a controversial but important topic. In recent years there is growing evidence which suggests that some chemical form(s) of Al could play an important role in governing the absorption and transport of Al in humans [F1-F5]. Unfortunately, very little is known about the concentrations and identities of Al species present in the environment and in biological systems. This problem is in large part due to the lack of analytical techniques capable of rapid and accurate determination of Al species present in various sample matrices.

Recently a controversial study which statistically links the ingestion of Al through drinking water and the increase frequency of AD has been reported [F6]. Although in this study no evidence of direct relationship between Al and AD has been established, it points out the possibility that Al in drinking water may be present in some unique chemical form(s) that makes it more bioavailable than Al found in food stuffs or medications. In this regard it is interesting to note that among the potential inorganic ligands normally present in water, equilibrium calculations suggested that only the fluoride ion will significantly affect Al speciation [F7]. The distribution of mononuclear fluoroaluminum species, e.g., AlF^{2+}, AlF_2^+, AlF_3 and AlF_4^-, in water is of particular interest since some of these monomeric Al species have been postulated to facilitate the transport of hydrolyzable Al species through hydrophobic membranes

and/or demonstrated to possess properties which alter biochemical pathways [F8].

Early analytical methods employed for Al speciation mainly involved some type of indirect method [F9]. The key step in all these methods was the use of cation-exchange columns to separate the labile monomeric (inorganic) from the non-labile monomeric (organic) fractions. Based on the concentration of the total monomeric Al, the labile monomeric concentration can then be calculated using thermodynamic-based speciation models. Recently direct determination of inorganic as well as organic Al species have been shown to be possible using ion chromatography (IC). For example, Bertsch and Anderson [F10] have demonstrated that fluoro- oxalato-, and citratoaluminum complexes can be separated and quantitated by IC, and that excellent quantitative agreement between predicted species concentrations (calculated from thermodynamic speciation model) and those determined by IC were obtained under various experimental conditions. More recently, Jones [F11] has applied an IC technique for the speciation of Al in reservoir and drinking water samples. In these studies major disadvantages of the use of IC methods for Al speciation included their inabilities to separate various inorganic or organic Al species with good efficiency and to resolve mixtures of inorganic and organic Al species into discrete chromatographic peaks under isocratic conditions.

In recent years capillary zone electrophoresis (CZE) has been shown to be a highly efficient technique for the separation of small inorganic as well as organic cations and anions. For example, simultaneous separation of ~ 10 alkali, alkaline earth and lanthanide metal cations within a single run has been demonstrated using CZE [F12]; also, the simultaneous analysis of weak organic acid anions (oxalate and citrate) and inorganic anions (chloride, sulfate, phosphate and carbonate) in diluted urine has been

achieved within the same analytical run in a simple and rapid manner [F13]. On the other hand, the use of CZE for the efficient separation of metal species with good resolution has also been shown to be feasible. For example, the determination of the oxyanionic species of arsenic, i.e., arsenite and arsenate, in urine was demonstrated [F13] and the separation of a mixture of metal complexes present in electroplating solutions, i.e., $Fe(CN)_6^{4-}$, $Fe(CN)_6^{3-}$, $Cu(CN)_4^{3-}$ and $Zn(OH)_4^{2-}$ were also reported [F14].

In this chapter the separation performance of CZE for the speciation of fluoro- and oxalatoaluminum complexes present in aqueous solutions was evaluated. Detection was performed using indirect absorption method with a background electrolyte containing imidazole as the UV absorber, which was first used by Beck and Engelhardt [F15] for the rapid CZE determination inorganic cations and aliphalic amines with excellent detection limits and separation efficiencies. Furthermore, the stability of Al species during CZE separation was examined by comparing measured and predicted concentration values (via the thermodynamic speciation model: SOILCHEM) obtained for the various fluoro- and oxalatoaluminum complexes and the uncomplexed Al under various experimental conditions.

EXPERIMENTAL

Chemical and Materials Aluminum nitrate, sodium fluoride, sodium oxalate and imidazole were analytical grade and purchased from J. K. Baker (Phillipsburg, NJ, USA) or Sigma (St. Louis, MO, USA). Doubly distilled deionized water obtained from a Barnstead Nanopure System (Dubuque, IA, USA) was used for the preparation of all buffer and sample solutions. Polyimide-coated fused-silica capillary with 75 μm i.d.

and 360 μm o.d. was obtained from Polymicro Technologies (Phoenix, AZ, USA).

Buffer and sample Solutions *All buffer solutions were prepared with a background electrolyte containing 5 mM of imidazole. Sample solutions were prepared by adding* solution containing the ligand of interest to an appropriate volume of $Al(NO_3)_3$ standard solution in a 100-ml polyethylene (PE) volumetric flask such that the final Al concentration was 0.25 mM. The pH of the buffer and sample solutions were adjusted with small amounts of 1 M sulfuric acid. Prior to use all solutions were filtered through a 0.45 M membrane filter and stored in the PE bottles to age for a minimum period of 24 h.

Instrumentation A home-built CZE instrument was used for all separations. An acrylic box with a safety-interlocked door designed to prevent operator contact with high voltage contained the Speelman voltage source (Model CZE 1000/30PN, Plainview, NY, USA) and a Linear Instrument UV/Vis absorbance detector (Model 204, Reno, NV, USA) which has been modified for on-line detection at 214 nm. Contact with solution was made via platinum electrodes. All CZE separations were carried out using 350 V/cm field strength. Samples were injected hydrodynamically at the anode (positive polarity) by raising the sample solution reservoir to a height of 10 cm for 10 s. Data were recorded using a Chromjet integrator (Spectra Physics, San Jose, CA, USA).

Capillary Preparation Capillary length was 45 cm with a detection window made by burning off 2mm of the polyimide coating at approximately 35 cm from the anode end of the capillary. Capillaries were washed with 1 N NaOH for 30 min, followed by rinsing with the buffer solution for 1 h and equilibration with the buffer solution overnight.

Speciation Calculations The theoretical species concentrations of Al in the sample solutions was calculated by utilizing the SOILCHEM program: an improved version of the thermodynamic geochemical speciation model-GEOCHEM [F16].

RESULTS AND DISCUSSION

Figure 5-1(a) shows the CZE separation of a standard solution of $Al(NO_3)_3$ using a background electrolyte buffer containing 5 mM imidizole at pH 3.5, and two sharp and well-defined peaks can be observed in the electropherogram. The early peak which appears at a migration time of ~ 3.5 min can be assigned to the "free" Al ion (Al^{+3}) since this species predominates in aqueous solution at pH less than 5. This positively-charged species would be expected to migrate faster toward the cathode (or detector) when compared to the predominant negatively charged solute present in the sample solution: NO_3^-, which appears as an "inverted" peak at a migration time of ~ 6.5 min. Appropriate amounts of nitric, hydrochloric and sulfuric acids were added to the buffer and sample solutions for pH adjustments and it was found that separation performance was dependent on the type of acid used. Sulfuric acid was found to provide the best resolution for the CZE separation of various Al species, *vide infra*, but it is not clear at this time why this is the case. It should be noted that based on thermodynamic calculations, the SO_4^{2-} ion could interact with the Al ion to form sulfatoaluminum complexes in the sample solutions. However, by adding a relatively large amount of SO_4^{2-} to the Al standard solutions (mole ratio SO_4: Al = 20:1), we found no significant difference in the retention time or peak area of the free Al ion peak as shown in Figure 5-1(a). This observation suggests that any sulfatoaluminum complexes formed in the sample solution are likely to exist as weak, electrostatic outer-

sphere complexes and are apparently readily dissociated during CZE separation. Similar observations have also been reported for the separation of sulfatoaluminum complexes using IC [F10].

Figure 5-1(b) shows that with the addition of F (as NaF) into the Al standard solutions, the peak area of the free Al ion peak was reduced significantly and additional peaks were produced in the CZE electropherogram. The major peak which appears at ~ 2.4 min can be assigned to Na^+ (comfirmed by the injection of NaF without the presence of $Al(NO_3)_3$). On the other hand, assignments of the two smaller peaks which appear at ~ 3.2 and 3.8 min, respectively, are not as straightforward. Table 5-1 compares experimental data and theoretical values generated by the SOILCHEM program. At a F/Al ratio of 0.5:1 and sample and buffer pH = 3.5 (experimental conditions of Figure 5-1 (b)), the predicted concentration values of Al^{3+}, AlF^{2+} and AlF_2^+ are shown to be in good agreement with experimental measurements, which suggests the formation of AlF^{2+} and AlF_2^+ species upon the addition of NaF into the Al standard solution. Furthermore, it was found that the total integrated areas of the free Al ion as shown in Figure 5-1 (a) and the cluster of three adjacent peaks (between 3.0 and 4.0 min) as shown in Figure 5-1 (b) are similar. These results, along with the fact that no interference peaks were obtained from the CZE separation of NaF alone, suggest that the two smaller peaks which are centered at ~ 3.2 and 3.8 min in Figure 5-1(b) are probably a result of a redistribution of Al between species of differing positive charges upon the addition of NaF and assignments of AlF^{2+} and AlF_2^+ could be made for these two additional peaks. In this case, it would be reasonable to assign AlF^{2+} as the early peak which appears at ~ 3.2 min since it possesses a higher positive charge and would be expected to migrate faster toward the detector when compared to AlF_2^+,

which was assigned as the latter peak appearing at ~ 3.8 min. However, using the same argument, it would be unreasonable to expect the Na^+ to migrate faster than AlF^{2+} as shown in Figure 5-1(b) and, similarly, the early appearance of AlF^{2+} when compared to the free Al ion (a positively triple charge species which appears at ~ 3.5 min) is not expected.

In an attempt to understand the migration order of the assigned peaks as shown in Figure 5-1(b), it is important to note that the mobility (or migration time) of a particular ion in CZE separation is dependent not only on the charge but also the size of the ion [F17]. For electrolytes dissolved in aqueous solutions the number of water molecules associated with the ions during their movement through the solution is likely to influence their overall size and mobility. Many experiments have been devised in attempts to determine the hydration of ions in aqueous solutions [F18,F19]. Unfortunately, the solvation (or hydration) number of many ions is not known with certainty. However, it is interesting to note that under the influence of intense electrical forces, the hydration numbers of NaCl and $AlCl_3$ have been reported to be 7 and 31, respectively [F18]. It is possible that under the experimental conditions described in Figure 5-1(b), the mobilities of the various ions are influenced by the degrees of hydration. The hydration number of the uncomplexed Al ions may be higher than that of Na^+ and AlF^{2+}, thus leading to an increase in the size and/or decrease of the charge of the free Al ion and resulting in a longer migration time.

Table 5-1 and Figure 5-2 show that good agreement between measured and predicted values extend over a range of pH and mole ratio values when the pH of the sample and background electrolyte buffer were matched. On the other hand, when the pH of the sample and buffer was unmatched, the experimental values of uncomplexed

Al and complexed fluoroaluminum species showed minimal changes and also exhibit good agreement with thermodynamic calculated values over a pH range of about one order of magnitude. These results suggest that these fluoroaluminum species exhibited good kinetic stability and maintained their integrity, i.e., minimal redistribution during CZE separation, under the present experimental conditions. The average limits of detection (LOD) for uncomplexed Al and complexed fluoroaluminum species was found to be about 0.3 ppm (S/N = 3) and the average relative standard deviations (n = 8) for mobilities and peak areas were < 0.5% and 4%, respectively. The relationship between peak area and concentration was linear in the range 0.3 to 15 ppm with the regression equation: A (peak area) = 1.04×10^4C (concentration) + 1.09×10^3. The correlation coefficient (r^2) was 0.9989 (n = 8).

Figure 5-3 shows the CZE separation of a sample solution containing mixed F and oxalate ligands (mole ratio Al:F:oxalate = 1:0.5:1). When compared to Figure 1(b), an additional peak which appears at ~ 4.0 min was produced with the presence of oxalate anion. Similarly, a peak which appears at ~ 4.0 min was also produced upon the addition of oxalate into Al standard solutions without the present of F. Figure 5-4 compares the experimental and thermodynamic calculated values of uncomplexed Al and monooxalatoaluminum species at varying mole ratio of oxalate and Al (in the absence of F) and indicates good agreement for these particular species, suggesting that that additional peak at ~ 4.0 min probably arose from the formation of monooxalatoaluminum species. The relatively long migration time obtained for this organic Al species is reasonable since it would have the smallest charge density due to its single positive charge and relatively large size (neglecting hydrating number), thus leading to lower mobility relative to the other positively charged species present in the

sample solution. Figure 5-3 shows that good resolution can be obtained for the simultaneous separation of inorganic and organic Al complexes within a single CZE run during a period of less than 5 min. This capability demonstrates that CZE possesses a distinct advantage over IC for the separation of sample solutions containing these particular mixed inorganic and organic ligands. Using IC only the uncomplexed Al and AlF^{2+} produced discrete chromatographic peaks while AlF_2^+ and monooxalatoaluminum species were observed to co-elute as a single peak under isocratic conditions [F10].

CONCLUSION

In summary, this work demonstrates that CZE can be used as a powerful technique for the rapid and efficient separation of fluoro- and oxalatoaluminum species present in aqueous solutions. More research is needed to examine the feasibility of using CZE for the separation of other small inorganic and organic Al complexes, as well as protein-bound and macromolecular Al species. In particular, experimental factors which affect the stability or integrity of the Al species during CZE separation and the effects of potential interference ions present in real samples which might form complexes with alumininum should be investigated in detail by comparing experimental and theoretical values.

Table 5-1 Measured (CZE) and Predicted (SOILCHEM-SOIL) Concentrations of Uncomplexed Al and Complex Fluoroaluminum Species in Solutions of Varying F:Al Mole Ratios and pH Values.

		Al^{3+}			AlF^{2+}			AlF_2^+		
F/Al[a]	pH	CZE[b]	CZE[c]	SOIL	CZE[b]	CZE[c]	SOIL	CZE[b]	CZE[c]	SOIL
0.5:1	3.2	.143	.141	.127	.104	.101	.115	.003	.008	.005
	3.5	.129	.134	.132	.115	.111	.113	.006	.005	.005
	4.0	.135	.130	.122	.112	.114	.124	.003	.006	.004
	4.2	.132	.137	.130	.113	.108	.114	.005	.005	.006
1:1	3.2	.075	.073	.058	.138	.148	.144	.037	.029	.048
	3.5	.068	.069	.059	.150	.149	.145	.031	.032	.046
	4.0	.066	.069	.060	.155	.156	.148	.029	.025	.042
	4.2	.075	.069	.059	.139	.139	.147	.036	.041	.044

[a]Total Al concentration = 0.25 mM

[b]pH of the sample and buffer solutions was matched in the range of 3.2 to 4.2

[c]pH of the buffer was fixed at 3.5 and pH of the sample solutions was adjusted from 3.2 to 4.2.

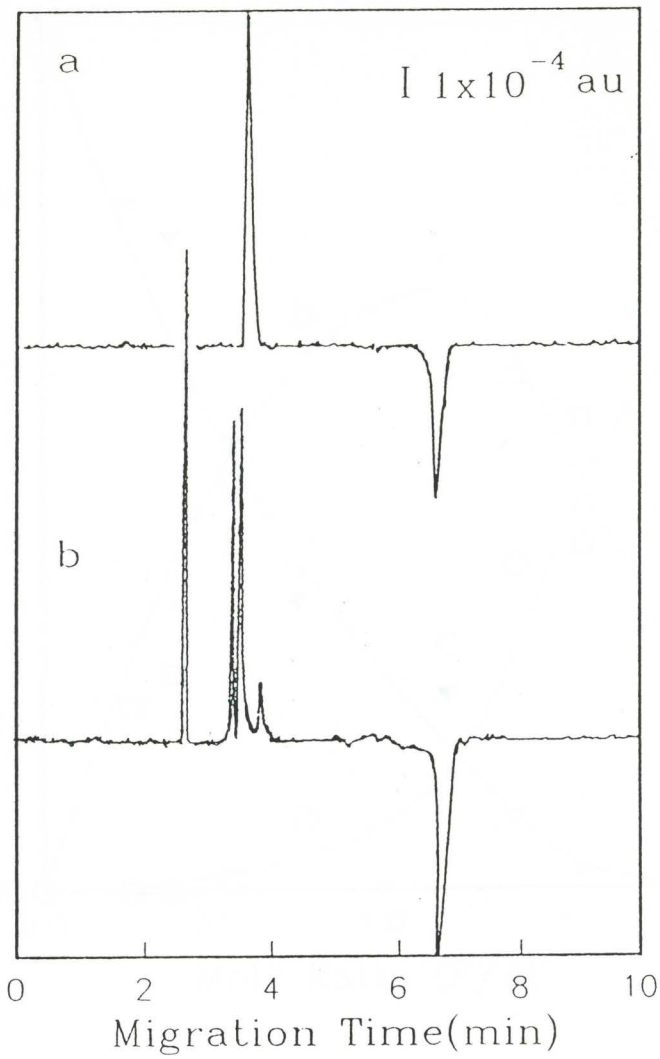

Figure 5-1 CZE electropherogram of a 0.25 mM $Al(NO_3)_3$ solution with (a) no F and (b) the addition of 0.12 mM of NaF. The pH of buffer and sample solutions was matched at 3.5.

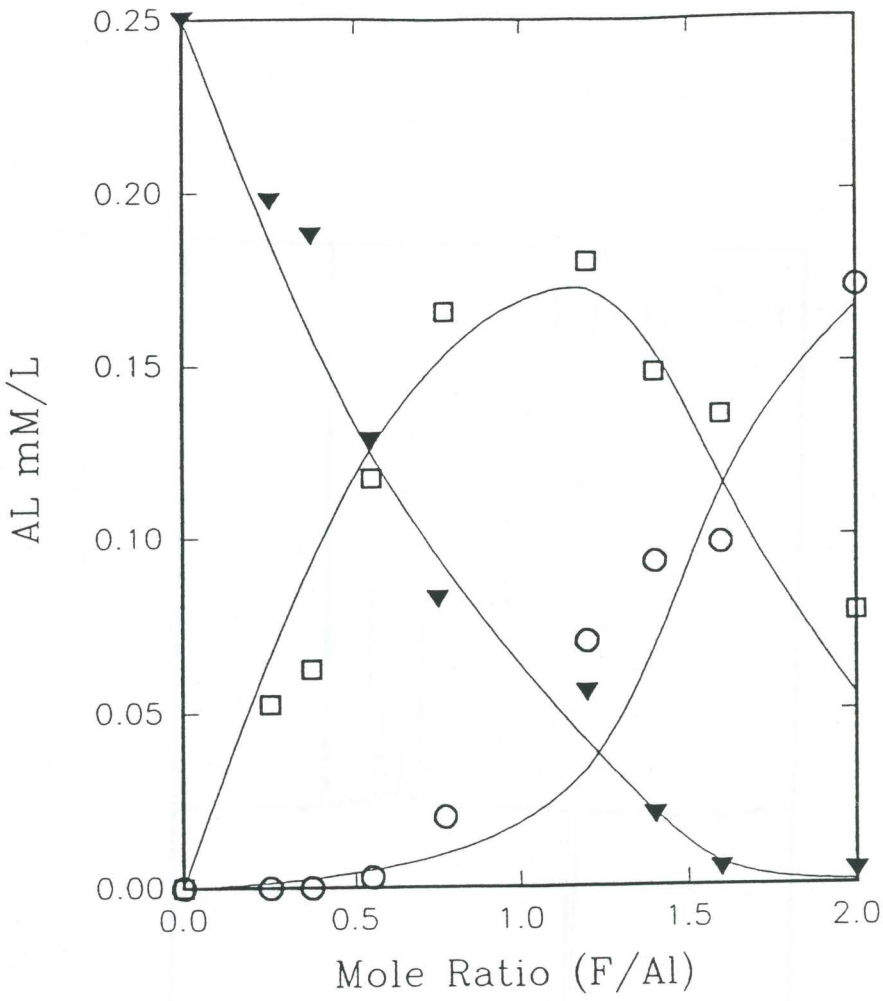

Fgure 5-2 Measured (symbols) and predicted (solid lines) concentrations of the uncomplexed and fluoro-complexed Al species at varying F:Al mole ratios with total Al concentration equal to 0.25 mM and pH of buffer and sample solutions equal to 3.5. ($\blacktriangledown = Al^{3+}$, $\square = AlF^{2+}$ and $\bigcirc = AlF_2^{+}$)

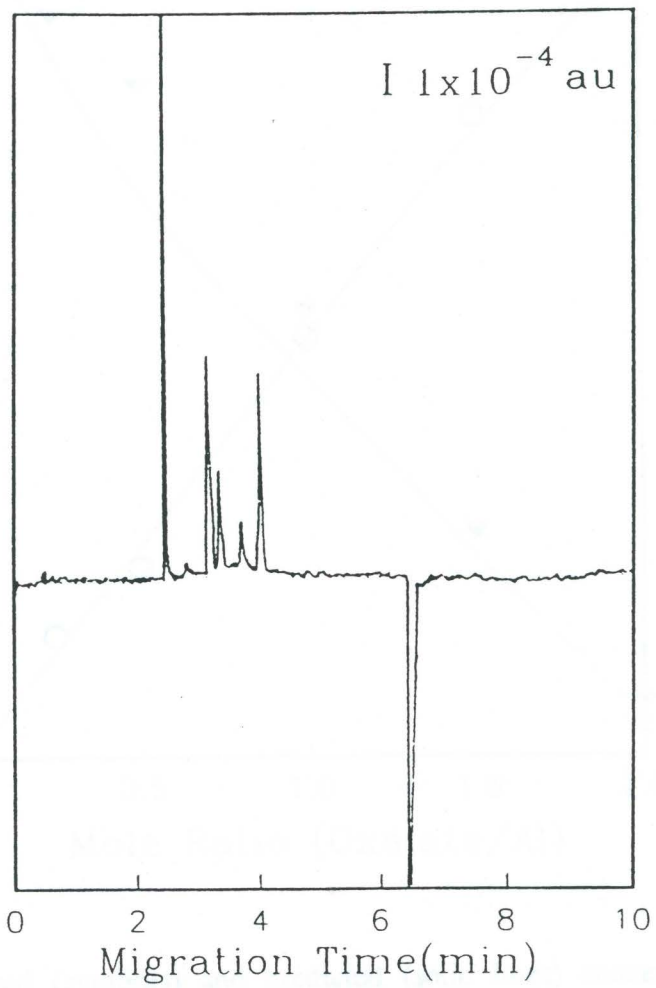

Figure 5-3 CZE electropherogram of a 0.25 mM $Al(NO_3)_3$ solution with the presence of 0.13 mM F and 0.25mM oxalate.The pH of buffer and sample solutions was matched at 3.5.

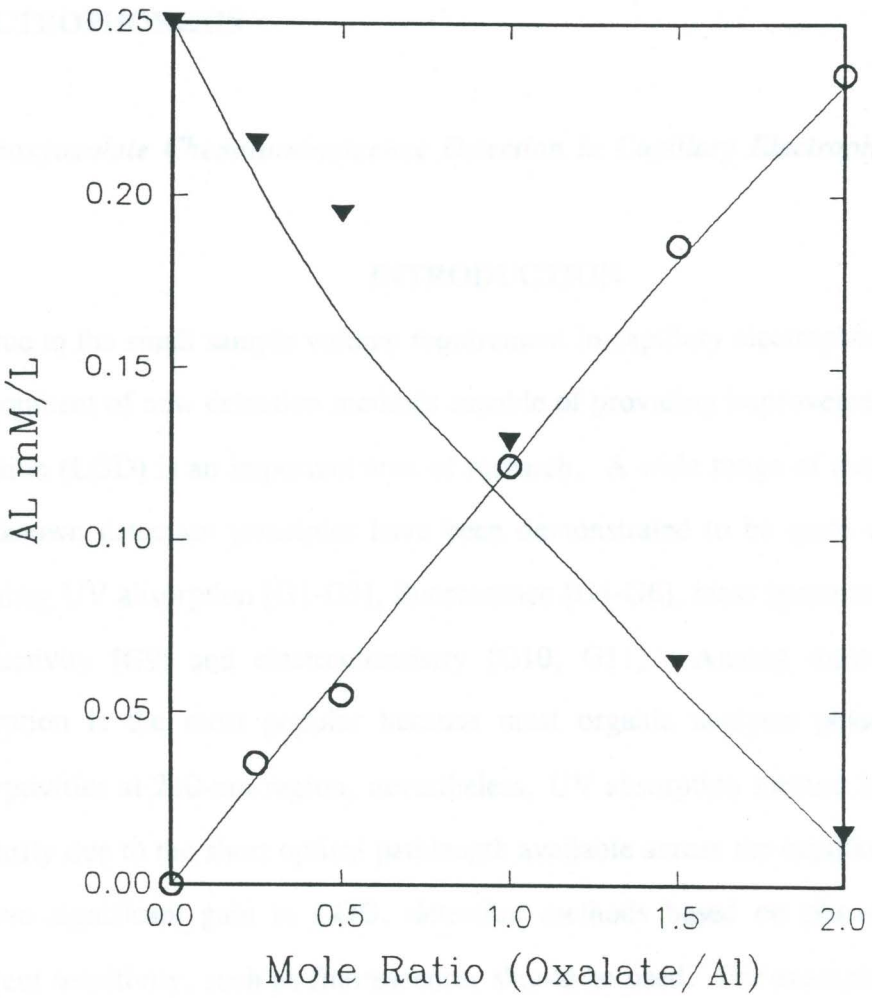

Figure 5-4. Measured (symbols) and predicted (solid lines) concentrations of the uncomplexed and monooxalato-complexed Al species at varying oxalate:Al mole ratios with total Al concentration equal to 0.25 mM and pH of buffer and sample solutions equal to 3.5. ($\blacktriangledown = Al^{3+}$, $\bigcirc$ = Al-oxalate^{+})

CHAPTER 6 IMPROVEMENT OF DETECIBILITY IN CAPILLARY ELECTROPHORESIS

I. *Peroxyoxalate Chemiluminescence Detection in Capillary Electrophoresis*

INTRODUCTION

Due to the small sample volume requirement in capillary electrophoresis (CE), the development of new detection methods capable of providing improvements in limits of detection (LOD) is an important area of research. A wide range of methods based on well-known detection principles have been demonstrated to be quite useful for CE, including UV absorption [G1-G3], fluorescence [G4-G6], mass spectrometry [G7,G8], conductivity [G9] and electrochemistry [G10, G11]. Among these methods UV absorption is the most popular because most organic analytes posses high molar absorptivities at 210-nm region; nevertheless, UV absorption method lacks sensitivity primarily due to the short optical pathlength available across the capillary column. To achieve significant gain in LOD, detection methods based on phenomena of high inherent sensitivity, such as fluorescence, should be used. For example, using a laser for fluorimetric excitation, detection of zeptomole (10^{-21} mol) quantities of analytes has been reported [G5,G6]. However, laser-induced fluorescence methods posses some disadvantages, such as the presence of significant background noise, e.g., Rayleigh and Raman scattering generated by the high-intensity laser, and the high price and complexity of most laser systems. These particular disadvantages could be, however, largely overcome by performing the fluorescence measurement via chemical excitation,

i.e., the generation of fluorescence in which the electronically excited state of the molecule is provided by a chemical reaction (chemiluminescence).

Chemiluminescence (CL) has been shown to be a highly sensitive method for detection in conventional [G12,G13] and microcolumn [G14] high-performance liquid chromatography (HPLC). Recently the feasibility of using CL as a detection scheme in CE has been demonstrated as well using the luminol CL system for sensitive detection of two luminol derivatives [G15]. It should be noted that, however, among the most common CL system, e.g., luminol, lucigenin and peroxyoxalate (PO)-CL reaction, the PO-CL system has been most widely used for post column detection in HPLC [G16]. The popularity of the PO-CL reaction, which is based on the oxidation of oxalate derivative in presence of a suitable fluorophore, is in part due to its high quantum efficiency and, perhaps more importantly, its ability to excite a wide range of different fluorophores when compared to other CL systems. Although the use of organic solvents is required in most common applications of PO-CL detection in HPLC involving reversed-phase columns due to the low solubility and instability of most oxalate derivatives in aqueous solutions, the post-column addition of PO-CL reagents to the column effluent containing the fluorophores to generate CL emission can be achieved with excellent sensitivity while maintaining good separation performance under optimized experimental conditions [G17]. The involvement of mixed aqueous-organic phase solvent systems, however, could present some major difficulties in the use of PO-CL reaction as a detection scheme in CE due to, for example, the influence of organic solvents on the migration behaviors of the analytes, which are strongly dependent on their mobilities in the aqueous electrophoretic buffer, and the possible effect of high electric field strength on the stability of the PO-CL reagents [G18].

Camilleri et al. [G19] have recently demonstrated that CE separation of proteins and peptides followed by elution under pressure (dynamic elution) can be achieved with little loss of resolution, thus allowing the possible use of CE as a micropreparative technique. In this section a similar two-step approach, involving switching off the CE power supply at an appropriate time and connecting the capillary to a syringe pump to effect dynamic flow, was demonstrated for the post-column detection of analytes in CE using the PO-CL reaction. Using dynamic elution, potential problems associated with incompatibilities between mixed aqueous-organic solvent and electrically driven separation systems are avoided. The effects of dynamic flow-rate and PO-CL reagent concentration on the CL signal intensity and /or peak width were examined for the measurements of three dansylated (Dns)-amino acids. LOD obtained using the present PO-CL method were compared to those of UV absorption method.

EXPERIMENTAL

Chemicals

Bis-(2,4,6-trichlorophenyl)oxalate (TCPO) was prepared using the procedures described by Mohan and Turro [G20]. Dns-glycine, Dns-L-arginine and Dns-L-leucine were purchased from Sigma (St. Louis, MO). Hydrogen peroxide (30%) and all other chemicals were of analytical grade from Aldrich (Milwaukee, WI). TCPO was dissolved in ethyl acetate and hydrogen peroxide was diluted with acetonitrile. All buffer solutions were made with distilled and deionized water.

Apparatus

CE separation was performed on a in-house-built instrument consisting of an acrylic box designed with a safety-interlocked door to prevent operator contact with a + 30 kV

high-voltage power (Glassman High Voltage, Whitehouse Station, NY), which was connected to the buffer reservoirs with platinum electrodes to effect CE separation. For on-line UV absorption detection, a detection window was made by burning off a small section of the polyimide coating at 40 cm from the anodic end of the electrophoretic capillary (55 cm x 75 μm I.D. x 144 μm O.D.) purchased from Polymicrotech (Phoenix, AZ). Absorption of analytes which migrate pass the detection window was measured using a Spectra-100 UV-Vis detector (Spectra Physics, San Jose, CA) set at 210 nm. For post-column CL detection, a post-column reactor which consisted of various fused silica capillaries held within a Swagelock stainless-steel tee and a detection cell was constructed.

Fig. 6-1-1 shows a schematic diagram of the post-column reactor. One arm of the tee contained the electrophoretic capillary which was inserted into the reaction capillary (10 cm x 200 μm I.D.x 400 μm O.D.; Supelo, Bellefonte, PA) situated at the opposite arm of the tee. The tee was connected to the detection cell via an adaptor and both the electrophoretic and reaction capillaries were inserted into the detection cell through the inner core of a PTFE tubing (400 μm I.D. x 1.5 mm O.D.), which served to protect the thin and fragile wall of the fused silica capillaries. The reaction capillary extended from the tee through the entire length of the detection cell whereas the electrophoretic capillary terminated at a fixed distance near the center of the detection cell; outlet capillary with smaller dimensions (20 cm x 100 μm I.D. x 195 μm O.D., Polymicrotech) was inserted into the opposite end of the reaction capillary to create a restricted area adjacent to the terminating end of the electrophoretic capillary to allow for mixing of PO-CL reagents and column effluent containing analytes to occur within this post-column region. Two reagent capillaries (15 cm x 75 μm I.D. x 144 μm O.D.,

Polymicrotech) inserted into the central arm of the tee were used to deliver the PO-CL reagents (TCPO and H_2O_2) into the mixing area through the small gaps that exist between outer surface of the electrophoretic capillary and inner surface of the reaction capillary. Dynamic elution of electrophoretic buffer and transport of the PO-CL reagents under pressure were achieved using two Sage syringe pumps (Model 341 B; Orion, Boston, MA).

To detect CL emission generated within the post-column mixing region, a detection window on the reaction capillary was made by burning off 2 mm length of the polyimide coating. The CL emission was collected via one end of an optical fiber bundle: 61 cm long x 1.6 mm diameter with a numerical aperture of 0.55 and an acceptance angle of 68^0 (Part No. 77520; Oriel, Stratford, CT) situated directly above the detection window and, the other end of the fiber bundle was interfaced to the detection system. The CL emission was isolated by a 10-nm band-pass filter centered at 520 nm (Corion, Holiston, MA) and was detected using a photomultiplier tube (Model 9558 B; EMI, Plainview, NY) operated at voltage between 700 and 800 V. The photocurrent was fed to a picoammeter (Model 7080, Oriel) and the signal was recorded on an integrator (Chromjet, Spectra-Physics).

Procedures

The CE separations were performed with a 20 mM sodium borate buffer (pH 8.9). Dns-amino acid stock solutions were prepared by dissolving appropriate amounts of the analytes into the buffer solutions. After making serial dilutions to obtained the desired concentrations, the sample solutions were electrokinetically injected into the CE system at anodic end by applying 9 k for 5 s. The electrophoretic capillary was treated by purging with 0.05 M NaOH for about 0.5 h and rinsed with the run buffer for 2 h

before use.

The CE separation of analytes followed by dynamic elution was accomplished by first turning on the power supply at 16.5 k for 3.2 min. During this time, the syringe pump connected to the reagent capillaries was turned on momentarily to provide a fresh supply of PO-CL reagents into the post-column mixing region. After 3.2 min, both the reagent supply pump and high-voltage power supply were turned off. The anodic and cathodic ends of the electrophoretic capillary were then removed from buffer reservoirs and attached to a syringe pump and one arm of the tee as shown in Fig. 6-1-1, respectively. Immediately afterward, delivering of the PO-CL reagents was resumed and dynamic elution of the analytes was started by turning on the two separated syringe pumps that were adjusted to appropriate flow rates.

RESULTS AND DISCUSSION

One of the most important factors which limits detectibilities in PO-CL based HPLC systems is that without the presence of fluorescent analytes, a relative low background CL signal can be detected when the column effluent is mixed with the PO-CL reagents [G13,G21]. Recent evidence suggests that this background signal may arise from reaction intermediates and/or products of the PO-CL reaction, and its intensity can be influenced by various experimental factors [G17,G22]. We found that the flow-rate of the PO-CL reagents (TCPO and H_2O_2) affected the background signal intensity as follows: at 2.5 μl/min or lower, the background current was found to remain relatively constant at 2.5 nA and it increased by a factor of about 2 at flow-rates higher than 4 μl/min (dynamic flow-rate of the CE running buffer was kept at an optimum rate of 1.7 μl/min, see below). Using a flow-rate of 1.7 μl/min for both the CL reagents and

running buffer, Fig. 6-1-2a and b shows that the concentrations of TCPO and H_2O_2 which produced the highest CL intensity for the post-column detection of Dns-L-leucine were found to be 5 mM and 0.3 m, respectively.

A major concern in using the present approach is that after CE separation, peak broadening due to diffusion and/or other processes may occur, resulting in loss of resolution during the dynamic elution process. Fig. 6-1-3 shows the effects of flow-rate due to dynamic elution on the relative peak width (measured at baseline) of three Dns-amino acids after CE separation. When compared to the normalized peak width of these analytes separated by CE without the influence of dynamic elution and detected by UV absorption method (Fig. 6-1-3: relative peak width = 1, at flow-rate = 0), it can be seen that broadening effects were reduced significantly as a result of an increase in the flow-rate, with the peak widths approaching those obtained without dynamic elution after about 2 μl/min; however, it should be noted that in conjunction with decrease in peak broadening a loss in separation selectivity was found at higher flow-rates. Fig. 6-1-4 shows the effects of flow-rate due to dynamic elution on the relative CL intensity of three Dns-amino acids. It is clear that optimal CL intensity occurred at low flow-rates ($<$ 1.5 μl/min) and started to decrease significantly, in particular for Dns-L-leucine and Dns-glycine, at flow-rate higher than ca. 1.7 μl/min. Importantly the results obtained in Fig. 6-1-3 and 6-1-4 indicated that in choosing a flow-rate for dynamic elution of the three Dns-amino acids, a compromise has to be made between separation and detection performance, and it appears that the optimum flow-rates fall in the range between ca. 1.5 and 2.0 μl/min.

Using the optimized conditions that have been determined for the flow-rates and PO-CL reagent concentrations, the separation and detection characteristics of the three Dns-

amino acids after CE separation followed by dynamic elution and post-column PO-CL detection are shown in Fig. 6-1-5a. For comparison purposes, Fig 6-1-5b shows the CE separation and detection of the same Dns-amino acids without the influence of elution under pressure and using on-line UV absorption method. It can be seen that although the peak widths of the three analytes were broadened as a result of dynamic elution and post-column CL reaction (baseline peak widths increased by a factor of about 3 to 4 at a flow-rate of 1.7 μl/min as shown in Fig. 6-1-3), the separation of all the Dns-amino acids can still be achieved with baseline resolution. The advantage of the present method is in the improvement of LOD using the PO-CL system for sensitive detection, Table 6-1 shows an improvement factor of 1 to 2 order of magnitude in mass or concentration LOD was achieved for measurements of the three Dns-amino acids using the present method. Average relative standard deviation (n=3) on peak height for the three dansyl amino acids measured using the PO-CL method as shown in Fig. 6-1-5a was about 4.1 %.

CONCLUSION

In this study, the feasibility of using the PO-CL system for the post-column detection of analytes after CE separation followed by elution under pressure has been demonstrated. Clearly, more investigations are needed to optimize the various experimental factors which affect detection and separation performance using the present method. For examples, the use of deuterated running buffer may minimize the loss of resolution due to slower rate of analyte diffusion within the higher viscosity buffer solution [G19]; modifications of the volume and geometry of the detection cell and connecting hardware may lead to less dispersion and/or higher degree of mixing

between analytes and reagents; and also, the change in temperature, pH and the addition of catalyst and organic modifiers may affect CL efficiency and/or kinetics. Many of these factors have already been investigated in detail for the optimal determination of analytes in post-column HPLC systems involving the PO-CL reaction [G12,G17] and the knowledge gain in this area could be directed toward the improvements of separation and detection performance using dynamic elution and PO-CL detection in CE.

Table 6-1 COMPARISON OF CONCENTRATION AND MASS DETECTION LIMITS BETWEEN ABSORBANCE AND CHEMILUMINESCENCE DETECTION METHODS

Dns-Amino acids	LOD (S/N = 3)	
	UV absorption	PO-CL
Dns-L-Argenine	42 fmol (2.4 μm)	1.2 fmol (71 nM)
Dns-L-Leucine	32 fmol (2.3 μm)	1.0 fmol (69 nM)
Dns-Glycine	50 fmol (3.8 μm)	1.5 fmol (114 nM)

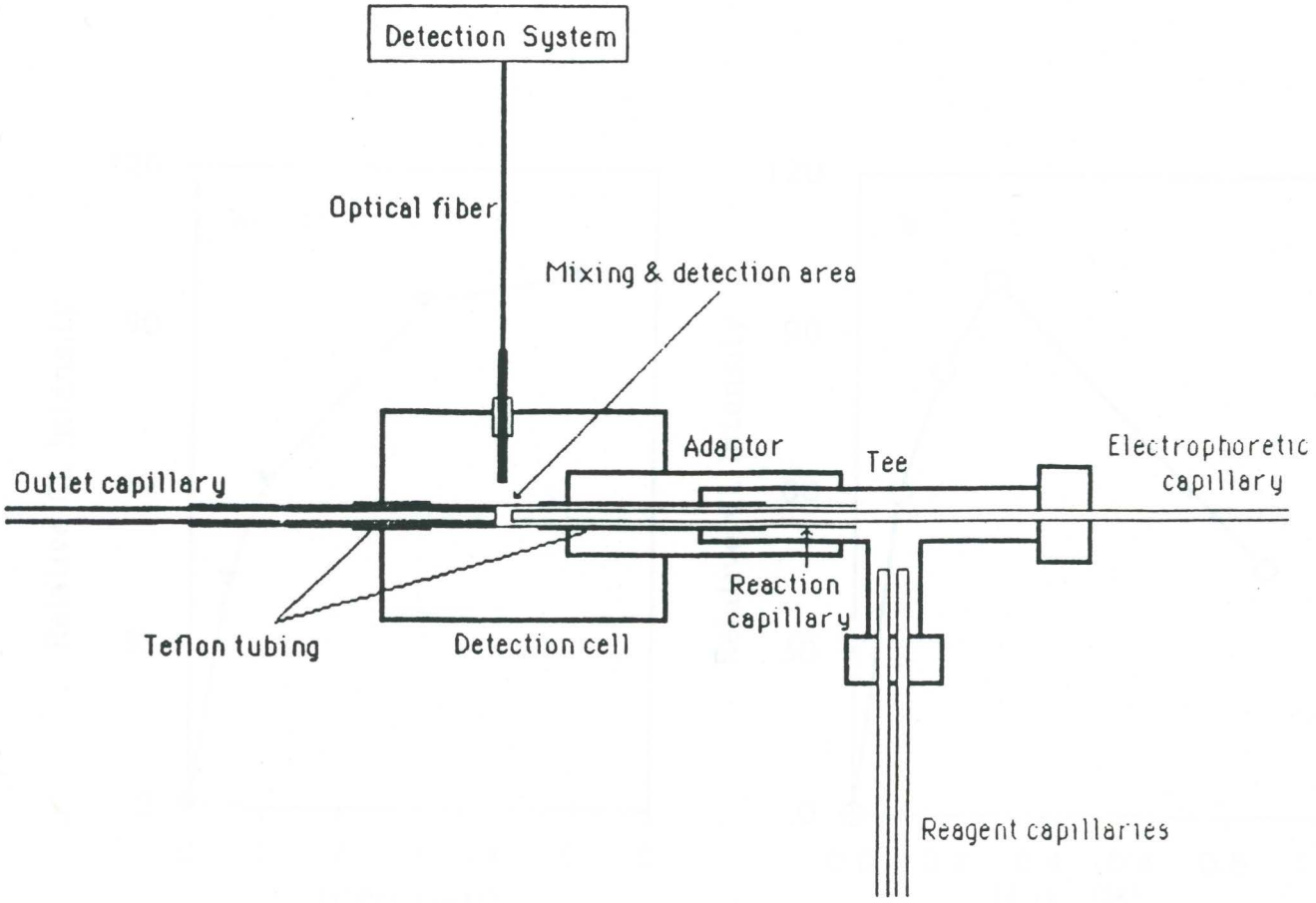

Figure 6-1-1. Cross-sectional view of the post-column reactor

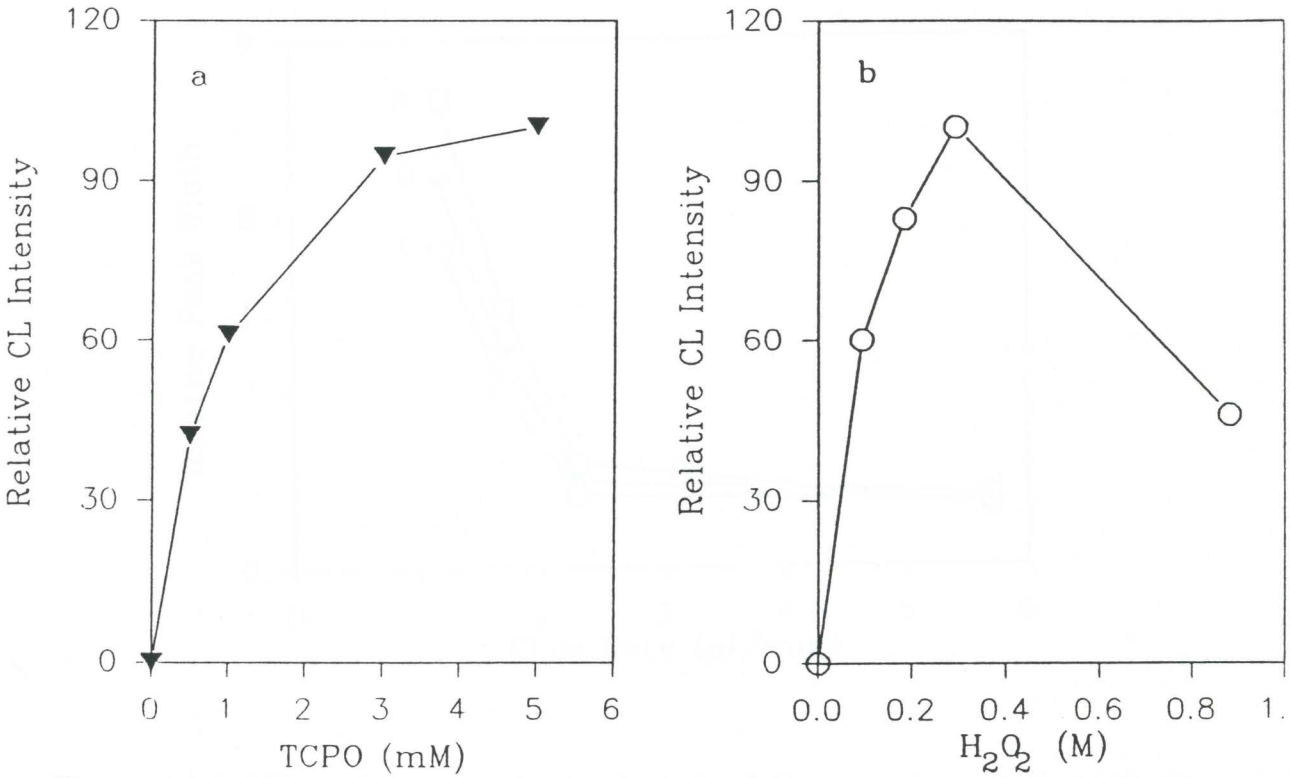

Figure 6-1-2 Effects of (a) TCPO and (b) H_2O_2 concentration on the relative CL intensity of 54 μM of Dns-L-leucine. The corresponding concentrations of TCPO and H2O2 in (a) and (b) were fixed at 5 mM and 0.29 M, respectively. Dynamic elution and PO-CL reagents flow-rate were set at 1.7 μl/min.

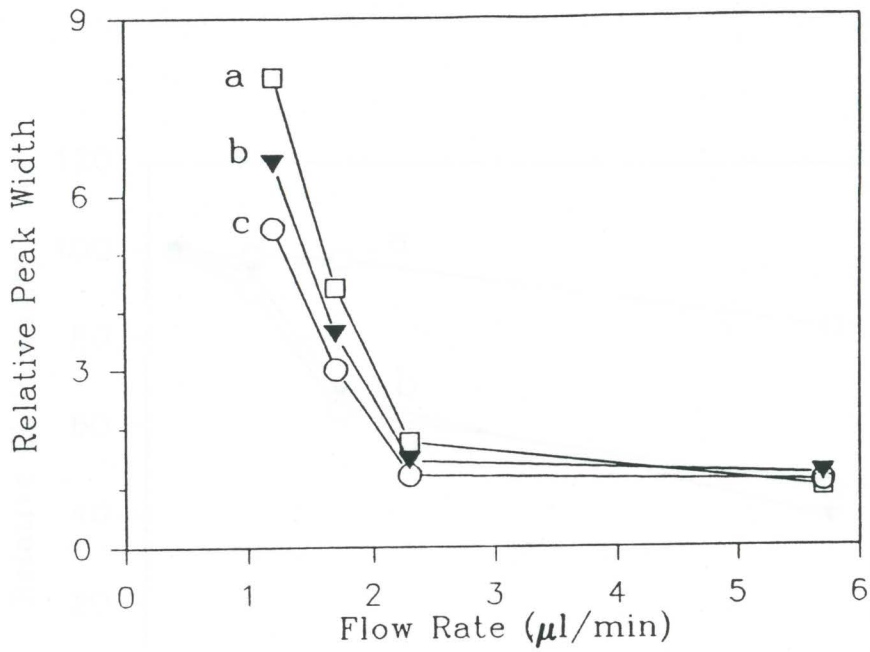

Figure 6-1-3 Effect of flow-rate due to dynamic elution on relative peak width (at baseline) of three Dns-Amino acids: (a) Dns-L-argenine=1.24 μM; (b) Dns-L-leucine=1.08 μM; (c) Dns-glycine=1.26 μM. Flow-rate for the PO-CL reagents was 1.7 μl/min and the respective concentrations for TCPO and H_2O_2 were 4.5 mM and 0.29 M.

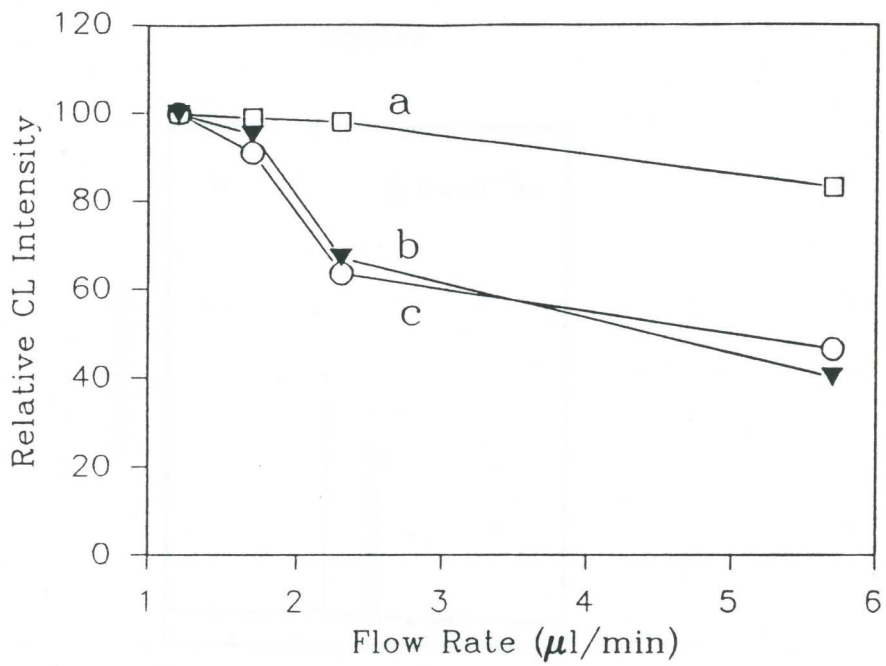

Figure 6-1-4 *Effect of flow-rate due to dynamic elution on the relative CL intensity of* (a) Dns-L-argenine, (b) Dns-L-leucine and (c) Dns-glycine. Experimental conditions were as in Figure 6-1-3.

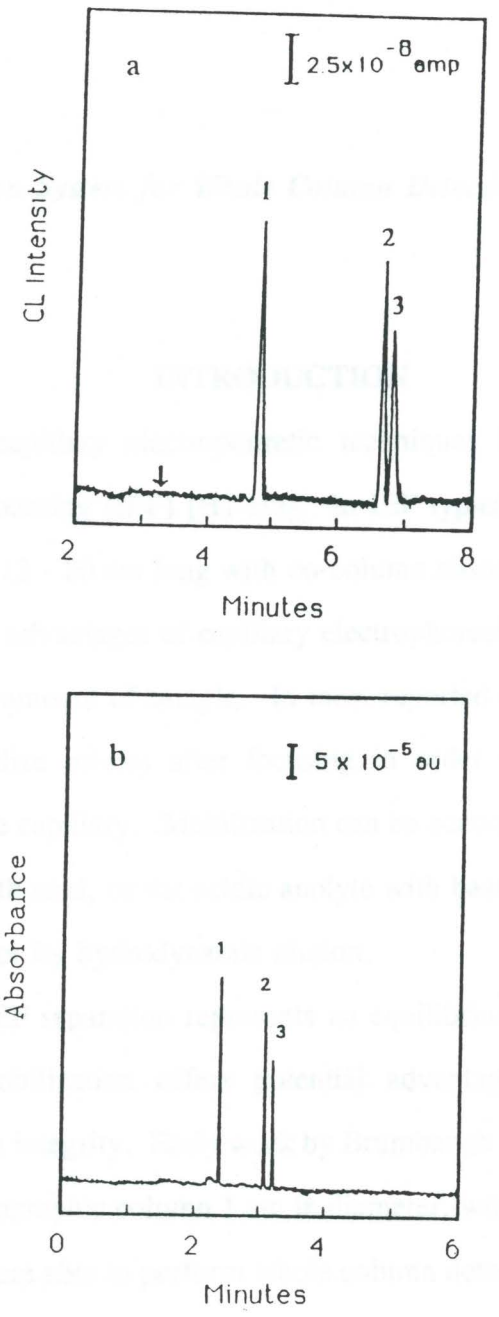

Figure 6-1-5 (a) CE separation of (1) 1.24 μM of Dns-L-argenine; (2) 1.08 μM of Dns-L-leucine and (3) 1.26 μM of Dns-glycine followed by dynamic elution and PO-CL detection. Dynamic elution and PO-CL reagents flow-rate were set at 1.7 μl/min. Concentrations of TCPO and H_2O_2 were 4.5 mM and 0.29 M, respectively. The arrow indicates the time at which the high-voltage power supply was turned off. (b) CE separation of (1) 62 μM of Dns-L-argenine; (2) 54 μM of Dns-L-leucine and (3) 63 μM of Dns-glycine and detected using on-line UV absorption method.

II. *Improved Detection System for Whole Column Detection in Capillary Electric Focusing*

INTRODUCTION

The success of capillary electrophoretic techniques have spawned interest in capillary isoelectric focusing (IEF) [H1-H5]. In IEF typical capillary dimensions are 25 - 200 μm i.d. and 12 - 20 cm long with on-column absorbance detection. Capillary IEF bears the general advantages of capillary electrophoresis, such as high efficiency, high speed and small amount of sample. In most reported capillary IEF techniques it is necessary to mobilize solutes after focusing in order to pass them through the detection region of the capillary. Mobilization can be accomplished by replacement of the basic catholyte with acid, or the acidic anolyte with base, by addition of salt to the catholyte or anolyte, or by hydrodynamic elution.

Since a focused IEF separation represents an equilibrium situation, whole-column detection without mobilization offers potential advantages both in time and in maintaining separation integrity. Early work by Brumbaugh and Ackers [H6] attempted to scan a gel-chromatographic column 1 cm in diameter, with limited success. Rowlen *et al.* [H7] recently were able to perform whole column detection on an HPLC column. More recently, Wu and Pawliszyn [H8] constructed a concentration gradient imaging detector in which a segment of capillary was illuminated by a laser beam, using a photodiode mounted on a scanner to measure the transmitted light, or diode array. While attractive in many regards, a disadvantage of this approach is that only a small segment (2cm) can be scanned, mechanical noise is still present in the scanning diode,

and detection is limited to fixed available laser wavelengths, neccessitating derivatization in many cases. This research group [H9] has recently demonstrated that a conventional light source can be used to scan the entire capillary by pulling the capillary past a fixed monochromator and diode, with results similar to that achieved using conventional (static) detection. In this paper a new whole column scanning device is demonstrated in which the S/N ratio was improved compared with earlier prototype. The advantages of this design are that examination of electropherograms during the course of development is possible and the need to handle the capillary after separation is eliminated.

EXPERIMENTAL

Instrumentation

Figure 6-2-1 is a schematic diagram of the capillary scanning apparatus. The detector was a Linear model 204 UV/Vis dual wavelength HPLC detector (Linear, Reno, NV) with output recorded on an integrator (Chromajet, Spectra-Physics, San Jose, CA). An optical fiber bundle (Superguide G-ES 20, Fiberguide, Stirling, NJ) was used to deliver light from the lightsource housed with the HPLC detection system. This radiation was re-focused to a spot of dimension ~ 0.5 mm onto the capillary using a bi-convex fused silica lens (model SBx010, Newport, Fountain Valley, CA) placed at the terminal end of the optical fiber. The photodiode was mounted on the oposite side of the light source as shown in Figure 6-2-1. The position of the optical fiber and photodiode was adjustable using a micro-positioner (model 450A, Newport). A precision moving stage was constructed and was driven via a rubber belt by a synchronous DC motor (model DA-1, 1 r.p.m., Hurst, Princetone, IN). The scan

speed was variable by replacing the drive gear. Contact with buffer solution and electrical leads was achieved through the use of specially designed buffer wells. The capillary was held in the detection apparatus by two holes (360 μm x 10 mm) drilled on the side wall of the cell. The scan cycles were controlled using a latching relay and two momentary switches at the maximum travel of the stage. The entire apparatus was enclosed in a black acrylic light-tight enclosure. The equipment for capillary electrophoresis was described in reference [H9].

Materials and Methods

Bovine albumin, ovalbumin, β-lactoglobulin B and carbonic anhydrase were obtained from Sigma (St. Louis, MO), pH 3-10 ampholytes from Fischer (Fair Lawn, NJ) and all other chemical were of analytical grade from Aldrich (Milwaukee, WI). Fused silica capillaries (various diameters) were purchased from Polymicro Technologies (Phoenix, AZ). The details of procedures for IEF and the pre-treatment of capillary were as described in our earlier report [H9].

RESULTS AND DISCUSSION

Whole column detection is limited by the noise levels which can be achieved, at least in comparison with static, conventional detection. With chromophores exhibiting appreciable molar absorptivities in the 10^4 range, the detection limits for conventional, commercial instrumentation is typically in the μg/ml range. For IEF, original analyte concentrations can be even lower, since they are focused, and hence, concentrated in the solution. Preliminary data indicate that optical noise in moving column detection arises from mechnical vibrations and from optical imperfections of the capillary, as

evidenced by the reduced noise when the outer capillary coating was stripped as shown in Figure 6-2-2. The improvement in the S/N ratio is due to the decreased in dynamic noise using a steady moving stage instead of the pulling operation in which vibration and friction were the major sources of dynamic noise. The mechnical vibration was also minimized using a rubber drive belt to move the scanning stage while insulating it from motor vibration. Because the capillary on the moving stage was not directly in contact with the drive motor, mechnical noise was substantially reduced compared to the pulling mechanism [H9]. However, it is still difficult to fabricate a precision moving stage which minimizes variation along direction perpendicular to the capillary movment. This positional variation was $\sim 25\mu$m in a 10 cm distance for this device which prevents the use of smaller i.d. capillaries. This positional variation is significantly decreased as larger capillaries are used. In Figure 6-2-2, the relationship between noise and capillary i.d. is presented.

In order to reduce the positional variation during capillary movement, small apertures ($\sim 360\mu$m) which held the outer diameter ($\sim 355\mu$m) of the capillary were made on the detection cell to align the position of capillary in the detection region. This enhancement in positional precision was accompanied by increased mechanical friction. In addition, we have found that the use of dual wavelength detection in order to further reduce noise due to capillary imperfections, light scattering, and vibration yields further improvements in S/N ratio. In order to maximize the effect of dual-wavelength detection the two wavelengths should be as far apart as possible. Limitations of the detector prevented experiments with wavelength variations larger than 10 nm due to the longer wavelength switching times required. Finally, the scanning electropherogram of several proteins in Figure 6-2-3 also shows an improvement in S/N ratio compared

to the previous design [H9].

CONCLUSION

In conclusion, this whole column detection method has significantly improved upon previous designs by further minimizing sources of dynamic noise. The significance of the further development of such a device would be widespread. In the area of IEF, this method provides an improvement over standard IEF separations, in which a mobilization step is required for detection. Parabolic flow or the need to change the inlet buffer limit the efficiency and utility of capillary IEF in its present form. Whole capillary detection is a possible solution to these problems and provides new challenges in capillary detection technology.

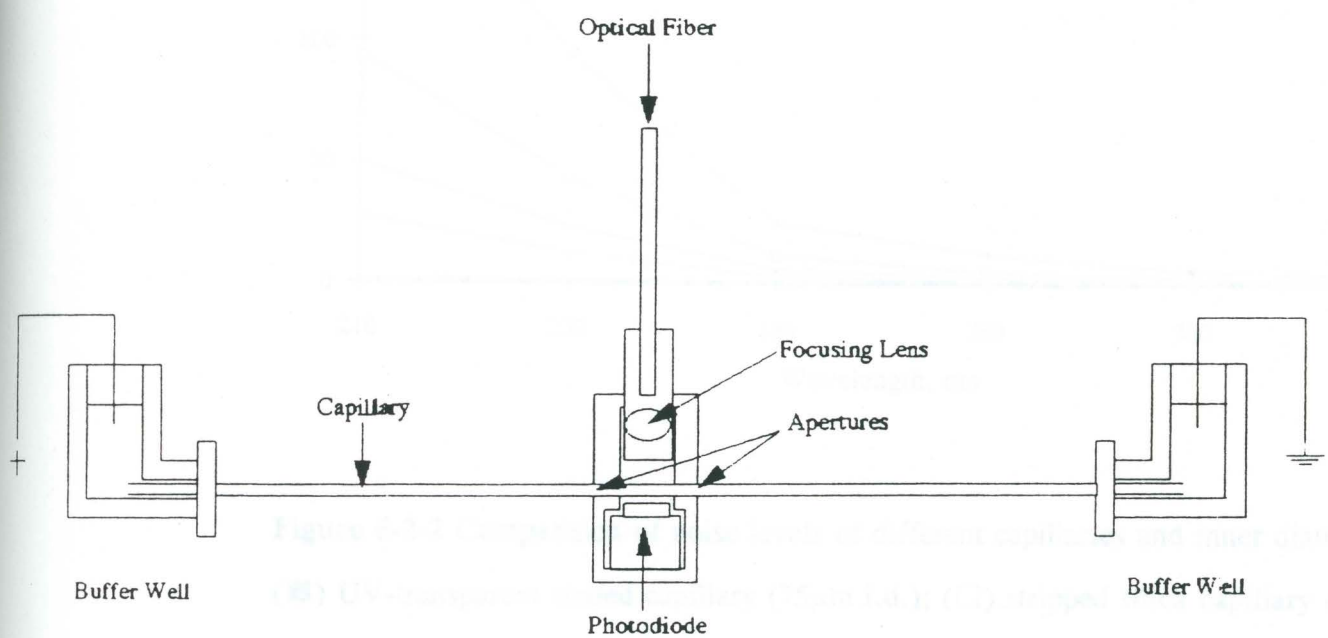

Figure 6-2-1 Cross-sectional view of the whole column detection system

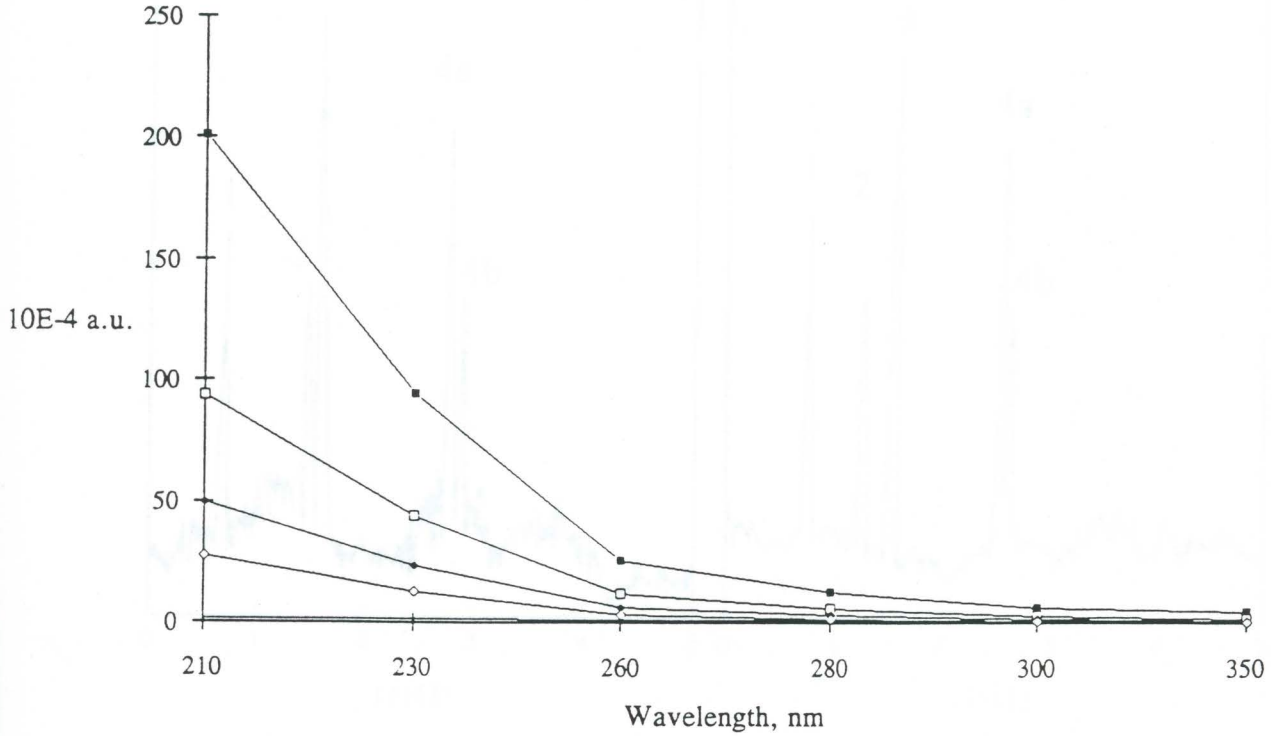

Figure 6-2-2 Comparision of noise levels of different capillaries and inner diameters: (■) UV-transparent coated capillary (75μm i.d.); (□) stripped silica capillary (75μm i.d.) measured by pulling mechanism; (♦) stripped silica capillary (75μm i.d.) and (◇) stripped silica capillary (254μm i.d.) measured by capillary scanning mode; (−) stripped silica capillary (75μm i.d.) measured by static. All capillaries were ~355 μm o.d. and filled with water, scanning or pulling speed was 0.25 mm/s.

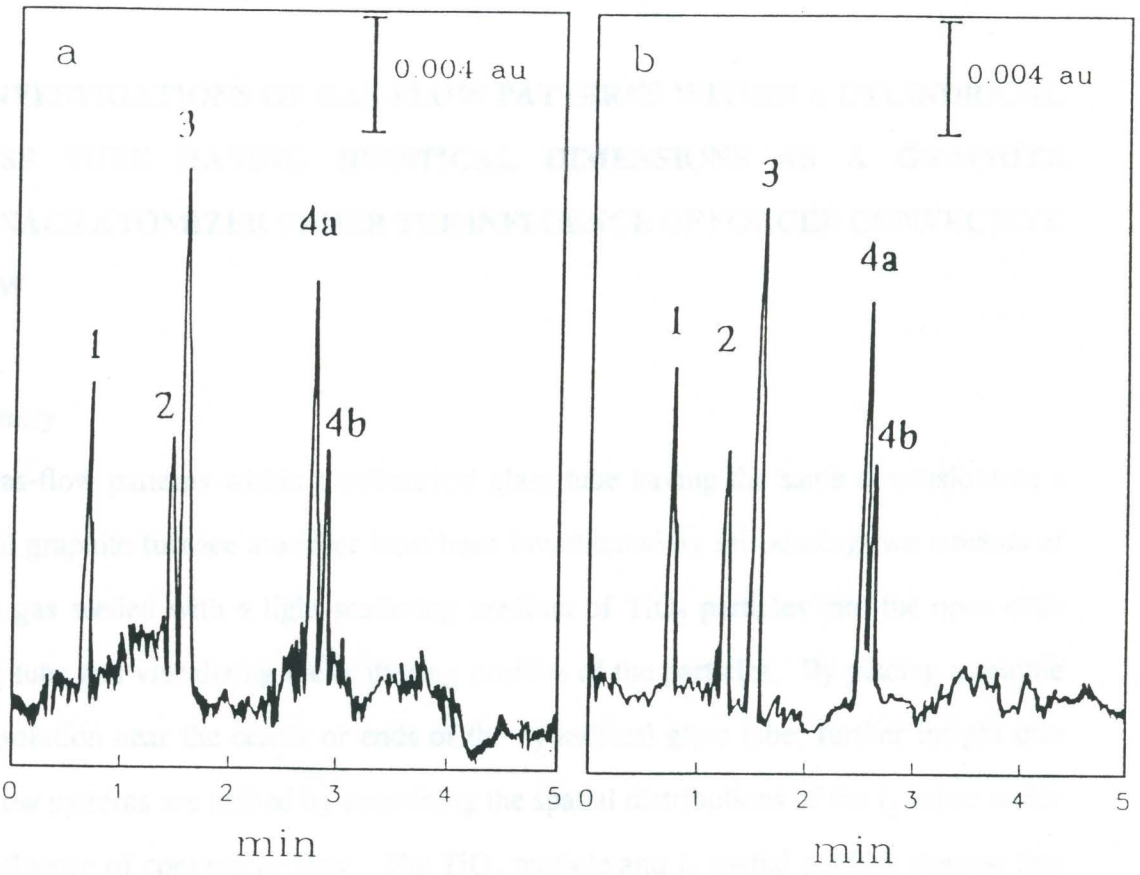

Figure 6-2-3 Isoelectropherogram measured using the capillary scanning device. (A) separated on a PEG 8M-10 treated capillary of 75μm i.d x 18 cm in 2% ampholyte (pH 3-10) and (B) separated on a bare capillary of 75μm i.d. x 18 cm in 1% Triton 100 R - 2% ampholyte (pH 3-10). Development voltage 8 kv; 6 min focusing time and scanning speed of 0.25 mm/s detection at 280 nm. Proteins: (1) ovalbumin; (2) bovine albumin; (3) β-lactoglobulin B; (4a) and (4b) carbonic anhydrase, 0.05mg/ml each.

APPENDIX

INVESTIGATIONS OF GAS-FLOW PATTERNS WITHIN A CYLINDRICAL GLASS TUBE HAVING IDENTICAL DIMENSIONS AS A GRAPHITE FURNACE ATOMIZER UNDER THE INFLUENCE OF FORCED CONVECTIVE FLOW

Summary

Gas-flow patterns within a cylindrical glass tube having the same dimensions as a typical graphite furnace atomizer have been investigated by introducing two streams of argon gas seeded with a light scattering medium of TiO_2 particles into the open ends of the tube and visualizing the scattering profiles of the particles. By placing a sample of I_2 solution near the center or ends of the cylindrical glass tube, further insight into gas-flow patterns are gained by examining the spatial distributions of the I_2 vapor under the influence of convective flow. The TiO_2 particle and I_2 spatial profiles suggest that at room temperature the argon streams follow a laminar-flow pattern in the bulk-flow region between the ends of the cylindrical tube and the sample introduction hole; however, at the junction region where the two argon streams converge and discharge from the dosing hole, local turbulences or eddies may be generated due to abrupt changes in gas-flow velocity and direction in the vicinity of an area (boundary layer) directly beneath the dosing hole.

INTRDUCTION

Confined or semi-enclosed Massmann-type electroatomizers are usually fabricated in the form of cylindrical tubes made from graphite and equipped with the means to maintain an internal purge gas flow [J1]. When applied in the drying and charring stages, the convective force of the purge gas is supposed to effectively clear vapors of the solvent and matrix, respectively, from the atomizer volume. During the atomization stage, the internal gas flow can be switched off, i.e., gas-stop condition, to prolong the residence time of the analyte vapor; on the other hand, it is sometimes desirable to maintain the internal purge gas flow even during the atomization cycle, i.e., gas-flow condition, to prolong the lifetime of the atomizer and/or to reduce sensitivity. A large number of papers have been published which deal with mechanisms of atom supply and removal within electroatomizers [J2-J10]. In general, under gas-stop condition, diffusion and vapor expulsion appear to be the dominant analyte loss mechanisms; however, under gas-flow condition in which forced convection is applied during the atomization stage, convection appears to play an important role in the removal of analyte from the atomizer. Although it has been shown that the effect of forced convection on mass transport within semi-enclosed electroatomizers is a function of the atomizer volume, the gas-flow rate, the atomizer temperature, and the gas-flow pattern within the atomizer, it is very difficult to quantitate the impact of forced convection on the removal of matrix and analyte because, in particular, very little is known about gas-flow patterns within the atomizer under various experimental conditions [J4].

In our earlier work involving the spatial mapping of sodium atom distribution with the graphite furnace atomizer under gas-stop and gas-flow conditions [J11], it was found

that the presence of internal gas flow appears to force most of the sodium atoms to localize on the bottom of the furnace rather than being immediately swept out of the furnace. This observation suggests that turbulences may be generated at various regions within the graphite tube and may have an impact on the redeposition of the analyte on the bottom of the furnace. In this work a first approximation of gas-flow patterns that may exist within the graphite furnace under the influence of forced convection is gained through the investigations of gas-flow patterns within a transparent cylindrical glass tube having the same dimensions as a typical graphite tube furnace by firstly, observing the scattering profiles of the purge gas (argon) flow after seeding it with a light scattering medium of TiO_2 particles and secondly, observing the spatial distributions of a probe species (I_2) after placing the sample solution at various locations within the cylindrical glass tube.

EXPERIMENTAL

A versatile and simple technique originally developed for studying gas-flow dynamics in unlit inductively-coupled plasma torches was modified for the present study in which gas-flow patterns within a cylindrical glass tube were observed by introducing a light-scattering medium into the argon flow and passing a thin plane of laser light into the tube. The schematic of the particle generator for seeding argon with TiO_2 particles can be found in detail elsewhere [J12]. Briefly, the argon gas was first passed through a flow meter and then introduced into a flask consisting of 100 ml of water to humidify the argon for the production of TiO_2 aerosol upon reaction of the water vapor carried by the argon flow with 20 ml of $TiCl_4$ (Alfa, Danver, MA, U.S.A.) placed in a second flask down stream. After the two flasks, mixing of the TiO_2-seeded argon stream with a pure argon stream was performed to dilute the particle concentration and to remove

any large particles by passing the two streams of gases through a 120 cm length of 3 mm i.d. Tygon tubing. The diluted gas stream was then made to pass through two drying tubes containing pellets of NaOH and $CaSO_4$ (Sigma, St. Louis, MO, U.S.A.) for the removal of hydrochloric acid and any residual moisture, respectively. Subsequently, the gas stream was split into two separate streams using a tee. Introduction of the two argon streams into a cylindrical glass tube fabricated to have the same dimensions as a Perkin-Elmer graphite tube furnace (28 mm long, 6 mm i.d., diameter of the sample introduction hole ~ 1.5 mm, Perkin-Elmer, Norwalk, CT, U.S.A., part number 0290-1821) was accomplished by inserting two 20-cm length Tygon tubings into the two opposite arms of the tee and the two open ends of the cylindrical glass tube. Scattering profiles of the argon flow were visualized at room temperature by projecting a thin plane of light into the cylindrical glass tube. Configuration of the optical system was similar to that shown in reference 12 in which the plane of light was produced by passing a laser beam from a 5 mW He-Ne laser (Uniphase, Sunnyvale, CA, U.S.A., Model 1105 P) through a series of spherical and cylindrical lenses.

Another simple experiment was performed to observe the spatial profiles of a probe species (I_2) under the influence of forced convection. A 1-ml of an ethanol solution saturated with I_2 (Sigma, St. Louis, MO, U.S.A.) was spotted with a 10-ml syringe into the center or near the ends of the cylindrical tube; subsequent vaporization of the sample solution and distribution of the I_2 vapor within various regions in the cylindrical tube under the influence of argon flow were studied by simply visualizing the yellowish color of the I_2 vapor under ambient room light and temperature.

RESULTS AND DISCUSSION

Gas dynamics within a graphite tube atomizer has been studied theoretically by Holcombe using a simplified model [J13] and laminar gas-flow patterns were shown to exist within the atomizer under gas-stop condition since the Reynolds number (Re) calculated even for extreme experimental conditions (average gas velocity = 1500 cm min^{-1} and tube radius = 0.3 cm) is less than 1, which lies well below the threshold limit (Re ~ 2300) for the formation of turbulent flow to occur; thus, velocity profiles within the cylindrical graphite tube take on a parabolic-flow pattern in which velocity approaches zero at the tube walls and increases toward the center. However, the effects of both the sample introduction hole and forced convection imposed by the internal purge gas on the gas-flow patterns were not considered in this model. It is interesting to note that the formation of turbulences or eddies has been shown to occur at flow conditions in which the value of Re is much lower than the threshold limit [J14]; a common example of this particular situation is when laminar flow streams encounter angularity or solid bodies in which there are abrupt changes in the flow direction and/or velocity. This is an important point since possible discharge of the purge-gas streams from the central sample introduction hole under the influence of forced convection may lead to drastic change in the local velocity and flow direction of the streamlines in the regions immediately below the dosing hole, thereby causing the formation of eddies in the vicinity of these regions even though the gas velocity within the tube is too low to meet the Reynolds criterion for turbulent flow to occur.

Qualitatively, Fig. 7-1 illustrates the scattering profiles of the medium of TiO_2 particles seeded in the argon flows that were introduced symmetrically at the open ends

of the cylindrical glass tube at a flow rate of 50 cc min^{-1}. It was observed that at the bulk-flow region between the ends of the tube and the sample introduction hole the particles appear to follow streamlines with steady and regular profiles that are characterized by a sharp curvature at the junction area where the two argon streams converge and discharge from the dosing hole, suggesting that the argon flow in this bulk-flow region is laminar in nature. It is interesting to observe from Fig. 7-1(a) that there exists a relatively large area which resembles the shape of a delta directly below the sample introduction hole in which scattering from the TiO_2 particles was not visually detectable, suggesting that convective force from the argon flow may be negligible in this "delta region". Furthermore, it was found that the size of this delta region decreased by $\sim 30\%$ as shown in Fig. 7-1(b) when the flow rate was increased to 150 cc min^{-1} or when the diameter of the sample hole was reduced to 1.0 mm. Thus, from a macroscopic viewpoint, it appears from Figs. 7-1(a) and (b) that there are two distinct regions within the cylindrical tube that are characterized by different gas-flow patterns: one appears to be governed by the convective force of the argon flow (laminar region) and the other possibly by diffusion due to the apparent lack of forced convection flow in this area (delta region). However, it is possible that there are microscopic regions within the cylindrical tube, in particular an area between the laminar and delta regions (boundary layer), in which local turbulences or eddies may be established due to abrupt changes in flow velocity and direction and cannot be detected by this visualization method.

Gas-flow patterns were further investigated by studying the spatial distributions of I_2 molecules within the cylindrical glass tube. Small amounts of a sample solution consisting of saturated I_2 in ethanol was deposited immediately below the sample

introduction hole and was allowed to vaporize under the influence of forced convection of the two opposing streams of argon flows introduced at the tube ends at a flow rate of 50 cc min^{-1}; qualitatively, Figs. 7-2(a-c) illustrate the density of I_2 vapor observed in this particular experiment. It is interesting to observe that I_2 molecules appear to concentrate in a region similar in size, shape, and location as the delta region immediately after vaporization has begun as shown in Fig. 7-1(a). This observation tends to support that there is indeed two distinct regions within the cylindrical tube with significantly different mass-transport mechanisms, resulting in the appearance of higher concentration of I_2 molecules in the central delta region as shown in Fig. 7-2(a). Furthermore, it was found that a few seconds after vaporization has begun, the concentration of I_2 molecules within the delta region appear to have partially dissipated while two narrow dark bands were found to build up along the boundary layer as shown in Fig. 7-2(b), suggesting an increase of I_2 density in this area and that the rate of mass transport of I_2 within the boundary layer is different than those in the laminar and delta regions.

To gain further insights into the mass transport of I_2 molecules within the cylindrical tube under the influence of symmetrical convective force of the argon flows, the experiment shown in Figs. 7-2(a) and (b) were repeated but this time the sample was placed near one end of the tube as shown in Fig. 7-2(c). It was very interesting to observe that a narrow dark band was produced a few seconds after vaporization had begun; however, there was no observable I_2 molecules in the laminar or delta regions. A similar narrow band can also be produced on the opposite side of the delta region when the sample was deposited near the opposite end of the tube.

The spatial distribution of I_2 molecules shown in Fig. 7-2(c) suggests that mass

transport of I_2 molecules within the boundary layer is perhaps governed by processes other than convection or molecular diffusion since I_2 cannot be visually detected in either the laminar or delta region. Specifically, one might envision that the higher density of I_2 in the boundary layer could be due to a decrease in the convective force (lower velocity) relative to the bulk flow; however, if this is the case, similar amounts of I_2 should also be observed near the walls of the glass tube at which velocity approaches zero assuming laminar flow. On the other hand, if molecular diffusion were a major mass transport mechanism within the boundary layer, one would expect to see a gradual increase in I_2 concentration in the delta region, but this is not the case. Thus, it is possible that some types of turbulences or eddies are generated in the boundary layer that may be responsible for the mass transport of I_2 molecules in this region. Furthermore, it is interesting to note that the time it took for the I_2 molecules to dissipate from the tube was about the same ($\sim$40 s) for both experiments as shown in Figs. 7-2(a) and (c) in which the sample was placed in the center and near the ends of the tube, respectively, suggesting the rate of I_2 removal in these experiments was dictated by the rate of mass transport within the boundary layer, which could be dominated by mechanisms such as eddy diffusion [J14]. It should be noted that the time it took for the I_2 molecules to dissipate from the tube without the influence of forced convection was about 2.5 minutes.

Turbulence phenomena in cylindrical tubes has been a subject of great interest to chemical engineers for many years and numerous mathematical models have been developed in an attempt to quantitatively describe mass transfer of solute in turbulent flow; of particular importance is the Reynolds model which describes turbulent flow near solid surfaces by recognizing an analogy between momentum and mass transfer

[J15]. Although this is a simplified model, it may perhaps shed some light into mass transport processes occurring within the boundary layer as shown in Figs. 7-2(b) and (c). In Reynolds model the turbulent core extends from the bulk flow in the x-direction (parallel to the tube wall) all the way to the surface of the tube wall, and velocity and concentration changes are significant only in y-direction (perpendicular to the tube wall). In the turbulent core, eddies or fluctuations are envisioned as lumps or aggregates of fluid-transferring matters which move back and forth across the flow stream in the y-direction only, involving the transfer of momentum from fluids moving in the x-direction. Since mass transfer is analogous to momentum transfer, it can be imagined that when a pulse of fluid moves from one level (y_1) to another (y_2) with a certain fluctuation velocity, it carries with it the concentration (as well as its momentum) appropriate to level y_1; at the same time another pulse of fluid moves from level y_2 to y_1, carrying with it momentum and concentration appropriate to level y_2.

Similar mass transport mechanisms as described by the Reynolds model may explain the observations as shown in Figs. 7-2(b) and (c). It is possible that once the I_2 molecules enter the boundary layer from the delta or laminar region by molecular diffusion or convection, the I_2 molecules, like the velocity, fluctuate with the eddy movements within the boundary layer. Small "pulses" of argon gas carrying the I_2 molecules may be fluctuating back and forth across the bulk argon flow in opposite direction towards the sample introduction hole and the bottom of the tube wall, resulting in an increase in flow resistance and convective mixing of the I_2 molecules within boundary layer. A closer examination of the dark narrow bands as shown in Figs. 7-2(b) and (c) supports this hypothesis since the bands appear to be comprised of a large number of small I_2 particulates, possibly formed as a result of an increase in the

number of collisions between I_2 molecules within the eddies in the boundary layer.

Although in this work the gas-flow patterns observed within the cylindrical glass tube were obtained at room temperature, the results should be useful towards the unraveling and understanding of complex gas-flow dynamics that occur within the graphite tube atomizer under typical experimental conditions; in particular, similar gas-flow patterns may exist within the graphite furnace during the drying and beginning of the charring stages in which a significant portion of the furnace gas may escape through the sample introduction tube, thus resulting in the possible formation of turbulences or eddies at the junction region directly beneath the hole during these time periods and thereby affecting the initial location of the sample droplet and/or the effective removal of the vapor of solvent and matrix.

The use of the present results for the correlation of gas-flow patterns that occur with the graphite furnace during the atomization stage would not be straightforward since expansion of hot gas towards the tube ends could occur during the initial heating period, especially under high heating rates as proposed by models developed by Holcombe [J13] and Chakrabarti *et al.* [J16]. On the other hand, Rademeyer *et al.* [J17] have made consideration in their model that in a furnace blocked at the ends, gas was assumed to escape mainly through the sample introduction hole and pointed out the unknown effects of combined convective force of the purge gas on the sample vapor beneath the hole. Furthermore, Welz *et al.* [J18] have recently suggested that since the furnace housing is semi-enclosed, i.e., windows exist on the ends of the furnace, the gas initially expands towards the tube ends would eventually exit out the dosing hole to relieve the internal pressure built up over time, thus increasing the rate of gas expulsion through the sample introduction hole a short period of time after the initial

heating period. If this is the case, the possible formation of turbulences or eddies due to abrupt changes in gas-flow velocity and direction as the gas discharge through the dosing hole would be of great interest since it might have a significant impact on the redeposition of analyte onto the graphite surface. Moreover, the present results suggest that the formation and distribution of particles within the furnace could be influenced by the gas-flow patterns. A recent paper published by L'vov *et al.* suggested that a cloud of carbon particles was formed in the course of the carbothermal reduction of Al_2O_3. Interestingly, the scattering intensity of these particles was found to be highest near the dosing hole, suggesting that the density and/or size of these particles may be influenced by the possible formation of turbulences near the dosing hole [J19].

To obtain a more representative picture of gas-flow patterns within the graphite tube furnace using the present visualization methods, it is perhaps necessary to modify the experimental set-up in such a way that rapid heating of the cylindrical glass tube is made possible so that the effect of gas expansion towards the furnace ends and/or sample introduction hole on the gas-flow patterns can be investigated. Furthermore, the development of mathematical models using, for example, the Monte Carlo method [J9] which takes into account the effects of various experimental parameters such as atomizer shape and dimension, diameter of sample introduction hole, flow velocity of the internal purge gas, initial and final furnace temperature, etc., would represent another important step forward for the understanding of the formation of turbulences or eddies within various regions inside the furnace atomizer and of the subsequent impact of this interesting and complex phenomenon on the characteristics of analytical signals for various elements.

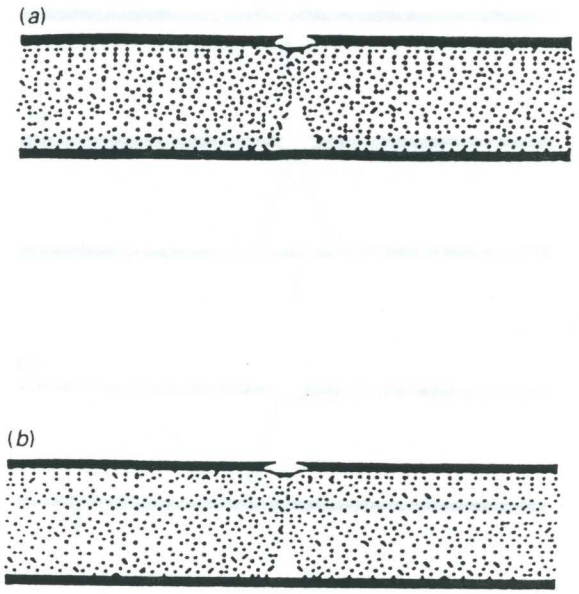

Figure 7-1 Scattering profiles of TiO_2 particles carried by the argon streams at a flow rate of (a) 50 cc min^{-1} and (b) 150 cc min^{-1} from each side of the tube. Note: the dots do not intend to represent the size of the particles but serve to illustrate qualitatively the flow patterns and relative concentration of the particles observed.

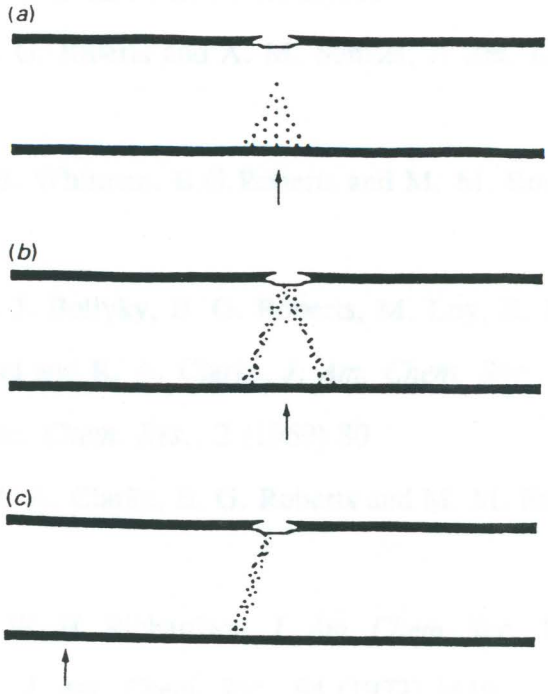

Figure 7-2 Spatial distributions of I_2 molecules under the influence of forced convection of argon at a flow rate of 50 cc min^{-1} from each side of the tube for the following conditions: (a) ~1 s after vaporization of I_2 has begun; (b) ~5 s after vaporization of I_2 has begun; and (c) same condition as (b) except for initial sample location. The arrows indicate approximately where the sample droplet was initially placed. Note: the dots do not intend to represent the size of any I_2 particulates formed but serve to illustrate qualitatively the relative concentration of I_2 observed.

REFERENCES

Chapter 1

1. E. A. Chandross, *Tetrahedron Lett.*, (1963)761

2. M. M. Rauhut, B. G. Riberts and A. M. Semsel, *J. Am. Chem. Soc.*, 88 (1966) 3604

3. L.J. Bollyky, R. H. Whitman, B.G.Roberts and M. M. Rouhut, *J. Am. Chem. Soc.*, 89 (1967) 6523

4. M. M. Rauhut, L. J. Bollyky, B. G. Roberts, M. Loy, R. H. Whitman, A. V. Lannotta, A. M. Semsel and R. A. Clarks, *J. Am. Chem. Soc.*, 89 (1967) 6515

5. M. M. Rauhut, *Acc. Chem. Res.*, 2 (1969) 80

6. D. R. Maulding, R. A. Clarke, B. G. Roberts and M. M. Rauhut, *J. Org. Chem.*, 33 (1968) 250

7. H. E. O'Neal and W. H. Richardson, *J. Am. Chem. Soc.*, 92 (1970) 6553

8. W. H. Richardson, *J. Am. Chem. Soc.*, 94 (1972) 1619

9. E. H. White, J. D. Miano, C. J. Watkins and E. J. Breaux, *Angew. Chem.*, 13(1974) 229

10. N. J. Turro and P. Lechtken, *J. Am. Chem. Soc.*, 95 (1973) 264

11. F. McCapra, *Pure Appl. Chem.*, 24 (1970) 611

12. P. Lechtken and N. J. Turro, *Mol. Photochem.*, 6 (1974) 95

13. M. M. Rauhut, B. G. Roberts, D. R. Maulding, W. Bergmark and R. Coleman, *J. Org. Chem.*, 40 (1975) 330

14. K. Honda, K. Miyaguchi and K. Imai, *Anal. Chim. Acta*, 177 (1985) 103 and 111

15. K. Imai, Y. Matsunaga, Y. Tsukamoto and A. Nishitani, *J. Chromatogr.*, 400 (1987) 169

16. W. R. Seitz and M. P. Neary, In D. M. Hercules (Editor), Contemporary Topics in Analytical Chemistry, Vol. I, Plenum, New York, 1977, p49

17. G. J. De Jong, N. Lammers, F. J. Spruit, R. W. Frei and U. A. Th. Brinkman, *J. Chromatogr.*, 353 (1986) 249

18. K. Imai, A. Nishitani and Y. Tsukamoto, *Chromatographia*, 24 (1987) 77

19. N. Hanaoda, R. S. Givens, R. L. Schowen and T. Kuwana, *Anal. Chem.*, 60 (1988) 2139

20. N. Hanaoka, H. Tanaka, A. Nakamoto and M. Takada, *Anal. Chem.*, 63 (1991) 2680

21. F. McCapra, J. Chem. Soc. Comm., 946 (1977)

22. W. Adam and J. C. Liu, *J. Am. Chem. Soc.*, 94 (1972) 2894

23. G. B. Schuster, *Acc. Chem. Res.*, 12 (1979) 366

24. J. Y. Koo and G. B. Schuster, *J. Am. Chem. Soc.*, 99 (1977) 6170

25. C. L. R. Catherall, T. F. Palmer and R. B. Cundall, *J. Chem. Soc., Faraday Trans.*, 80 (1984) 823 and 837

26. F. J. Alvarez, N. J. Parekh, B. Matuszeweski, R. S. Givens, T. Hignchi and R. L. Schowen, *J. Am. Chem. Soc.*, 108 (1986) 6435

27. T. G. Curtis and W. R. Seitz, *J. Chromatogr.*, 134 (1977) 343 and 513

28. F.E.P. Mikkers, F. M. Everaerts and Th. P. E. Verheggen, *J. Chromatogr.*, 11 (1979) 169

29. J. W. Jorgenson and K. D. Lukacs, *Anal. Chem.*, 53 (1981) 1298

30. S. Terabe, K. Otsuka, K. Ichikawa, A. Tsuchiya and T. Ando, *Anal. Chem.*, 56 (1984) 113

31. S. Terabe, K. Otsuka and T. Ando, *Anal. Chem.*, 332 (1985) 219

32. K. Otsuka, S. Terabe and T. Ando, *J. Chromatogr.*, 348 (1985) 39

33. H. Nish, N. Tsumagai, T. Kamamoto and S. Terabe, *J. Chromatogr.*, 465 (1989) 331

34. F. M. Everaerts, Graduate Reports, University of Technology, Eindhoven (1964)

35. R. J. Weime, in E. Heftman (Editor), Chromatography: Laboratory Handbook of Chromatography and Electrophoresis Method, Van Nostrand, New York, 3rd Ed., (1975)

36. A. W. Adamson, Physical Chemistry of Surfaces, 2nd Ed., Interscience, New York, Chapter 4 (1967)

37. A. Tsuda, K. Normura and G. Nakgawa, *J. Chromatogr.*, 264 (1983) 385

38. E. Grushka and R. J. McCormick, *J. Chromatogr.*, 471 (1989) 421

39. J. C. Giddings, United Separation Science, John Wiley and Sons, New York, Chapter 4 (1991)

40. E. Grushka, R. M. McCormick and J. J. Kirkland, *Anal. Chem.*, 61 (1989) 241

41. J. C. Giddings, *Sep. Sci.*, 4 (1969) 181

42. S. Terabe, K. Otsuka, K. Ichikawa, A. Tsuchiya and T. Ando, *Anal. Chem.*, 56 (1984) 111

Chapter 2

A1. Kobayashi, S.; Sekino, J.; Honda, K.; Imai, K. *Anal. Biochem.* 122 (1981) 99-104.

A2. DeJong,G.J.; Lammers,N.; Spruit, F.J.; Brinkman, U.A.Th.; Frei, R.W. *Chromatographia* 18 (1984) 129-133.

A3. Kwakman,P.J.M.; Brinkman, U.A.Th.; Frei, R.W.; DeJong, G.J.; Spruit, F.J.; Lammers, N.; Van Den Berg, J. *Chromatographia* 24 (1987) 395-399.

A4. Sigvardson, K.W.; Birks, J.W. *Anal. Chem.* 55 (1983) 432-435.

A5. Sigvardson, K.W.; Kennish, J.M.; Birks, J.W. *Anal. Chem.* 56 (1984) 1096-1102.

A6. Koziol, T.; Grayeski, M.L.; Weinberger, R. *J. Chromatogr.* 317 (1984) 355-366.

A7. Grayeski, M.L.; DeVasto, J.K. *Anal. Chem.* 58 (1987) 1203-1206.

A8. Van Zoonen,P.; Gooijer,C.; Velthorst,N.H.; Frei,R.W. *J.Pharm.Biomed.Anal.* 5 (1987) 485-492

A9. Baeyens,W.; Bruggeman, J.;Dewaele, C.; Lin, B.; Imai, K. *J. Biolumin. and Chemilumin.* 5 (1990) 13-23.

A10. Curtis, T.G.; Seitz, W.R. *J. Chromatogr.* 134 (1977) 343-350.

A11. Curtis, T.G.; Seitz, W.R. *J. Chromatogr.* 134 (1977) 513-516.

A12. Alvarez, F.J.; Parekh, N.J.; Matuszewski, B.; Givens, R.S.; Hizuchi, T.; Schowen, R.L. *J. Am. Chem. Soc.* 108 (1986) 6435-6439.

A13. Mohan, A.G.; Turro, N.J. *J. Chem. Ed.* 51 (1974) 528-530.

A14. Uchiyama, S. Uchiyama, M. *J. Liq. Chromatogr.* 3 (1980) 681-691.

A15. Hanaoke, N.; Tanaka, H.;Nakamoto, A.;Takada, M., *Anal. Chem.* 63 (1991) 2680-2685.

B1. N. Wu and C. W. Huie, *Anal. Chem.*, 64 (1992) 2465

B2. R. Weinberger, C. A. Mannan, M. Cerchio and M. L. Grayeski, *J. Chromatogr.*, 288(1984) 445

B3. R. Weinberger, *J. Chromatogr.*, 314 (1984) 155

B4. N. Hanadoka, R. S. Givens, R. L. Schowen and T. Kuwana, *Anal. Chem.*, 60 (1988) 2193

B5. N. Hanadoka, H. Tanaka, A. Nakamoto and M. Takada, *Anal. Chem.*, 63 (1991) 2680

B6. L. Eals, "Clinical Chemistry of the Porphyrins" in The Porphyrins, Vol. VI; Biochemistry, Part A, D. Dolphin ed. Academic Press, New York (1979) pp 665-804

B7. F. De Croo, G. A. Bens and P. De Moerloose, *J.High Resolt. Chromatogr. Chromatogr. Comm.*, 3 (1980) 423.

B8. T. G. Curtis and W. R. Seitz, *J. Chromatogr.*, 134 (1977) 343

B9. M. M. Rauhut, L. J. Bollyky, B. G. Roberts, M. Loy, R. H. Whitman, A. V. Lannotta, A. M. Semsel and R. A. Clarke, *J. Am. Chem. Soc.*, 89 (1967) 6515; M. M. Rauhut, *Acc. Chem. Res.*, 2 (1969) 80

B10. B. mann and M. L. Grayeski, *Biomed. Chromatogr.*, 5 (1991) 47

B11. R. Weinberger and E. Sapp, *J. Chromatogr.*, 516 (1990) 271

B12. P. M. Johson, S. L. Perkins and S. W. Kennedy, *Clin. Chem.*, 34 (1988) 103

B13. A. Junker-Buchheit and H. Jork, *J. Planar Chromatogr.*, 1 (1988) 214

Chapter 3

C1. J. R. Chowdhury, A. W. Wolkoff and I. M. Arias, in C. R. Scriver, A. L. Beaudet, W. S. Sly and D. Valle (Eds.), The Metabolic Basis of Inherited Diseases, Vol. 1, Part 8, McCGraw-Hill, New York, 1989, pp 1367-1408.

C2. M. Roth, M. in H. Ch. Curtius and M. Roth (Eds.) Clinical Biochemistry: Principles and Methods, Vol. II, Part XII, Walter de Gruyter, New York, 1974.

C3. D. White, G.A. Haidar and J. G. Reinhold, *Clin. Chem.*, 4 (1958) 211.

C4. A.A. Lamola, J. *Invest. Dermatol.*, 31 (1981) 114.

C5. R.F. Chen, *Arch. Biochem. Biohys.*, 160 (1974) 106.

C6. J.H. Aiken and C.W. Huie, *Anal. Lett.*, 24 (1991) 167.

C7. M. Roth, *Clin. Chim. Acta*, 17 (1967) 487.

C8. A. Townshend, *Analyst*, 115 (1990) 495.

C9. L.J. Kricka, *Clin. Chem.*, 37 (1991) 1472.

C10. K. Sigvardson and J.W. Birks, *Anal. Chem.*, 55 (1983) 432.

C11. S. Albrecht, H. Brandl, and E. Köstler, *Z. Klin. Med.*, 23 (1989) 2071.

C12. A. Cu, G. Bellah and D.A. Lightner, *J. Am. Chem. Soc.*, 97 (1975) 2579.

C13. A.G. Mohan and N.J. Turro, *J. Chem. Educ.*, 51 (1974) 528.

C14. A.F. McDonagh and F. Assisi, *Fed. Eur. Biochem. Soc. Lett.*, 18 (1971) 315.

C15. J. Fog and E. Jellum, *Nature*, 198 (1963) 88.

C16. J.J. Lee and G.D. Gillispie, *Photochem. Photobiol.*, 33 (1981) 757.

C17. M.M. Rauhut, *Acc. Chem. Res.*, 2 (1969) 80.

C18. R. Weinberger, *J. Chromatogr.*, 314 (1984) 155.

C19. C. Gooijer, P. van Zoonen, N.H. Velthorst and R.W. Frei, *J. Biolumin. and Chemilumin.*, 4 (1989) 479.

C20. B. Mann and M.L. Grayeski, *Anal. Chem.*, 62 (1990) 1532.

C21. C.D. Tran and G.S. Beddard, J. *Am. Chem. Soc.*, 104 (1982) 6741.

C22. C.D. Tran and G.S. Beddard, *Biochim. Biophys. Acta*, 687 (1981) 497.

C23. S. Kobayashi and K. Imai, *Anal. Chem.*, 52 (1980) 424.

C24. C.D. Tran, *Appl. Spectrosc.*, 41 (1987) 512.

C25. C.H. Hempe, H.K. Silver and D.O. O'Brian, in Current Pediatric Diagnosis and Treatment, Large Medical Publications, London, 1974, pp. 9878.

C26. C.E. Cornelius, in J.J. Kaneko and C.E. Cornelius (Eds.) Clinical Biochemistry of Domestic Animals, Vol. 1, Academic Press, New York, 1970, pp. 161.

C27. J. Fog and A.F. Bakkeh, *Scand. J. Clin. Lab. Invest.*, 20 (1967) 88.

C28. O.S. Wolfbeis and M. Leiner, *Anal. Chim. Acta*, 167 (1985) 203.

C29. A.J. Weber and M.L. Grayeski, *Anal. Chem.*, 59 (1987) 1452.

Chapter 4

D1. J. R. Chowdhury, A. W. Wolkoff and I. M. Arias, in C. R. Scriver, A. L. Beaudet, W. S. Sly and D. Valle (Editors), *The Metabolic Basis of Inherited Disease*, McGraw-Hill, New York, 6th edition, 1989, pp. 1367-1410.

D2. J. J. Lauff, M. E. Kasper, T. W. Wu and R. T. Ambrose, *Clin. Chem.*, *28* (1982) 629.

D3. T. W. Wu, G. A. Levy, S. Yin, J. X. Au, P. D. Greig, S. M. Strosberg, M. Ettles, M. Abecassis, R.A. Superina, B. Langer, L. M. Blendis, M. J. Philips and B. R. Taylor, *Clin. Chem.*, *36* (1990) 9.

D4. N. Blanckaert, P. M. Kabra and F. A. Farina, *J. Lab. Clin. Med.*, *96* (1980) 198.

D5. S. Onishi, S. Itoh, W. Kawada, K. Isoba and S. Sugiyama, *Biochem. J.*, *185* (1980) 281.

D6. C. K. Lim, R. V. A. Bull and J. M. Rideout, *J. Chromatogr.*, *204* (1981) 219.

D7. T. Uesugi and S. Adachi, *J. Chromatogr.*, *277* (1983) 308.

D8. J. J. Lauff, M. E. Kasper and R. T. Ambrose, *Clin. Chem.*, *29* (1983) 800.

D9. J. Singh and L. D. Bowers, *J. Chromatogr.*, *380* (1986) 321.

D10. R. Weinberger and E. Sapp, *J. Chromatogr.*, *516* (1990) 271.

D11. S. Terabe, K. Otsuke, K. Ichikawa, A. Tsuchiga and T. Ando, *Anal. Chem.*, *56* (1984) 111.

D12. A. S. Cohen, A. Paules, B. L. Karger, *Chromatographia*, *24*, (1987) 15.

D13. S. Terabe, M. Shibata and Y. Miyashita, *J. Chromatogr.*, *480* (1985) 219.

D14. K. Otsuka, S. Terabe and T. Ando, *J. Chromatogr.*, *332* (1985) 219. 15.H .

Nishi, T. Fukuyama, M. Matsuo and S. Terabe, *J. Chromatogr.*, *515* (1990) 233.

D16. H. Nishi, T. Fukuyama and M. Matsuo, *J. Chromatogr.*, *515* (1990) 245.

D17. N. Blanckaert, *Biochem. J.*, *185* (1980) 115.

D18. W. R. Eberlein, *Pediatrics*, *25* (1960) 878.

D19. C. C. Kuenzle, N. G. Cumarasamy and K. J. Wilson, *J. Biochem.*, *251* (1976) 801.

D20. R. Tenhumen, *Ann. Med. Exp. Biol. Fein., Suppl.*, *6* (1965) 1.

D21. J. Ostrow, D. Murphy and H. Nancy, *Biochem. J.*, *120* (1970) 311.

D22. M. Roth, in H. Ch. Curtius and M. Roth (Editors), *Clinical Biochemistry - Principles and Methods*, Walter de Gruyter, New York, 1974, pp. 1372-1389.

D23. J. J. Lee and G. D. Gillispie, *Photochem. Photobiol.*, *33* (1981) 757.

D24. P. D. Grossman, J. C. Colburn, H. H. Lauer, R. G. Nielsen, R. M. Riggin, G. S. Sittampalam and E. C. Richard, *Anal. Chem.*, *61* (1989) 1186.

D25. J. H. Aiken and C. W. Huie, *Anal. Lett.*, *24* (1991) 167.

D26. R. P. H. Thompson and A. F. Hofmann, *J. Lab. Clin. Med.*, *82* (1973) 483.

D27. J. J. Lauff, M. E. Kasper and R. T. Ambrose, *J. Chromatogr.*, *226* (1981) 391.

D28. T. Wang, J. H. Aiken, C. W. Huie and R. A. Hartwick, *Anal. Chem.*, *63* (1991) 1372.

D29. E.S. Yeung, *Acc. Chem. Res.*, *22* (1989) 125.

E1. R. Williams, Z. S. Fu and W. L. Hinze, *J. Chromatogr. Sci.*, 28 (1990) 298

E2. H. Nishi, T. Fukuyama, M. Matuso and S. Terabe, *Anal. Chim. Acta*, 236 (1990) 281

E3. M. C. Carey and D. M. Small, *Arch. Intern. Med.*, 130 (1972) 506

E4. G. E. Barker, P. Russo and R. A. Hartwick, *Anal. Chem.*, 64 (1992) 3024

E5. R. O. Cole and M. J. Sepaniak, *LC o GC*, 10 (1992) 380

E6. R. Weinberger, E. Sapp and S. Moring, *J. Chromatogr.*, 516 (1990) 271

E7. B. Farruggia and G. Pico, *Gen. Physiol. Biophys.*, 11 (1992) 219

E8. K. Otsuka, S. Terabe and T. Ando, *J. Chromatogr.*, 348 (1985) 39

E9. R. K. Gilpin, S. E. Ehtesham and R. B. Gregory, *Anal. Chem.*, 63 (1991) 2825

E10. Y. H. Chu, L. Z. Avila, H. A. Biebuyck and G. W. Whiteside, *J. Med. Chem.*, 35 (1992) 2915

E11. G. Barker, W. J. Horvath, C. W. Huie and R. A. Hartwick, *J. Liq. Chromatogr.*, in press

E12. P. Lundahl, E. Greijer, M. Sandberg, S. Cardell and K. O. Eriksson, *Biochim. Biophys. Acta*, 873 (1986) 20

Chapter 5

F1. C.T. Driscoll, J.D. Barker, Jr. and C.L. Schofield, *Nature,* 284 (1980) 161.

F2. R.B. Martin, *Clin. Chem.* 32 (1986) 1797.

F3. M.A. Akeson and D.N. Munns, *Biochim. Biophys. Acta,* 984 (1989) 200

F4. G.S. Zubenko and I. Hanin, *Brain Res.,* 498 (1989) 381.

F5. R.A. Yokel, V. Lidums, P.J. McNamara and U. Ungersted, *Toxic. Appl. Pharm.,* 107 (1991) 153.

F6. C.N. Martyn, C. Osmond, J.A. Edwardson, D.J.P. Barker, E.C. Harris and R.F. Lacey, *Lancet,* 1 (1989) 59.

F7. J. Johansson, *Acta Chim. Scand.,* 14 (1980) 771.

F8. T.L. Macdonald and R. Bruce Martin, *Trends in Biochem. Sci.,* 13 (1988) 15.

F9. T.J. Sullivan, H.M. Seip and I.P. Muniz, *Inter. J.Environ. Anal. Chem.,* 26 (1986)61 F10.P.M. Bertsch and M.A. Anderson, *Anal. Chem.,* 61 (1989) 535.

F11. P. Jones, *Intern. J. Environ. Anal. Chem.,* 44 (1991) 1.

F12. A. Westen, P.R. Brown, P. Jandik, W. K. Jones and A. L. Heckenberg, *J. Chromatogr.,*593 (1992) 289.

F13. B.J. Wildman, P.E. Jackson, W.R. Jones and P.G. Alden, *J. Chromatogr.,* 546 (1991) 459.

F14. M. Aquilar, X. Huang and R.N. Zare, *J. Chromatogr.,* 480 (1989) 427.

F15. W. Beck and H. Engelhardt, *Chromatographia,* 33 (1992) 313.

F16. D.R. Parker, L.W. Zelazny and T.B. Kinraide, *Soil Sci. Soc. Am. J.,* 51 (1987) 488.

F17. B.L. Karger, A.S. Cohen and A. Guttman, *J. Chromatogr.,* 492 (1989) 585.

F18. R.A. Robinson and R.H. Stokes, *Electrolyte Solutions*, Butterworths, London, 2nd Ed., 1965, pp. 49-73.

F19. A.L. Horvath, *Handbook of Aqueous Electrolyte Solutions: Physical Properties, Estimation and Correlation Methods*, Ellis Horwood Limited, Chichester, 1985, pp.1934.

Chapter 6

G1. *Y. Walbroehl and J. W. Jorgenson, J. Chromatogr.*, 315 (1984) 135

G2. M. Krejci, K. Tesarik and J. Pajurek, *J. Chromatogr.*, 191 (1980) 17

G3. T. Tsuda and G. Nakagawa, *J. chromatogr.*, 268 (1983) 369

G4. J. W. Jorgenson and K. D. Luckacs, *Anal. Chem.*, 53 (1981) 1298

G5. S. Wu and N. J. Dovichi, *J. Chromatogr.*, 480 (1989) 141

G6. J. V. Sweedler, J. B. Shear, H. A. Fishman, R. W. Zare and R. Scheller, *Anal. Chem.*, 63 (1991) 496

G7. R. A. Smith, J. A. Olivares, N. T. Nguyen and H. R. Udseth, *Anal. Chem.*, 60 (1989) 436

G8. M. Moseley, L. Deterding, K. Torner and J. W. Jorgenson, *J. Chromatogr.*, 480 (1989) 197

G9. X. Huang and R. N. Zare, Anal. Chem., 63 (1993) 2193

G10. F. E. P. Mikkers, F. M. Everaerts and Th. P. E. M. Verheggen, *J. Chromatogr.*, 169 (1979)

G11. R. A. Wallingford and A. G. Ewing, *Anal. Chem.*, 59 (1987) 1763

G12. S. Kobayashi and K. Imai, *Anal. Chem.*, 52 (19800 424

G13. W. Sigvardson and J. W. Birks, *Anal. Chem.*, 55 (1983) 432

G14. M. L. Grayeski and A. Weber, *Anal. Lett.*, 17 (1984) 1953

G15. R. Dadoo, L. A. Colon and R. N. Zare, *J. High Resolut. Chromatogr.*, 15 (1992) 133

G16. K. Robards and P. J. Worsfold, *Anal. Chim. Acta*, 266 (1992) 175

G17. P. J. M. Kwakman and U. A. Th. Brinkman, *Anal. Chim. Acta*, 266 (1992) 175

G18. R. Brina and A. J. Bard, *J. Electroanal. Chem.*, 238 (1987) 277

G19. P. Camilleri, G. N. Okafo and C. Southan. *Anal. biochem.*, 196 (1991) 178

G20. A. G. Mohan and N. J. Turro, *J. Chem. Educ.*, 51 (1974) 528

G21. R. Weinberger, C. A. Mannan, M. Cerchio and M. L. Grayeski, *J. Chromatogr.*, 288 (1984) 445

G22. N. Hanaoka, H. Tanaka, A. Nakamato and M. Takado, *Anal.Chem.*, 63 (1991) 26

H1. S. Hjerten, and M. Zhu, J. Chromatogr., 346 (1985) 256

H2. S. Hjerten, J. Liao, and K. Yao, K, J. Chromatogr., 387 (1987) 127

H3. T. Dulffer R. Herb, H. Hermann, and U.Kobold, Chromatographia, 30 (1990) 11

H4. K. W. Yim, J. Chromatogr., 559 (1991) 401

H5. M. Zhu, D. L. Hansen, S. Burd, and F. Gannon, J. Chromatogr., 480 (1989) 311

H6. E. E. Brumbaugh and G. K. Ackers, J. Biol. Chem., 243 (1968) 6315

H7. K. L. Rowlen, K. A. Duell, J. P. Avery and J. W. Birks, Anal. Chem., 63 (1991) 575

H8. J. Wu and J. Pawliszyn, Anal. Chem., 64 (1992) 224

H9. T. Wang and R. A. Hartwick, Anal. Chem., 64, 1745-7 (1992)

Appendix

J1. Falk, H., *CRC Critical Reviews in Analytical Chemistry*, 19 (1988) 29.

J2. L'vov, B. V., *Atomic Absorption Spectrochemical Analysis*, Hilger, London, 1970.

J3. Sturgeon, R.E., Chakrabarti, C.L.,Langford, C.H., *Anal. Chem.*, 48 (1976) 1792

J4. Van den Broek, W. M. G. T., and de Galen, L., *Anal. Chem.*, 49 (1977) 2176.

J5. Frech, W., Zhou, N. G., and Lundberg, E., *Spectrochim. Acta*, 378 (1982) 691.

J6. Fuller, C. W., *Analyst*, 101 (1976) 798.

J7. Paveri-Fontana, S., and Tessari, G., *Proc. Anal. At. Spectrosc.*, 7 (1984) 243.

J8. Smets, B., *Spectrochim. Acta*, 35B (1980) 33.

J9. Güell, O. A., and Holcombe, J. A., *Spectrochim. Acta*, 43B (1988) 459.

J10. Welz, B., Radziuk, B., and Schlemmer, G., *Spectrochim. Acta*, 43B (1988) 749.

J11. Huie, C. W., and Curran, Jr., C. J., *Appl. Spectrosc.*, 44 (1990) 1329.

J12. Childers, A. G., and Hieftje, G. M., *Appl. Spectrosc.*, 40 (1988) 680.

J13. Holcombe, J. A., *Spectrochim. Acta*, 38B (1983) 609.

J14. Davies, J. T., *Turbulence Phenomena*, Academic, London, 1972, pp. 4-93.

J15. Skellard, A. H. P., *Diffusional Mass Transfer*, Wiley, New York, 1974, pp. 231-243.

J16. Chakrabarti, C. L., Wu, S., Karwowska, R., Rogers, J. T., and Dick, R. *Spectrochim. Acta*, 40B (1985) 1663.

J17. Rademeyer, C. J., Human, H. G. C., and Faure, P. K., *Spectrohim. Acta*, 41B (1986) 439.

J18. Welz, B., Sperling, M., Schlemmer, G., Wenzel, N., and Marowsky, G., *Spectrochim. Acta*, 43B (1988) 1187.

J19. L'vov, B. V.; Romanova, N. P. and Polzik, L. K., *Spectrochim. Acta*, 46B (1991) 1001.